Carnegie Mellon University

CARNEGIE INSTITUTE OF TECHNOLOGY

THESIS

SUBMITTED IN PARTIAL FULFILLMENT OF THE REQUIREMENTS

FOR THE DEGREE OF Doctor of Philosophy

TITLE Structural Design and Economic Analysis of Suspension Bridges Constructed Using FRP Deck

PRESENTED BY Elfatih Ahmed

ACCEPTED BY THE DEPARTMENTS OF

Civil and Environmental Engineering

James H. Garrett — ADVISOR, MAJOR PROFESSOR — December 11, 2014 — DATE

David A. Dzombak — DEPARTMENT HEAD — December 11, 2014 — DATE

APPROVED BY THE COLLEGE COUNCIL

Vijayakumar Bhagavatula — DEAN — January 12, 2015 — DATE

Structural Design and Economic Analysis of Suspension Bridges Constructed Using FRP Deck

A dissertation submitted in partial fulfillment of the requirements for

the degree of

Doctor of Philosophy

in

Civil Engineering

Elfatih Ahmed

B. Sc., Civil Engineering, University of Khartoum

Master of Engineering, Civil Engineering, Howard University

Department of Civil and Environmental Engineering
Carnegie Mellon University
Pittsburgh, Pennsylvania, USA

December 2014

ACKNOWLEDGEMENTS

My sincere gratitude goes to Professor James H. Garrett, Jr. for his support and guidance. I respect his devotion to produce excellent academic research. Jim’s devotion and attention to details, in spite of his busy schedule, helped me to improve the proposal and dissertation drafts substantially. I am grateful to Dr. Juan Sobrino for his advice on the design process. Juan’s comments and suggestions from the proposal stage through the final dissertation were invaluable. I would like to express my sincere appreciation to my thesis committee members, Professor Irving Oppenheim and Professor Matteo Pozzi for their critical and valuable comments on the proposal and the dissertation.

I greatly appreciate the financial support I received from a Dean’s fellowship in my first year in graduate studies at Carnegie Mellon University. This funding helped me to complete the dissertation.

I also would like to thank the staff at Carnegie Mellon University particularly Maxine Leffard for her great help.

I would like to thank my wife Mona for her support. Her support enables me to pursue careers in both the engineering practice and academic research.

ABSTRACT

Bridges built today are larger, but also lighter, more slender, and more efficient structures than they were a century ago. As the free span of future suspension bridges increases, so does the need for reducing dead loads. Using Fiber Reinforced Polymer (FRP) deck for suspension bridges is one way to achieve significantly lighter dead loads. Although the cost of FRP materials is more than double the cost of conventional concrete and steel deck, the hypothesis of this research is that the savings in the anchoring system and foundation and the reduction in weight of the main cables and suspenders will result in an *overall cost reduction.* It is also the hypothesis of this research that the use of FRP deck will impair the aerodynamic stability of suspension bridges.

Significant studies have been performed on the use of FRP materials in bridge structures. The Federal Highway Administration initiated research on FRP composite bridge decks in the early 1980s, primarily focused on deck strength and stiffness. In addition, several research projects have been conducted for health monitoring and to assess the long-term performance of FRP materials in bridge construction. Overall, the results suggest that long-term structural response was consistent and well within acceptable strength and serviceability design limits.

For the research described in this dissertation, a parametric study was performed considering several bridges of different spans, materials, soil conditions, and material unit prices to study the economic and aerodynamic implications of using FRP deck in suspension bridges. Two groups of suspension bridges with 200 m, 400 m, and 600 m free spans were designed, one group using a reinforced concrete deck and the other group using the much lighter FRP deck. Since soil conditions affect the design of the anchorage and the overall cost of the bridges, three different soil types were considered in this research. The three soil conditions that were considered in this research were sound rock, medium sand, and stiff clay. Then, the aerodynamic stability was examined for all of the bridges using Selberg's approach. Three-dimensional finite element analyses was performed for each bridge to obtain the values for the torsional moment of inertia and the vertical and torsional frequencies. These values were used in Selberg's equation to determine the flutter speed of each bridge. A linear elastic analysis was performed to validate the three-dimensional finite element analysis results.

The predicted flutter speeds obtained from the linear elastic approach and the finite element approach were within 9% for all the spans and deck materials. The use of FRP deck reduced the predicted flutter speed of the 200 m span bridge, 400 m span bridge, and 600 m span bridges by 35%, 36%, and 37%, respectively.

Sensitivity cost analysis was performed of the 200 m, 400 m and 600 m span bridges founded in three different soil types. The three soil types considered were sound rock, medium sand, and stiff clay. The maximum savings was realized in the case of the weakest soil with the least resistance to the main cables tension force: stiff clay.

Consistent with the research hypothesis, the cost of the FRP deck is more than twice the cost of the concrete deck, yet the overall cost savings for using an FRP deck were 30% to 42% of the cost using a concrete deck depending on span length and soil conditions.

While earlier studies have demonstrated that the life cycle cost analysis could be advantageous in the long term because it requires less maintenance, the findings of the research described in this dissertation showed that the use of FRP deck could result in a 30% to 42% reduction in initial construction cost.

Table of Contents

List of Figures

List of Tables

Chapter 1 - Introduction

This chapter includes a brief overview of the topic, the objectives of this research, and a preview of the chapters that follow.

1.1 Overview

The last century witnessed significant developments in the field of bridge engineering, which resulted in the design and construction of larger but also lighter, more slender, and structures that are more efficient. Today, suspension bridges such as the Akashi-Kaikyo Bridge in Japan (Figure 1.1) reach a free span of almost 2,000 m. Proposed future bridges would span even greater distances; for example, the design of the Strait of Messina Bridge has a free span of 3,300 m. Unlike other types of bridges, suspension bridges are supported only in four points at the cable ground anchorage system (Figure 2.1) shows the suspension bridge components). The need for reducing the dead load of suspension bridges becomes increasingly important as the free span becomes longer. The use of Fiber Reinforced Polymer (FRP) deck for suspension bridges will result in significantly lighter dead loads than the loads that result from conventional steel and concrete deck. A typical 200 m FRP bridge deck weighs 25 psf while a concrete deck spanning the same distance as the FRP deck weighs 119 psf (www.fhwa.dot.gov). Such reduction in dead loads will result in a reduction of the forces on the cables, the anchorage system, and the foundation. The hypothesis of this research is that the use of composite decks in suspension bridges will result in significant reductions in construction costs and will influence the aerodynamic stability of these bridges. Although the cost of FRP materials is more than double the cost of conventional concrete and steel deck, the hypothesis is that the savings in the anchoring system and foundation and the reduction in weight of the main cables and suspenders will result in an overall cost reduction.

This proposed research considers the use of FRP composites only for the deck and uses conventional construction materials for all other elements of the bridge—reinforced concrete for the towers and steel strands for the main cables and suspenders.

Significant research has been performed on the use of FRP materials in bridge structures. The Federal Highway Administration initiated research on FRP composite bridge decks in the early 1980s, primarily focused on deck strength and stiffness. In addition, several research projects have been conducted on health monitoring and to assess the long-term performance of FRP materials in bridge construction. Overall, the results suggest that long-term structural response was consistent and well within acceptable strength and serviceability design limits.

Figure 1.1: Akashi-Kaikyo Bridge, Japan

Some studies of life cycle costs of bridges using FRP deck have concluded that the use of FRP deck will result in higher initial cost but lower life cycle costs in the long term. For example, a study performed in Japan by Nishizaki, et al. (2006), found FRP bridge deck to be more efficient when longer life (100 years) is required in severely corrosive environments. Another study suggested that under extremely soft ground conditions, composite suspension bridges might offer significant advantages over steel suspension bridges in reducing the total cost (Meiarashi, et al. 2002). A North Carolina study (Eheln 1999) examined life cycle costs for three FRP deck types and compared them to the costs for a conventional concrete bridge deck; the study found that wood core FRP was a life-cycle cost-effective alternative to conventional reinforced concrete.

While earlier studies have demonstrated that the life cycle cost analysis could be advantageous in the long term because it requires less maintenance, the findings of this study show that the use of FRP deck could result in a lower initial construction cost.

1.2 Objectives

The objectives of the research described in this research are twofold:

1. To explore the aerodynamic implications of reducing the dead weight of the deck of suspension bridges by using FRP composite for deck materials. Composite concrete deck on steel girders is effective for suspension bridges with span lengths up to 600 m. For span lengths greater than 600 m, this concrete composite deck system will affect the aerodynamic stability of the bridge. Therefore, this study focused on short to medium span suspension bridges from 200 m to 600 m span bridge length.

2. To explore the economic implications of using FRP deck in suspension bridges. The cost of FRP deck is higher than the cost of concrete deck. However, significant savings can be achieved by using a lighter FRP deck because it will reduce the size and cost of the steel girders, cables, tower foundations and anchorage system. This research studied these savings versus the extra cost of the FRP deck under three different soil conditions.

1.3 Organization of the Dissertation

Chapter 2 discusses suspension bridges, including history and development, components, and historical development of theories that predict aerodynamic stability. Various aerodynamic phenomena are described and various theories of predicting aerodynamic stability are discussed.

Section 2 of the chapter discusses FRP deck, including its behavior, properties, and life cycle cost studies that have been performed in the past.

Chapter 3 presents the research questions and the approaches to answer them. The first research question is in regards to the aerodynamic behavior of suspension bridges constructed with an FRP deck as compared to others constructed from traditional concrete composite deck. The second question addresses the economic implications of using such deck. To answer the first question, 200 m, 400 m, and 600 m suspension bridges with an FRP deck and concrete deck were designed. After completion of the design of these bridges, flutter speeds were computed for all of the bridges and a parametric study was performed to compare the aerodynamic behavior of all the bridges. To answer question 2, an economic comparative study was performed for all the bridges under three different soil conditions.

Chapter 4 describes the design procedure followed for the design of all the bridges using the base model of the 200 m span bridge as an example to show the detailed design procedure. It includes design specifications, codes adopted for this research, and trial models performed to achieve live load deflection limits and design requirements. In addition, it details the design procedure for the towers and anchorage systems. This chapter also presents the results and data for the final designs of 200 m Span suspension bridges with an FRP deck on steel girders and concrete deck on steel girders. Chapter 5 presents the results and data for 400 m and 600 m Span suspension bridges with an FRP deck on steel girders and concrete deck on steel girders.

Chapter 6 shows the procedure and methodology for calculations of flutter speeds for all the bridges. Selberg's equation (Selberg 1961) was used to determine the flutter speed. Two methods were used to obtain the aerodynamic parameters such as torsional and vertical frequencies to be used in Selberg's flutter speed computations. One method uses the linear elastic approach. The second method is a three-dimensional finite element non-linear analysis utilizing (MIDAS-Civil) software capabilities. In addition, the results of the flutter speeds computed by two different methods for all the bridges are presented in this chapter.

Chapter 7 presents the comparative economic analysis of all the bridges. Soil conditions affect the design and quantities of the anchorage system. Considering that the use of FRP deck reduces the cable tension force that is exerted on the anchorage, various types of soil conditions were studied and presented in this chapter. The anchorage systems and tower foundations were designed for all the bridges on sound rock, medium sand, and stiff clay. This chapter is concluded with a discussion of various cost reductions obtained by using FRP deck in various soil conditions and various span lengths.

Chapter 8 discusses the findings of this research and compares these findings with the initial hypothesis. Moreover, the chapter recommends future research. A similar comparative study of streamlined shape deck constructed from steel and composite materials could be useful. Application of this study's findings for existing suspension bridges, such as the Bronx Whitestone Bridge, to minimize the dead load on the hangers and cables could offer effective solutions for rehabilitation of these bridges. It could lead to a suitable solution for the aging suspension bridges that were not designed for today’s live loads and need a reduction of the dead loads.

Chapter 2 - Research Background

This chapter includes a brief history of suspension bridges, an overview of suspension bridge components, and a discussion of the aerodynamic forces that must be taken into account in bridge engineering and how these forces are calculated, an overview of Fiber Reinforced Polymers (FRP), and an overview of previous research considering the economics of using FRP in the construction of bridges.

2.1 Suspension Bridges

This section describes the different components of a suspension bridge and their locations, materials and functions. In addition, it discusses the aerodynamic behavior of suspension bridges and the development of the theories for prediction of the aerodynamic behavior of suspension bridges.

2.1.1 History and Evolution

Early suspension bridges were constructed for pedestrians (pedestrian bridges). They consisted of cables formed from twisted vines. The cables were attached to tress or other permanent objects located on riverbanks or at the edge of valleys.

Military engineers made effective use of rope bridges. In 1734, the Saxon army built an iron-chain bridge over Oder River at Glorywitz, Germany; it was reportedly the first metal suspension bridge in Europe. The first metal suspension in North America was the Jacob's Creek Bridge in Pennsylvania, USA. It was designed and erected by James Finley in 1801 (Podolny, W., 2006).

A major milestone in the history of suspension bridges was the opening of the Brooklyn Bridge over the East River in New York in 1883. It has a center span of almost 500 m and a side span of 286 m, making the total cable supported length more than 1 km. Roebling designed it before his death in 1869. It is regarded as the ancestor of all modern suspension bridges (Buonopane, 1993).

In 1930s, engineers explored slender deck and stiffening girders for suspension bridges, but the failure of Tacoma Narrows Bridge in 1940 under aerodynamic forces led the return to an aerodynamically stable stiffening girder such as box girders. By the late 1980s, three suspension bridges (the Golden Gate Bridge in San Francisco, California, USA, the Verrazano-Narrows Bridge in New York, USA, and the Humber Bridge in Hull, England, UK) have main spans of more than 1,200 m (Billington, 2012). Today, suspension bridges are able to reach main span lengths of almost 2,000 m, such as the Akashi-Kaikyo Bridge in Japan (1998) and even 3,300 m main span for the proposed future Strait of Messina Bridge.

2.1.2 Suspension Bridge Components

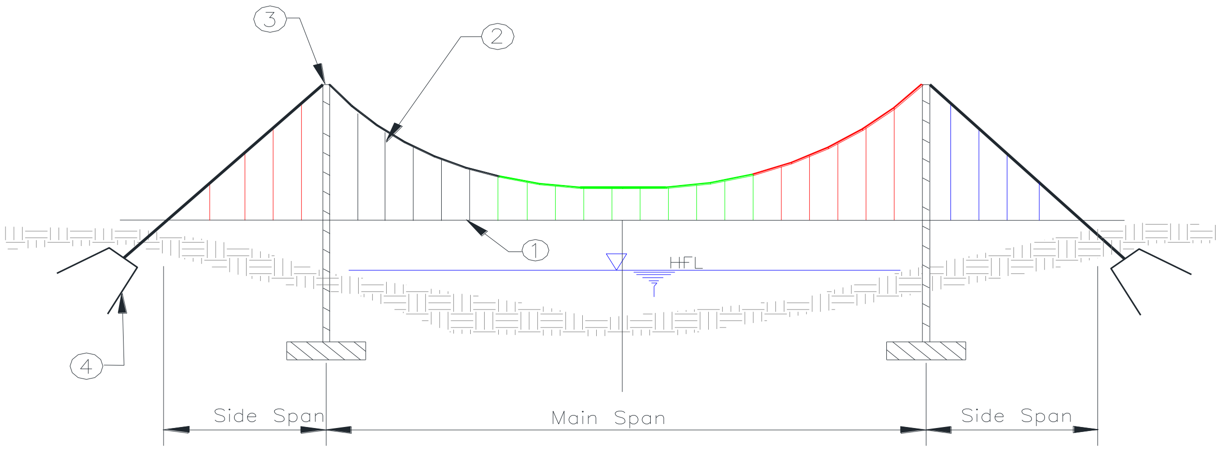

Figure 2.1: Terminology for Suspension Bridge Components

This section discusses the components of suspension bridges, their locations, functions, and materials. Figure 2.1 describes the components of suspension bridges.

The key components of the bridge shown in Figure 2.1 are:

- Stiffening girders (or stiffening truss) with the bridge deck;
- Cable system supporting the stiffening girder;
- Towers (or pylons) supporting the cable system; and
- Anchor blocks (or anchor piers) supporting the cable system vertically and horizontally.

Each of these components are described in the next three sections.

2.1.2.1 Stiffening Girders with the Bridge Deck

In highway bridges, a concrete deck will consist of a slab with a thickness of 200 mm to 300 mm supported by floor girders (cross–girders) spaced at a distance of 3,000 to 5,000 mm.

Longitudinal girders and cross-girders are usually made of steel or concrete. Longitudinal girders could be steel plate girders or truss girders (stiffening truss). An edge girder deck system consists of heavy girders along the plane of the cables in either side of the deck. Cross-girders span transversely between these girders with a concrete deck spanning longitudinally between cross-girders. A composite steel system is not feasible for a span over 600 m (Detroit River International Crossing Bridge Type Study Report, July 2007). Other types of deck cross section includes orthotropic box girders. They are only economical for very long spans where minimum superstructure weight is necessary and aerodynamics are critical.

2.1.2.2 Cable System

In a suspension bridge, the cable system carries the deck through the hangers (suspenders), which transmit the loads to the main cable. Cables are usually composed of parallel wire, parallel strands, and locked-coil strands. There are various types of cables used for suspension bridges. Helical bridge strands (spiral strands) and parallel wire strands are commonly used in suspension bridges.

2.1.2.3 Towers (Pylons) and Anchor Blocks

Towers or pylons support the main cable. They experience various forces such as wind, as well as vertical and horizontal forces from the main cables tension. The most influential force is the vertical component of the main cables tension. They are constructed from steel or concrete. Although the self-weight of the concrete is much heavier, concrete pylons are competitive to a height of 250 m and, depending on local conditions, they may be competitive beyond that. The choice between steel and concrete depends on the speed of erection and soil condition. This research uses concrete for pylon materials.

In earth-anchored suspension bridges, the main cables forces are transmitted to the earth through the anchor block. The individual strands of the main cables are connected to the concrete block. The most common type of anchor block is the gravity type. This type uses a large vertical force from the dead weight of the concrete to resist the uplift from the vertical component of the main cables tension. The dead load should be sufficient to resist the horizontal component of the main cables tension. The resistance force to the horizontal component of the main cables tension comes from the dead load multiplied by the soil coefficient of friction.

2.1.3 Aerodynamic Stability

This section discusses the historical background of the understanding of wind impact on suspension bridges. It also describes wind phenomena that affect suspension bridges and the development of the theories for the prediction of suspension bridge response to wind.

The computed flutter speed obtained using a particular method of analysis is compared to the design flutter speed. Design flutter speed varies and depends on many factors. These factors include site location, exposure category, nature of the terrain, and specific bridge owner requirements. A detailed discussion and example of design flutter speeds are presented in Chapter 6, Section 6.2.

2.1.3.1 Historical Background

In the design of long span suspension bridges, the local wind activity and its impact on that bridge is of primary concern. The failure of the Tacoma Narrows suspension bridge in 1940

(Figure 2.2) led to a deep realization of the importance of understanding the effect of wind on suspension bridges.

Figure 2.2: Tacoma Narrows Bridge Collapse, 1940

Before the failure of the Tacoma Narrows Bridge, the required stiffness of suspension bridges was based only on the ratio of live load deflection to span length. The design live load for the Tacoma Narrows Bridge was only 1,500 lb/ft., compared with 3,000 lb/ft for the Bronx-Whitestone Bridge and 4,000 lb/ft for the Golden Gate Bridge (Barelli 2006). The slenderness of the Tacoma Narrow Bridge design resulted from its smaller design loads. The collapse of the Tacoma Narrows Bridge showed that the traditional measure of stiffness was inadequate, and a minimal absolute stiffness was required in order to deal with wind-induced oscillations. Section 2.1.3.2 describes the aerodynamic phenomena that can affect suspension bridges. Section 2.1.3.3 describes the development of theories that predict suspension bridge response to wind.

2.1.3.2 Aerodynamic Phenomena

The aero-elastic wind phenomena that affect the bridge deck of suspension bridges are vortex shedding and flutter.

2.1.3.2.1 Vortex Shedding

Simiu and Scanlan (1986) state that when a body is subjected to wind flow, the separation of flow occurs around the body. This produces force on the body: a pressure force on the windward side and a suction force on the leeward side. The pressure and suction forces result in the formation of vortices in the wake region, causing structural deflections on the body (Figure 2.3).

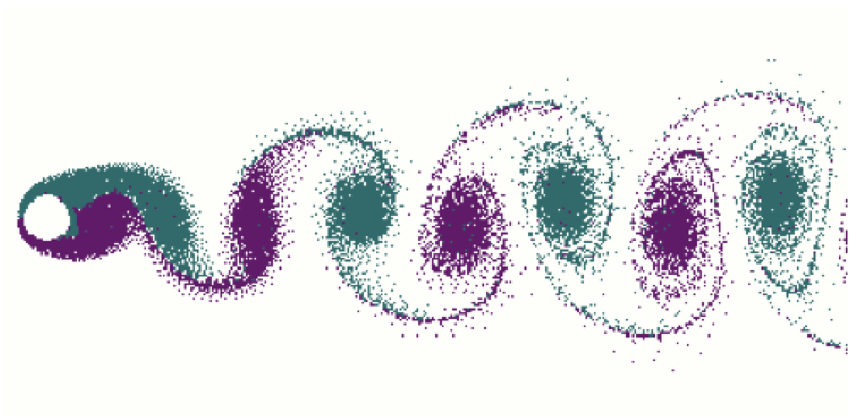

Figure 2.3: Vortex Shedding Behind a Cylindrical Structure (Simon Key, 2005)

The process of vortex shedding is highly influenced by the effect of viscosity. Only a viscous fluid will satisfy a no-slip condition of its particles on the surface of a body immersed in the flow. Even if the viscosity is very small, this condition will hold; however, its influence on the flow regime will be confined to a small region: the boundary layer along the body. Within this boundary layer, the velocity of the fluid changes from zero on the surface to the free-stream velocity of the flow.

At surfaces with high curvature, there can also be an adverse pressure gradient. The influence of the viscosity and the velocity of the flow are defined by the Reynolds number:

$$R_E = \frac{pVD}{u}$$ **(2.1)** [Simiu and Scanlan 1986]

Where,

R_E = Reynolds number

p = Density of the fluid

V = Velocity of the fluid relative to the cylinder

D = Diameter

u = Dynamic viscosity of the fluid

Strouhal defined a dimensionless shedding frequency, the Strouhal number, to characterize this process:

$$S = \frac{N_3 D}{U}$$ **(2.2)** [Strouhal, V.C. 1878]

Where,

S = Strouhal number

N_s = Frequency of full cycles of vortex shedding

D = Characteristic dimension of the body projected on a plane normal to the mean flow velocity

U = Velocity of oncoming flow.

As demonstrated in the above equations, the most important physical parameter of a two-dimensional body exhibiting vortex-induced oscillations is the size and shape of the body (Parkinson 1989). Zdravokovich also emphasized the influence of the angle of attack (1996). From the above discussion, it could be concluded that vortex shedding phenomena would be impacted less by the reduction of bridge deck mass than by the shape and size of the bridge deck and the wind angle of attack.

2.1.3.2.2 Flutter

Flutter is an aero elastic phenomenon in which two degrees of freedom of a structure couple in a flow-driven, unstable oscillation. Flutter can be defined as a condition of negative aerodynamic damping wherein the deflection in the structure grows to enormous levels until failure occurs. The motion is characterized by the fluid regime feeding energy into the structure during each cycle, thus counteracting the structural damping. If there is no flow, any oscillation caused by a disturbance will decay due to the presence of damping (Simiu and Scanlan, 1986).

When the speed of flow is gradually increased, the rate of apparent damping of the oscillation first increases. With further increase in flow speed, however, a point is reached where the damping decreases again. The point where the effective damping is equal to zero is referred to as the critical flutter condition. Here the oscillation just maintains its amplitude. Above the critical speed, any small disturbance grows and initiates an oscillation of great amplitude.

2.1.3.3 Development of Theories for Prediction of Suspension Bridge Response to Wind

This section offers a historical background of the development of the theories of bridge aero-elasticity. These theories include the simplified methods and the computational fluid dynamic method.

2.1.3.3.1 Simplified Methods

Ammann introduced the "stiffness index" as a simple measure of suspension bridge response to wind (Ammann 1953). In deriving the index, he considered the simplest model of suspension bridge: a beam supported by a parabolic cable. He then calculated the half-span uniform load, which causes a one-foot deflection at the quarter point of the main span. This loading condition was selected because it simulates the deflected shape of the bridge in its first asymmetric mode.

The formula includes two terms, one representing the cable component and one the stiffening girder component:

$$S = \frac{8.2q}{f} + \frac{2457.6EI}{L^4}$$ **(2.3)** [Ammann 1953]

$$S = \frac{8.2q}{f} + \frac{0.07I}{(10^{-3} \times L)^4}$$ **(2.4)** [Ammann 1953]

Using $E = 193 \text{ X } 10^6$ kN/m^2

Where,

q = Weight of the suspended structure (kN/m)

f = Cable sag (m)

I = Moment of inertia of the stiffening girders in m^4

L = Span length (m)

Although he derived his equation analytically, Ammann then treated the formula empirically and modified it to better fit with the performance history of previous designs. He doubled the coefficient in front of the truss term in order to better account for damping, and added a correction term to account for the side span's length L_S.

$$S = \left(\frac{8.2q}{f} + \frac{0.14I}{(10^{-3} \times L)^4}\right)\left(1 - 0.6\frac{L_s}{L}\right)$$ **(2.5)** [Ammann 1953]

According to Rothman, Ammann considered an index above 370 desirable, and one above 600 optimal (Rothman 1984).

In 1943, D.B. Steinman presented his own method of calculating the "spring constant" of a suspension bridge, *K*, using a conservation of energy method (Steinman 1943). For a bridge vibrating in a mode of *n* equal segments he presented the formula:

$$K = n^2 \frac{\pi^2}{L^2} H_q + n^4 \frac{\pi^4}{L^4} EI$$ **(2.6)** [Steinman 1943]

If we look at the asymmetric mode,

$$n = 2$$

$$H_q = \frac{qL^2}{8f}$$ **(2.7)** [Steinman 1943]

$$K = \frac{\pi^2}{2}\left(\frac{q}{f}\right) + 16\pi^4 \left(\frac{EI}{L^4}\right)$$ **(2.8)** [Steinman 1943]

Steinman's formula takes the same form as Ammann's equation, except with different coefficients.

$$S = 8.2\left(\frac{q}{f}\right) + 2457.6\left(\frac{EI}{L^4}\right)$$ **(2.9)** [Steinman 1943]

The early work of Ammann and Steinman showed the important parameters that influence the aerodynamic stability of suspension bridges. The parameters are the weight of the suspended structure, cable sag, moment of inertia of the stiffening girders, and span length.

Although these equations will not be used in this research, they define the parameters that are to be considered for the study of the aerodynamic stability of suspension bridges. Current theories depend strongly on the use of classical pseudo-static force coefficients (drag, lift, and momentum) and their derivatives, so-called flutter derivatives.

Bleich conducted early pioneering work on bridge flutter analysis in 1948. He addressed bimodal-coupled bridge flutter consisting of fundamental vertical bending and torsional modes of vibration using airfoil aerodynamic theory. This analysis framework led to extensive numerical studies concerning the influence of bridge mass and frequency parameters on the critical flutter velocity.

These numerical studies provided a basis for the empirical formula suggested by Selberg (1961) for estimating the critical flutter velocity of bridges with a flat plate section. Another advancement in this area came with the introduction of flutter derivatives and the development of their identification schemes through wind tunnel testing. This approach offers a realistic modeling of aerodynamic forces on bluff bridge sections (Scanlan 1979).

2.1.3.3.2 Computational Fluid Dynamic Method

Most recently, however, due to the advancement of computer speed and capabilities, numerical methods have been used to predict suspension bridge response to wind. Morgenthal (2005) developed a numerical scheme that incorporates the natural wind characteristics and the aero-elastic properties of the bridge deck to obtain time-history analysis of the dynamic response. G.Szabó and J. Györgyi (2009) used Computational Structural Dynamics (CSD) and (CFD). They developed three-dimensional Fluid-Structure Interaction (FSI) using ANSYS MFX multi-field solver. The cross section of the model was 200 mm wide and 30 mm deep. The

Computational Solid Dynamic (CSD) model was created using the Finite Element Method (FEM).

The FEM mesh consists of regular rectangular four-node shell elements with six degrees of freedom per node. Cable elements were modeled using link elements without bending capabilities. The CFX module of ANSYS uses Finite Volume Method to model the wind force. This technique requires subdividing the domain of the flow into cells. For the CFD modeling, they used 200,000 cells. The meshing was finer around the bridge and coarser in the further reaches of the computational domain. To get the critical flutter speed, Szabó and Györgyi increased the inlet flow velocity gradually in different runs. They calculated the critical speed by monitoring the amplitude of motion from the different runs. They considered the critical speed as the speed at which the amplitude of motion starts growing. To validate their results, they used a simplified beam model for the bridge and a simple load model for the wind. As in the CSD-CFD simulation, they increased the inflow velocity wind until they reached the critical flutter speed. They concluded that the results they obtained from the CSD-CFD simulation and the simplified beam model were close.

2.2 FRP Composites

FRP composites technology has been incorporated into the industrial world for about 70 years. The technology has been utilized in the aerospace industry since the 1960s. More recently, however, it has been used as bridge material. The first all-composites bridge was the Miyun Bridge built in Beijing, China in 1982 (Sahirman 2003). Chongqing Glass Fiber Product Factory (China) was responsible for its manufacture. The National Composites Network reported the first all-composites pedestrian bridge was Aberfeldy Foot Bridge built in 1992 in Scotland by Maunsell Structural Plastics (www.ncn-uk.co.uk). The first FRP-reinforced concrete bridge deck in the U.S. was built in 1996 at McKinleyville, West Virginia (Sahirman 2003). The first all-composite vehicular bridge in the U.S. was built at Russell, Kansas in 1996. It was manufactured by Kansas Structural Composites, Inc. (www.ncn-uk.co.uk).

Examples of some FRP bridge decks are shown in Figure 2.4.

Illustration	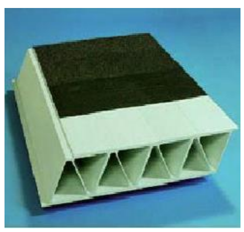	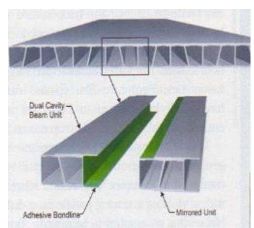	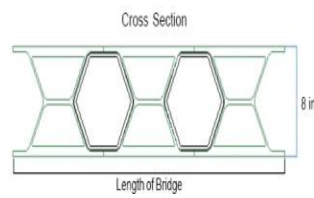
Deck Type	Dura Deck	Dura Span Deck	Super deck
Manufacturer	Fiber Composites	Marietta Composites	Creative Pultrusion

Figure 2.4: FRP Bridge Deck Examples

2.2.1 Material Behavior

FRP bridge deck systems offer the benefits of a high strength-to-weight ratio and environmental resistance. The Federal Highway Administration advisory on FRP composites bridge technology indicates that a typical 200 mm (8") FRP deck with its wearing surface weighs 122 kg/m^2 (25 psf) versus 581 kg/m^2 (119 psf) for a standard 240 mm (9.5”) concrete deck (www.fhwa.dot.gov). The Federal Highway Administration initiated research on FRP composite bridge decks in the early 1980s to transfer fiber-reinforced polymer composite technology to the design and construction of bridge decks (www.fhwa.dot.gov). This has led to the design and testing of numerous Glass Fiber Reinforced Polymer (GFRP) deck types.

The most common types being manufactured use either adhesively bonded pultruded shapes or sandwich construction. Extensive laboratory and field-testing has provided valuable performance data, enabling manufacturers to modify designs. The majority of this testing has focused on deck strength and stiffness.

Alagusundaramoorthy, et al. examined the behavior of FRP composite bridge deck panels under service load, wheel load, and failure load (2006). Laboratory testing was performed at Kentucky Structural Engineering Laboratory, and the results were used to model the First Salem Bridge in Salem, Ohio for the Ohio Department of Transportation (ODOT). The FRP bridge deck panels were fabricated and supplied by four different manufacturers. They tested the FRP panels and reinforced concrete panels for flexural, shear, and deflection. The test results were compared with the performance criteria (i.e., flexure, shear, and deflection) per ODOT specifications. The performance criteria specified by the Ohio Department of Transportation are based on strength (shear and flexural) and serviceability (deflection). All tested FRP bridge decks satisfied the performance criteria. The panels were tested to failure. The safety factor against failure varied from three to eight.

Several research projects have been conducted for health monitoring and to assess the long-term performance of FRP materials in bridge construction. Farhey (2006) reported the results of extensive health monitoring of the Tech 21 Bridge. Tech 21 is a Smith Road Bridge that is located west of Hamilton, Butler County, Ohio, USA. The bridge was designed and constructed using composite materials for all components of the bridge. The objective of the research was to provide a qualitative and quantitative long-term structural performance evaluation for a composite infrastructure. This two-lane bridge is the first fully instrumented all-composite bridge in the U.S. The health monitoring system was installed during its fabrication and construction. It was embedded in its structural components. No degradation or adverse performance outcomes were noted in the materials of the Tech 21 Bridge during four years of continuous monitoring. Researchers concluded that the bridge's stable structural response history demonstrates the durability of the materials, the integrity of the structural components, and environmental stability through multiple climate cycles. Overall, the long-term structural response was consistent and well within acceptable strength and serviceability design limits.

Hwai-Chung Wu, et al. also addressed the durability of FRP composite bridge deck (2006). The durability performance of FRP materials was examined under variable weather conditions. Specimens of typical FRP bridge deck materials were subjected to freeze-thaw cycling between 4.4º and -17.8˚C in media of dry air, distilled water and saltwater. The specimens were also subjected to a constant freeze of -17.8˚C. The average flexural strength of the specimens in dry air, distilled water and saltwater was 496.6 MPa, 453.2 MPa, and 480.6 MPa, respectively. A constant freeze at -17.8˚C resulted in a minor increase in flexural strength. The impact of the number of cycles and the duration of exposure was studied. The deterioration of the FRP composites was more sensitive to the number of cycles than the duration of exposure.

Despite an acceptable, overall performance of GFRP bridge decks, there was evidence that some of the decks had experienced wearing surfaced delimitation problems (O'Connor 2002). Wattanadechachan, et al. (2006) studied the thermal compatibility and durability of the wearing surface of GFRP bridge deck.

The objective of their study was to propose a wearing surface system with improved long-term performance characteristics that bonds well to the GFRP deck and provides the necessary riding skid resistance to traffic load. They investigated four different types of wearing surface materials. These types were polymer concrete, polymer modified concrete, asphalt, and polymer modified asphalt.

Preliminary tests showed that polymer concrete bonded very well to GFRP panel surfaces; however, it had poor wear resistance at elevated temperatures. On the other hand, polymer modified concrete had poor bond strength to GFRP panel surfaces, but it had excellent wear resistance to traffic loads.

They also investigated a hybrid wearing surface system made up of one layer of polymer concrete and one layer of polymer-modified concrete. They concluded that polymer concrete exhibits excellent adhesion to GFRP surfaces under the temperature range investigated (-23º to 60˚C (-10º to 140˚F)). However, polymer-modified concrete and polymer-modified asphalt did not exhibit good adhesion to GFRP surfaces. The asphalt-wearing surface exhibited a very good bond to GFRP panels; however, it exhibited very low stiffness when subjected to high temperatures.

A hybrid-wearing surface exhibited excellent adhesion to GFRP surfaces during all thermal compatibility tests. No delimitation or cracks were observed of the hybrid-wearing surface during the tests that they performed.

2.2.2 Economic Analysis

Nishizaki, et al. (2006) conducted a life cycle cost case study for two pedestrian bridges, one made of all composite materials and the other constructed using pre-stressed precast concrete. The FRP Bridge was built in Okinawa, Japan, in 2,000 and is called Okinawa Road Park Bridge. Three cases of the precast concrete bridge were studied. Case-1 is the base case, which has no protective coating. Case-2 is similar to Case-1, but uses an epoxy resin coated reinforcing bars and tendons. Case-3 is similar to Case-2 with an additional coat of paint on the concrete surface. The initial cost of each case was ¥58.370M, ¥60.750M, and ¥64.500M, respectively. At the time of the study, 1 U.S. dollar equaled approximately 105 Japanese yen ($1=¥105). Two cases of the FRP bridge were considered. Case-4 is the actual bridge that was built, and Case-5 was a modified design suggested by the authors to reduce the cost. In Case-5, the authors used an aluminum handrail instead of FRP rail and modified the design of the joints in the deck. These modifications caused the construction cost of the FRP bridge to be reduced from ¥80.51 M to ¥69,260 M. Since the FRP structure does not corrode, the authors allowed minimum maintenance costs for small-scale repair. For precast concrete bridges, maintenance costs were determined from historical cost data of similar bridges.

The 50-year life cycle costs for Case-1 to Case-5 were ¥100.87M, ¥60.75M, ¥91.5M, ¥90.51M, and ¥72.76M, respectively. The 100-year life cycle costs for Case-1 to Case-5 were ¥127.87M, ¥85.25M, ¥118.5M, ¥100.51M, and ¥76.26M, respectively. The study showed that the lowest 50-year life cycle cost was the concrete bridge with the epoxy resin coated reinforcing bars and pre-stressed strands (Case-2), while the 100-year life cycle cost showed the modified design of the FRP bridge (Case-5) had the lowest cost. The researchers concluded that FRP bridge deck is more efficient when longer life is required in severely corrosive environments.

Meiarashi, et al. (2002) studied the life cycle costs of two highway suspension bridges, one made of conventional steel and another constructed with advanced all-composite carbon fiber reinforced polymer (CFRP). The two bridges studied were 800 m long. They used a sag ratio of 1/10 for the steel suspension bridge and 1/20 for the CFRP bridge. The decks of the FRP bridge and the steel bridge have the same dimensions. The deck of the FRP bridge is made of CFRP rectangular cell boxes. The deck of the steel bridge is trapezoid-shaped stiffening boxes made of steel plates. The main cables and the hanger cables of the FRP bridge are made of carbon fiber cables, while steel strands are used for the steel bridge. The finite element method was used to model the two bridges.

The maximum vertical deflection obtained from the finite element analysis is 2.27 m for the steel bridge and 6.44 m for the CFRP bridge. As expected, the maximum cable tension force was larger for the steel bridge, 68.3 MN as compared to 27.6 MN for the CFRP bridge. Wind speed to generate flutter was 123 m/s for the CFRP bridge and 162 m/s for the steel bridge. The researchers indicated that the FRP bridge has a lower critical flutter speed than the steel bridge because it has less mass; however, they also stated that the critical flutter speed of the FRP bridge is still higher than the design critical speed of 63 m/s.

They used Highway Bridge Specifications (Japan Road Association 1996) as specifications to design the two bridges. They obtained the estimated present and future costs of the CFRP pultrusion product from multiple FRP manufacturers in Japan. The initial construction costs of the steel bridge and the all-composite suspension bridge were calculated. Then, a life-cycle comparative analysis was conducted comparing the all-steel bridge and the all-composite bridge. For the material prices, the life cycle cost analysis did not demonstrate the CFRP bridge to be cost effective over the all-steel bridge; however, under extremely soft ground conditions, the CFRP bridge may offer significant advantages over the steel bridge in reducing the total cost.

The study used CFRP instead of GFRP in the comparison study. CFRP is significantly more expensive than GFRP. If GFRP were used instead of CFRP, the conclusion of the life cycle analysis could have changed.

Constructing the towers and other parts of the suspension bridge using composite materials is extremely expensive. In the design of suspension bridges, while it is important to reduce the dead weight in the deck, there is no economic benefit for reducing the weight of the towers. Typically, horizontal forces rather than vertical forces control the design of the tower and its foundation because the horizontal forces cause tension while the vertical forces cause compression on the towers (Figure 2.5). The weight of the tower will increase the compression and reduce the tension in the towers caused by the horizontal force. Therefore, reducing the weight of tower material may not result in construction cost savings.

The anchorage system must provide significant resistance to the horizontal component of the main cables tension forces as shown in Figure 2.6. The pile cap is usually connected to the towers through a ground link slab to help resist the horizontal force (Figure 2.6). Heavier towers will significantly help resist the horizontal force. Building the towers using composite materials will reduce the dead weight and would not provide the required horizontal force resistance.

The study assumed zero maintenance costs for the composite bridge in their life-cycle cost analysis, while Nishizaki, et al. (2006) considered minimum maintenance costs for the FRP bridge discussed above.

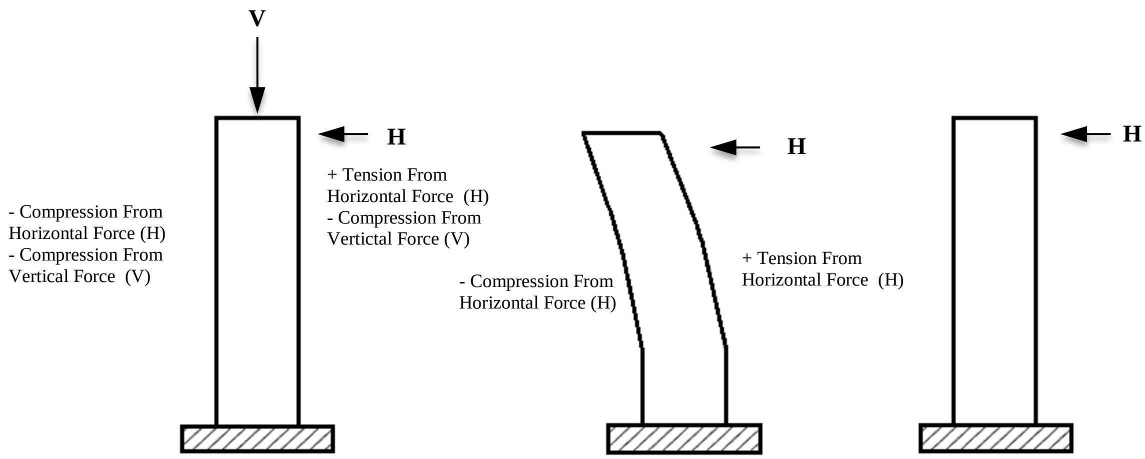

Figure 2.5: Horizontal & Vertical Forces Acting on a Suspension Bridge Pylon

(Shows the dead weight role in stabilizing the horizontal force)

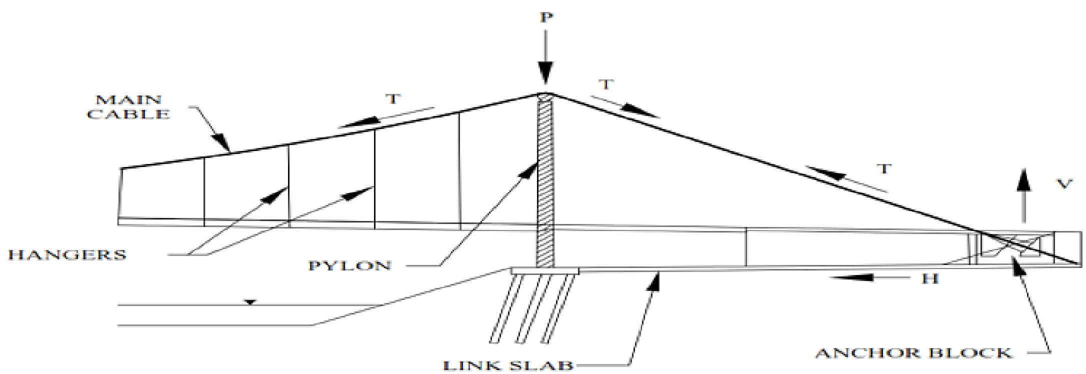

Figure 2.6: Design of the Anchorage System

This proposed research considers the use of FRP composites only for the deck and uses conventional construction materials for all other elements of the bridge—reinforced concrete for the towers and steel strands for the main cables and suspenders. The main objective of this research is to reduce the dead weight of the deck and therefore the cables, hangers and anchorage system.

Eheln (1999) examined life cycle costs for three FRP deck types and compared them to a conventional concrete bridge deck. The three types of FRP deck considered were the Seeman composite resin infusion molding process (SCRIMP), Wood-Core (WC) and Pultruded Plank (PP). The conventional concreted deck used in the analysis is 22 cm (8.5 in.) thick and made of 21 MPa concrete. Reinforcing steel runs both parallel and perpendicular to traffic flow. The variation of prices of each materials is assessed using the Monte Carlo simulations.

The concrete deck and the three FRP decks were designed to satisfy the structure's performance requirements, such as minimum loads, maximum deflections between the support, and minimum service life. The performance requirement of the deck is to be able to carry HS-20 loads, to satisfy L/800 span deflection requirements, and to last a minimum of 40 years. [The authors indicated that the North Carolina Department of Transportation (NCDOT) requires the 40-year life of the deck; the general AASHTO requirement is 75 years]. Initial costs and maintenance costs for the four bridge deck alternatives were obtained from private industry, FRP designers, FRP fabricators, and government agencies, primarily the North Carolina Department of Transportation.

The study considered agency user costs in the life cycle cost analysis. It also considered initial costs; operation, maintenance and repair (OM&R) costs; and disposal costs. The total life cycle cost for the concrete deck, WC, SCHRIMP and PP are $266,305, $267,986, $537,828, and $621,933, respectively. Although the concrete and WC decks have comparable costs ($266,305 vs $267,986), the Monte Carlo simulations indicated that the WC deck is a life cycle cost effective alternative to conventional reinforced concrete (in a probabilistic sense).

Chapter 3 - Research Questions and Approach

This chapter presents the questions addressed in this research and the approach taken to obtain answers to those questions.

3.1 Research Questions

The initial cost of an FRP bridge deck is higher than a conventional deck, such as reinforced concrete or steel deck. However, its lower weight will lead to smaller hangers, cables, and towers, as well as less anchorage. Since FRP materials are more corrosion resistant, FRP bridge deck is expected to be more cost effective in a life cycle analysis than traditional materials. As previous life cycle cost studies indicate, the initial construction cost of an FRP bridge is higher than a conventional bridge; however, FRP bridges could be cost effective in the long term. The hypothesis of this research (in contrast with the previous studies) is that a suspension bridge with an FRP deck will have a lower initial construction cost than a conventional suspension bridge. This discussion leads to the first question:

1. Would suspension bridges with span ranges from 200 m to 600 m free span constructed from FRP deck be cost effective as compared to those constructed with reinforced concrete deck?

    1.1. How do the costs of suspension bridges (200 m to 600 m free span) constructed with an FRP deck compare to those constructed with a concrete deck?

    1.2. How would the variation of soil conditions impact the comparative economic analysis of suspension bridges (200 m to 600 m free span) constructed from an FRP deck and those constructed from a concrete deck?

Using a lightweight deck for a suspension bridge may affect the aerodynamic stability of the bridge. This leads to the second question:

2. How would the suspension bridges discussed in questions 1.1 and 1.2 above behave aerodynamically?

3.2 Approach

This section describes the approach to research questions 1 and 2 of Section 3.1.

Suspension bridges are usually economical for spans in excess of 1,000 ft. (~300 m), yet many suspension bridges with spans as short as 400 ft. (~130 m) were built to take advantage of their aesthetic features.

Although not closely defined, suspension bridges with spans between 300 m to 600 m are designated as moderate span suspension bridges (Structural Steel Designer Handbook, 2006). This study has focused on short and medium span suspension bridges with free spans between 200 m and 600 m. Composite concrete deck on steel floor girders is the least expensive deck type. Steel built-up sections (steel plate girders) cost between $2,500/ton to $3,500/ton as compared to steel plate box deck that costs between $9,000/ton to $12,000/ton.

A concrete deck is generally comprised of a slab with a thickness between 200 mm and 300 mm supported by stringers or floor beams spaced at 3,000 – 5,000 mm. The main advantage of the concrete slab is the low cost of the slab itself. On the other hand, the greater weight of the concrete slab requires a greater cross section of cables, hangers, towers and anchorage systems. Reduction of the deck weight can be obtained by using FRP bridge deck. A typical 200 mm FRP bridge deck weighs about 1 kPa (25 psf), while a concrete deck spanning the same distance as the FRP deck weighs 5.7 kPa (119 psf) (www.fhwa.dot.gov).

To answer question 1.1, a parametric study of suspension bridges with free spans between 200 m to 600 m was performed. Three suspension bridges with span lengths of 200 m, 400 m, and 600 m were designed with a reinforced concrete deck supported by steel plate girders as stiffening girders and steel floor beam (Figures 3.1, 3.2, and 3.3). Another group of suspension bridges with similar span lengths were designed using FRP deck material. Soil conditions will affect the design of the anchorage systems. To answer question 1.2, three different types of soils were considered in the design of the concrete and FRP bridge models.

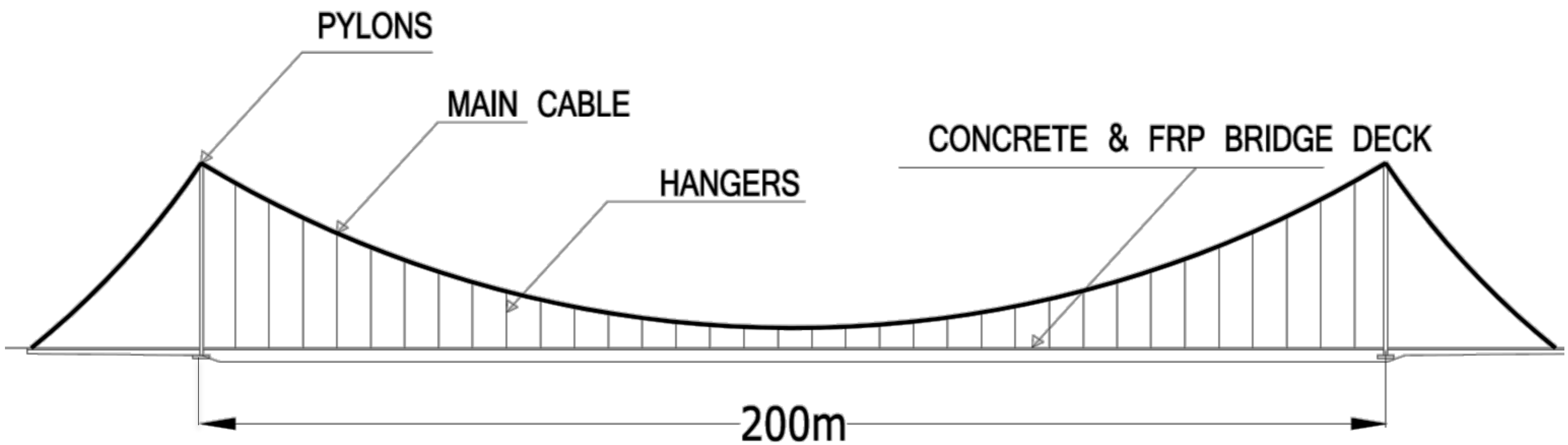

Figure 3.1: Suspension Bridge with 200 m Free Span

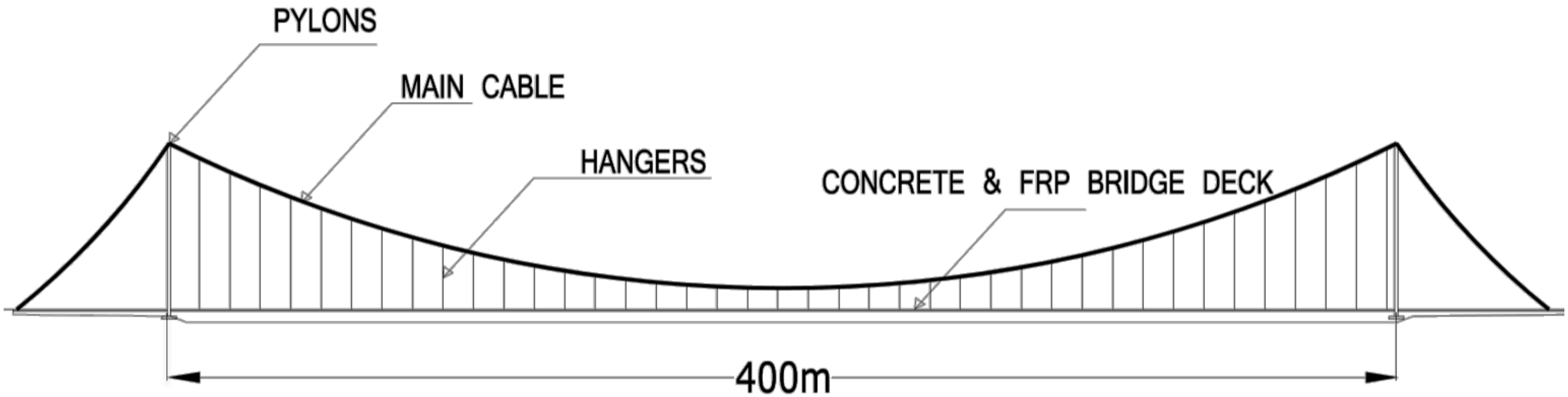

Figure 3.2: Suspension Bridge with 400 m Free Span

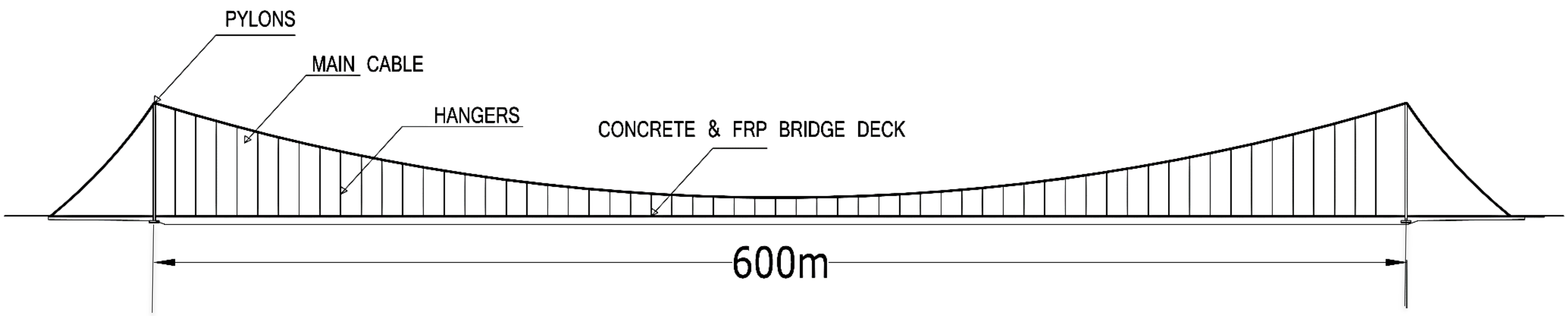

Figure 3.3: Suspension Bridge with 600 m Free Span

3.2.1 Design Philosophy

This section describes the design philosophy for all the bridge models discussed in Section 3.1. The deck system will consist of longitudinal girders and cross-girders supporting a reinforced concrete or an FRP deck. The deck will be designed to span between the cross-girders. Currently, reinforced concrete decks are designed using the limit-states principle to ensure sufficient strength against bending. A serviceability limit state such as deflection is examined after strength requirements are satisfied.

Although serviceability criteria are usually examined after strength design is performed, the lower elastic modulus for FRP causes serviceability to control the design. Suspension bridges with an FRP deck will have lower cable tension forces and therefore smaller anchorage systems than those with a concrete deck. This fact is particularly important in weak soil conditions where massive anchorage systems will be required for the concrete deck option. To study the impact of soils on the comparative economic analysis, three types of ground conditions will be considered for each bridge. The anchorage systems and the pylon foundations will be designed using three different soil characteristics.

3.2.2 Codes and Standards

Optimum design was performed in accordance with AASHTO LRFD Bridge Design Specifications, Fifth Edition 2010. The Euro code EN 1993-1-11 will be used for the design of the hangers and main cables.

3.2.3 Material Properties

Material properties of commercially available GFRP bridge deck vary for different bridge deck types. Material properties such as Young Modulus and strength depend on the amount of the fiber. Table 3.1 shows average values of material properties of adhesively bonded pultruded type (Kim, 2004). For the main cables and hangers, parallel wire strands were used in accordance to ASTM A421. For longitudinal girders and cross-girders, ASTM steel grade 50 was used with yield strength of 345 MPa.

Table 3.1: Material Properties

Materials	**Unit**	**Concrete-30**	**GFRP**	**Steel**	**Strands**	
Elements		Deck Case-1	Deck Case-2	Girders	Main Cables	Hangers
Density	kN/m³	25	-	78	78	78
Weight	kN/m²	5	1.2	-	-	-
Elastic modulus	GPa	23	25	205	197	197
Poisson's ratio		0.2	0.25	0.3	0.3	0.3

3.2.4 Design of the Towers, Anchorage, and Foundation

The pylon (tower) material selected for all of the suspension bridge models is concrete. Concrete is cost-effective material for towers measuring up to 250 m in height. Pylon dimensions and stiffness were selected during the design iterative process to obtain an optimum design that meets the deflection criteria. Then the design of each pylon was checked against the compressive force exerted on the pylon from the cable and the self-weight of the pylon itself. A minimum tower dimension of 2 m x 2.5 m was adopted for the concrete deck case to provide working area around the saddles on top of the towers. For the FRP case, the design dimensions of 2 m x 1.65 m were considered sufficient to provide the required space because the saddles for the FRP case are smaller than those for the concrete case. To simplify the pylon design process, stresses resulting from wind and other out-of-plane forces are subtracted from the allowable compressive stress of the tower material is used. A typical allowable stresses of 60% to 80% of the concrete allowable compressive stresses were used for the design of the towers (Gimsing, 1997). The reduction in the allowable stresses is to allow for wind forces and other forces that are acting on the towers but not considered in the design. An average value of 70% of the allowable compressive stresses of the concrete was used in this analysis for the design of the towers under axial forces only. Figure 3.4 shows the horizontal and vertical components of the main cables tension that were used in the tower design.

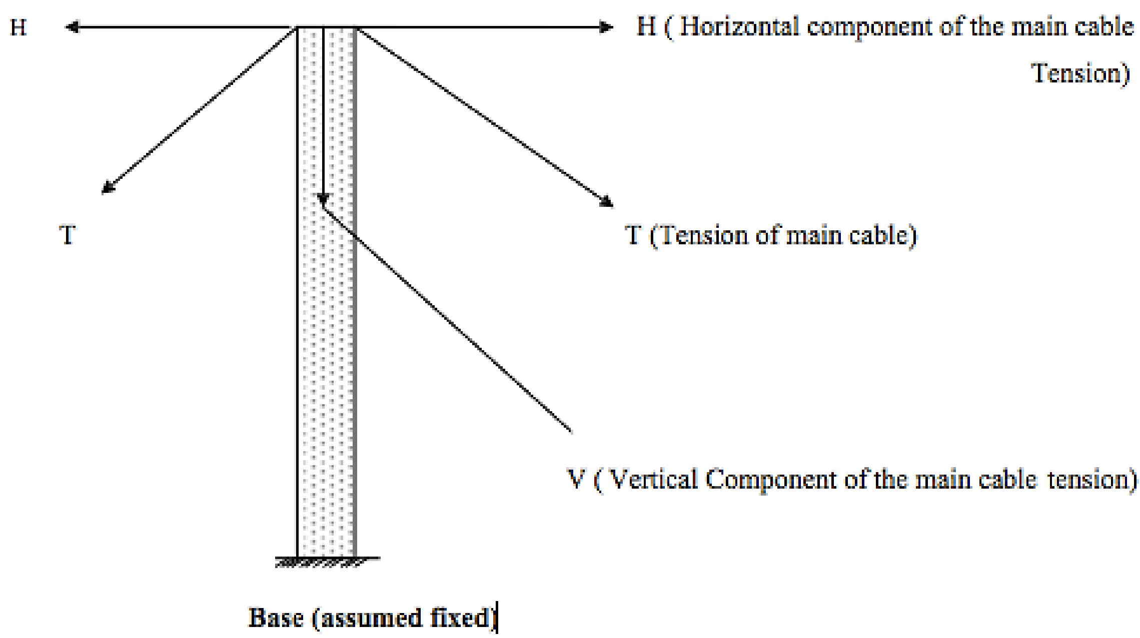

Figure 3.4: Cable Forces Acting on Pylon

This reduction is used to allow for the effects of other loads, such as wind and the horizontal force component exerted by the main cables tension forces.

3.2.5 Design of the Anchorage System

Concrete gravity anchorage was selected for the anchorage system for all of the models. Figure 3.5 shows the forces acting on the anchorage block. The main cables tension forces is analyzed into a horizontal component force resisted by the soil anchorage block friction. The other component of the main cables tension is the vertical component, which produces uplift of the concrete block and is resisted by the weight of the concrete block. The design of the anchorage system is controlled by the friction interaction between the concrete block and the soil and the horizontal component of the main cable tension force. In addition, the bearing capacity of the soil will influence the geometry of the anchorage block. For this comparative analysis, the cost of the anchorage block is calculated based on the amount of concrete required to resist the horizontal component of the cable tension forces.

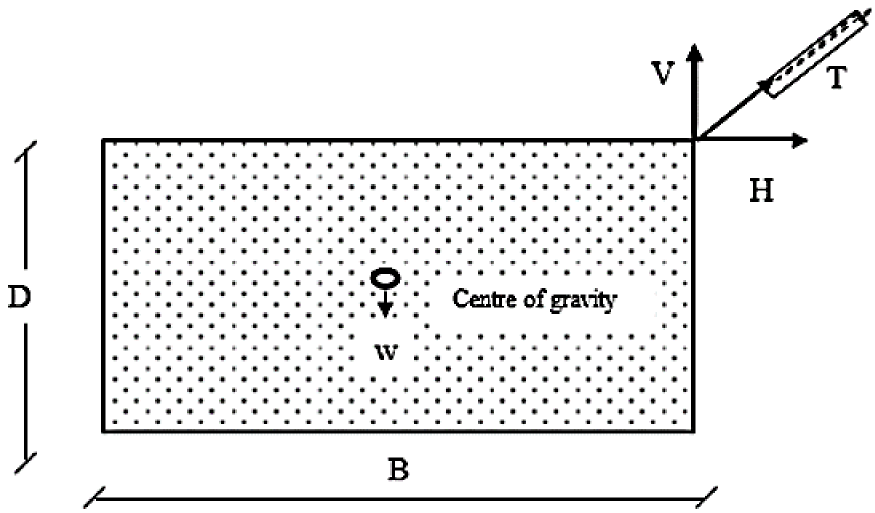

Figure 3.5: Forces Acting on the Concrete Anchorage Block

To determine the dimensions of the anchorage block, the weight of the block can be determined by equation 3.1. Equation 3.2 and 3.3 defines the relationship between the vertical force, *V*, and the horizontal component of the main cables tension, *H*.

D = Anchorage concrete block depth

B = Anchorage concrete block width

$$R_H = \mu R_V \tag{3.1}$$

$$W = V + R_v \tag{3.2}$$

$$= V + H/\mu \tag{3.3}$$

Where

V = Vertical component cable tension force

H = Horizontal component of cable for tension

μ = Coefficient of function between soil and the concrete block

R_H = Horizontal soil reaction on concrete block

R_V = Vertical soil reaction on concrete block

The use of a lighter deck will reduce the cable tension and the anchorage block. Such reduction in the cable tension force is much needed in weak soils. To study the impact of the soil conditions on using FRP deck, three types of soil were considered for each model. Sound rock, medium sand, and stiff clay were considered for each model.

The coefficient of friction of each soil type is listed in Table 3.2, obtained from Department of the Navy, Naval Facilities Engineering Command, Foundation and Earth Structures Design Manual, Alexandria, VA (1982). The allowable bearing capacities were obtained from U.S. Army Corps of Engineers, Engineer Manual 1110-1-1905, Washington, DC (1992).

Table 3.2: Soil Properties of Three Soil Types

	Coefficient of Friction	Allowable Bearing Capacities ksf, (kPa)
Sound rock	0.70	90, (4320)
Medium sand	0.50	4.7, (226)
Stiff clay	0.40	4.3, (206)

The value of the coefficient of friction for medium sand is an average of the range given in the Department of the Navy design manual (1982) of 0.45 - 0.55. The value used for stiff clay was an average of 0.3 - 0.5.

The allowable bearing capacity for rock is an average of three values of 8,000 kPa, 2,880 kPa, and 1,920 kPa. The allowable bearing capacity for medium sand is an average of 288 kPa, 240 kPa, and 144 kPa; for clay, it is an average of 384 kPa, 192 kPa, and 48 kPa.

3.2.6 Aerodynamic Stability

3.2.6.1 Effect of Mass on the Aerodynamic Behavior of Suspension Bridges

Not only the mass but also the distribution of the mass of the structure determines the aerodynamic stability of the structure. The following is a detailed explanation of the mass effect on the aerodynamic behavior of suspension bridges.

The following is referencing Gimsing's (1997) equations.

Consider the simple model of Figure 3.6 showing a symmetric mass, G, supported by two springs each with a spring constant C.

For the vertical oscillation, the natural frequency is determined by:

$$n_v = \frac{C}{G} \tag{3.4}$$

Whereas the frequency n_t of the torsional oscillation becomes:

$$n_t = \frac{C_t}{I_m} \tag{3.5}$$

I_m is the mass moment of inertia. With the mass concentrated in the cable planes, as shown in Figure 3.7, the mass moment of inertia becomes:

$$I_m = \frac{G\ b^2}{4} \tag{3.6}$$

This leads to a torsional frequency equal to:

$$n_t = \frac{2C}{G} \tag{3.7}$$

With the mass distributed across the width b, as indicated in Figure 3.8, the mass moment of inertia becomes:

$$I_m = \frac{Gb^2}{12} \tag{3.8}$$

With the frequency of the torsional model becomes:

$$n_t = \frac{6C}{G} \tag{3.9}$$

In this case, the ratio between the torsional and the vertical frequency will be:

$$\frac{n_t}{n_v} = \sqrt{3} \tag{3.10}$$

In a real structure, the mass distribution will be similar to Figure 3.8, somewhere between the extremes of Figure 3.6 and Figure 3.7. The main girders or main trusses directly below the cable planes will have a mass distribution according to Figure 3.6, whereas the bridge deck and the floor beams will have a mass distribution according to Figure 3.7.

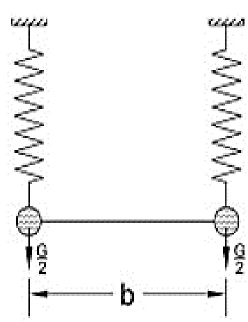

Figure 3.6: Dynamic Model with Two Masses Concentrated at the Supporting Springs

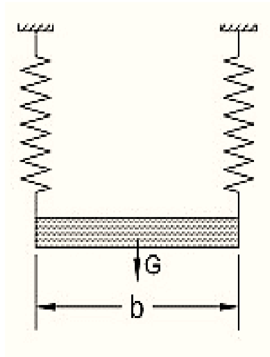

Figure 3.7: Dynamic Model with a Symmetric Mass Uniformly Distributed between the Two Supporting Springs

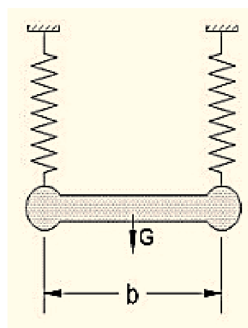

Figure 3.8: Dynamic Model Comprising a Symmetric Mass Supported By Two Springs

It can be concluded from the preceding analysis that deck mass is one factor that influences the aerodynamic stability of a bridge. The distribution of the deck mass and its relationship with the mass of the main girders and the main cables is another factor that influences the aerodynamic stability of suspension bridges.

A lighter deck, such as an FRP deck, will lead to smaller main girders and main cables. The relationship between the mass of the main girders and main cables with the mass of the FRP deck itself will determine the aerodynamic stability of FRP suspension bridges.

3.2.6.2 Calculations of Flutter Speed

To answer question 2, flutter speed will be computed for each structure. To compare the aerodynamic behavior of each structure, a three-dimensional finite element analysis was performed to obtain the dynamic parameters, such as the torsional and vertical frequencies of each structure. Selberg's equations to predict flutter speed were used. This equation agrees reasonably well with the test results when it is used for streamlined decks. For bluff shape decks, a factor of 0.43 is recommended for use (Gimsing, 1997). The equation to compute critical flutter speed v_f is:

$$v_f = 0.52 v_d \sqrt{\left[1 - \left(\frac{n_v}{n_t}\right)^2\right] b \sqrt{\frac{m}{I_m}}} \qquad \textbf{(3.11)} \text{ [Selberg 1961]}$$

Where,

$$v_d = \text{Divergence speed} = \frac{2}{b}\sqrt{\frac{c_t}{\pi p}} \qquad \textbf{(3.12)}$$

n_t = Torsional frequency

n_v = Vertical frequency

c_t = Torsional spring constant

I_m = Mass moment of inertia

m = Mass

To compute the critical flutter speed using Selberg's formula, the torsional frequency, vertical frequency, and mass moment of inertia need to be computed. Two methods were utilized to compute the aerodynamic parameters such as torsional and vertical frequencies. One method is to obtain the value of the torsional and vertical frequencies and moment of inertia from the Finite Element Model (FEM). The other method is to use the spring constants approach presented by Viana, (2005).

For I-steel plate girders supporting a concrete or an FRP deck a factor of .43 is used to count for the bluff body negative influence in the aerodynamic stability. The flutter speed calculated in equation 3.11 is for streamed-lined shape deck. For a bluff body, a reduction factor should be applied.

Chapter 4 - Design Procedure for the Base Model 200 m Span Suspension Bridge with Concrete and FRP Decks

This chapter describes the design process that was performed for all the bridges. In addition, it provides detailed design calculations for two 200 m span suspension bridges. One bridge was designed with a concrete deck; the other bridge was designed with an FRP deck.

4.1 General Design Procedure

A 200 m suspension bridge was designed and analyzed for a concrete deck and an FRP deck. Initially, a panel consisting of longitudinal girders and cross-girders was designed using AASHTO design criteria. The panel is assumed to span between the hangers and be simply supported by the hangers. It is a conservative assumption, but it is reasonable to get initial sizes to use in the finite element model (FEM) as shown in Figure 4.1.

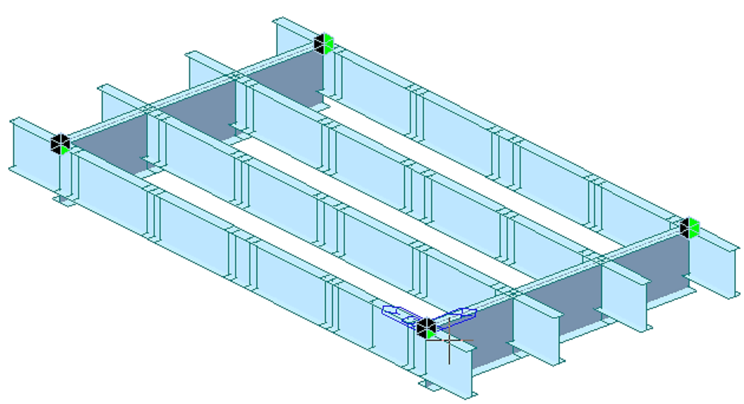

Figure 4.1: Typical Deck Panel between Hangers (FEA Model)

To obtain optimum design of the concrete deck, a composite action with the steel girders is considered (Figure 4.2 and Figure 4.3). Zihong Liu studied composite action of FRP deck on steel girders (2007). His study concluded that composite action between FRP decks and steel girders should not be considered in the design. Therefore, all of the FRP models were considered as non-composite decks (Figure 4.4).

Non-composite decks will result in a conservative design and heavier steel floor girders. However, heavier steel girders will improve the overall aerodynamic stability of the bridge.

After a typical panel was designed for concrete and FRP decks, the main cables size and hangers were designed. The tension in the main cables was calculated using the linear elastic method (Podolny, 2006).

T = Tension in the main cables = H/cosα **(4.1)**

Where,

H = Horizontal tension in main cables = w L^2/8d **(4.2)**

α = Angle of cable inclination at anchor points

(w) = (Live + Dead) Load per each cable/m

L = Span of the bridge = 200 m

d = Cable sag -10% of the span length = 20 m

After obtaining preliminary sizes of the main cables, hangers, and floor beams, three-dimensional finite element non-linear analysis was performed for each model. The MIDAS-Civil structural analysis was utilized for the design and analysis of each bridge.

MIDAS-Civil performed completed state analysis, which include the initial equilibrium state analysis and the final state analysis. At the initial equilibrium state, the structure is in a balanced condition under self-weight, and the deflection due to the self-weight has already occurred. This stage is referred to as the initial equilibrium state of the suspension bridge. The initial equilibrium state analysis provides the coordinates and tension forces in the main cables and hangers due to self-weight. The tension forces in the main cables and hangers obtained from initial equilibrium state analysis were converted into increased geometric stiffness of these components. Then, the completed state analysis of the suspension bridge was performed to check the behavior of the structure with the modified stiffness's under additional loads, such as live and wind loads. Complete description of the MIDAS-Civil software analysis procedure along with initial forces in the hangers and main cables are given in Appendix III.

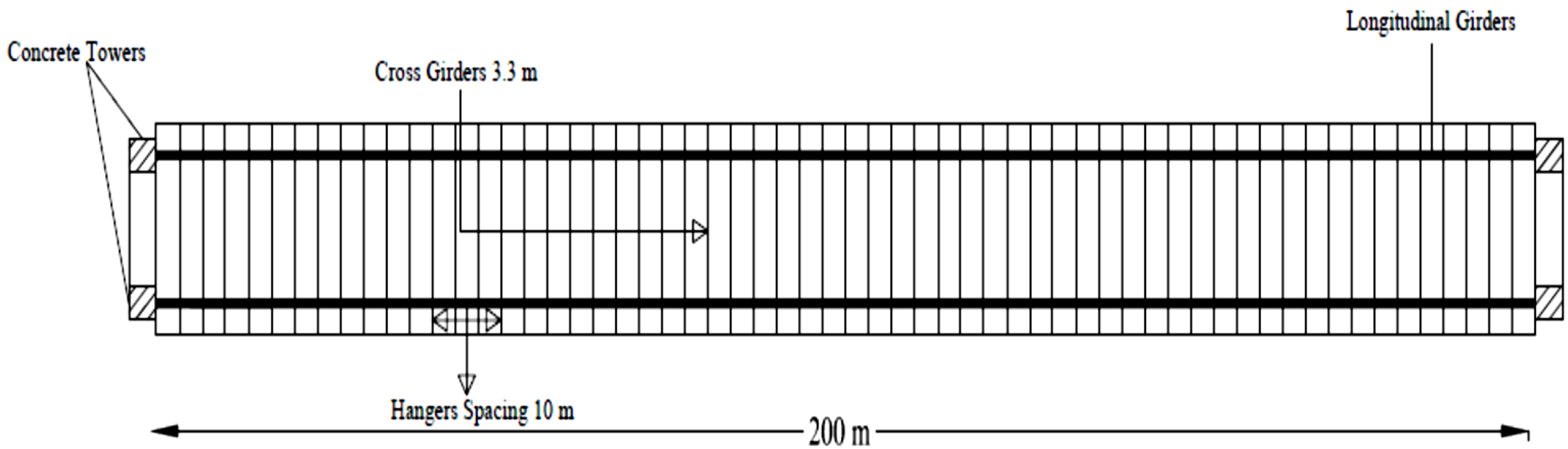

Figure 4.2: Plan (Concrete Deck)

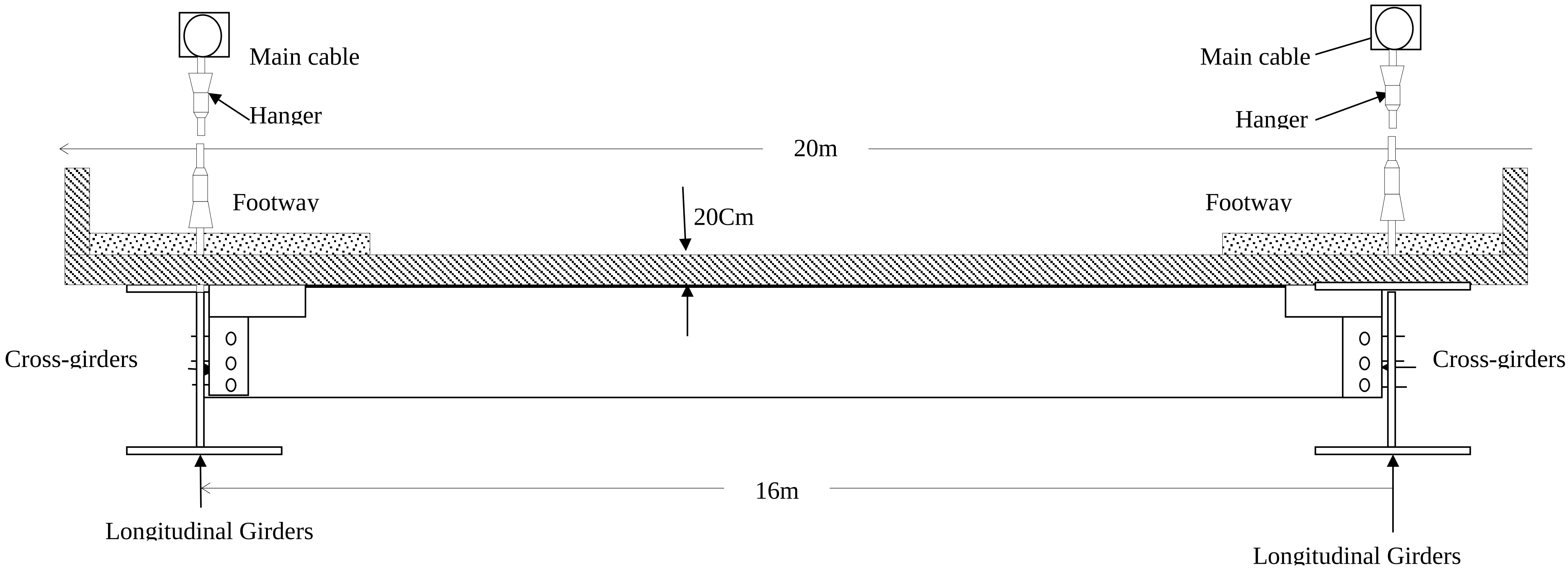

Figure 4.3: Section (Concrete Deck)

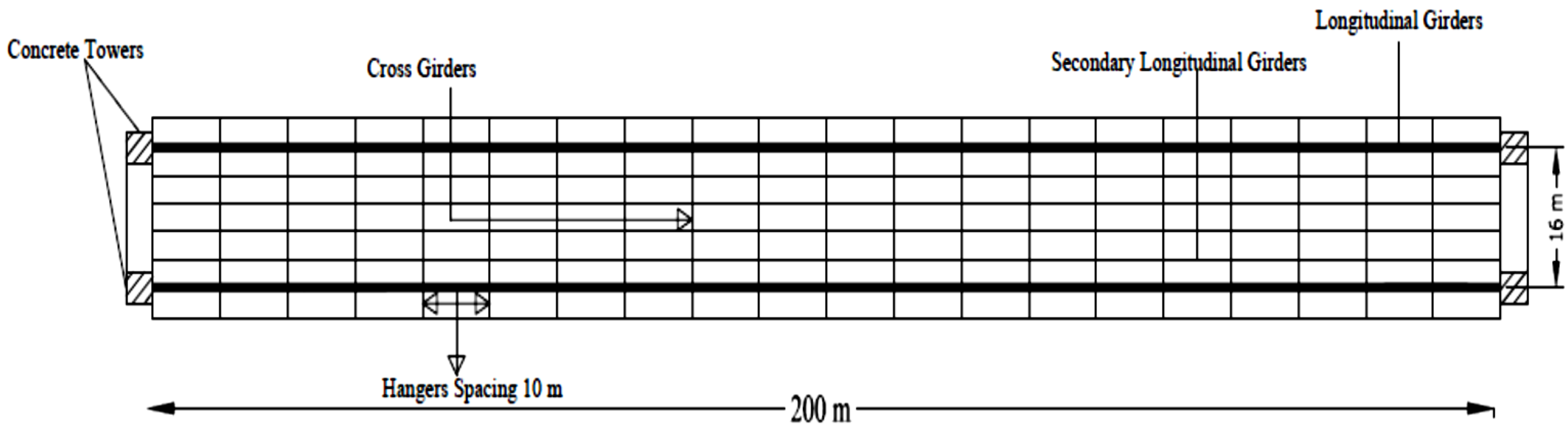

Figure 4.4: Plan (FRP Deck)

4.2 Boundary Conditions

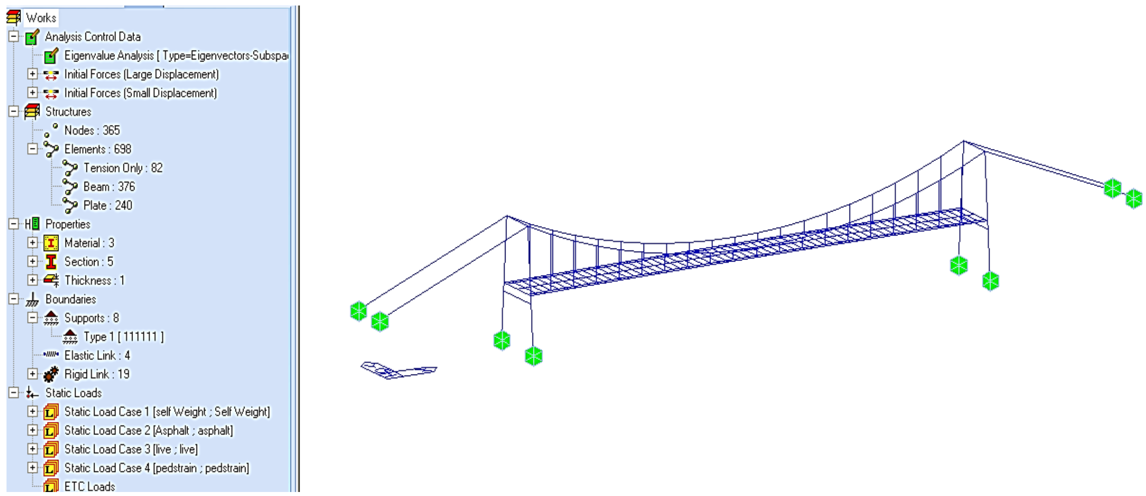

Figure 4.5: Boundary Conditions

The connections between the towers and deck are modeled as fixed joints at one-end and expansion joints at the other end as shown in Figure 4.5. The expansion joint allows the longitudinal movement of the deck due to thermal expansion and contraction.

At the fixed end, bearing rotations were allowed while displacements were not allowed in all directions. At the expansion end, bearing rotations were allowed in all directions while displacements were only allowed in the longitudinal direction.

4.3 Results of the Finite Element Analysis

The results of the three-dimensional finite element non-linear analysis were checked against a linear elastic analysis to compare the results of the tension on the hangers and main cable.

The maximum deflection under traffic loads (using AASTHO lane loads and 25% of truck loads) is limited to L/300 for all models (Podolny, 2006) and (Vickneswaran, 2011). Several design iterations were performed to comply with the deflection limits of L/300.

Several adjustments of the size of the longitudinal girders, hangers, main cables, and tower stiffness were performed to achieve the L/300 deflection limit. Through several runs of various finite element models and by adjusting the design of each structural component, the design of each model with a concrete and an FRP deck was achieved. Three finite element models of the 200 m suspension bridges with concrete decks were analyzed with three different cable sizes to achieve the minimum cable size that meets the deflection criteria (Table 4.1 and Table 4.2).

Three additional models for the concrete deck case with three different tower sizes were analyzed to study the effect of the tower size in the live load deflection. Three finite elements models were performed of the 200 m suspension bridges with FRP decks using three different cable sizes to meet the deflection criteria, L/300. Three additional models for the FRP deck case with three different tower sizes were analyzed to study the effect of the tower size in the live load deflection. When performing the finite element analysis, it was realized that the size of the main cables has the largest influence on the live load deflection of the bridge. The stiffness of the deck has also influenced the live load deflection. The stiffness of the tower has less influence on live load deflection.

The first trial used the following sizes of the bridge components

- Steel cross sections for the main girder and cross-girder as shown in Figure 4.6 and Figure 4.7.

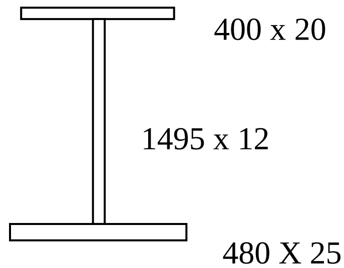

Figure 4.6: Section of the Cross-girder

(All dimensions are in mm)

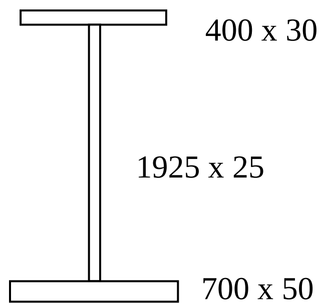

Figure 4.7: Section of the Main Girder

(All dimensions are in mm)

- Hanger cable diameter: two 60 mm diameter strands with equivalent diameter of 0.0848 m.

- Tower size: (2.5 m x 2.0 m).

The three models have common bridge elements with the same dimensions for each model. They are listed in Table 4.1.

Table 4.1: Element Dimensions Used for All Bridge Models

Item	Unit	Dimensions
Girder (top flange)	mm	400 x 30
Girder (web)	mm	1925 x 25
Girder (bottom flange)	mm	700 x 50
Cross-beam (top flange)	mm	400 x 20
Cross-beam (web)	mm	1495 x 12
Cross-beam (bottom flange)	mm	480 x 25
Main tower	m	2 x 2.5
Hanger diameter	m	0.0848
Strand main cable	m	0.07

Three finite element models were created and analyzed of the 200 m span bridge with a concrete deck using three different main cables sizes. The other element dimensions used were presented in Table 4.1. The results are tabulated in Table 4.2.

Table 4.2: Live Load Deflection for Concrete Case

Item	**Unit**	**Model 1**	**Model 2**	**Model 3**
Number of strands	No.	12	14	16
Equivalent main cable diameter	m	0.221	0.242	0.262
Live load deflection	m	0.49	0.45	0.38

Selected model for the concrete bridge

Live load deflection

Three other trials were performed to study the tower size effect on the live load deflection:

- Hanger cable equivalent diameter: 2 cables with a diameter of 60 mm; equivalent diameter = 0.0848 m;
- Main cables equivalent diameter: 16 cables with a diameter of 0.07 m; equivalent diameter = 0.262 m; and
- The tower size was changed as shown in Table 4.3:

Table 4.3: Design Models for Different Tower Sizes of the 200 m Span Bridge with a Concrete Deck

Model Number		Model 1	Model 2	Model 3
Tower size	m^2	1.5 x 2	1.75 x 2.25	2 x 2.5
Live load deflection	m	0.56	0.47	0.38

Selected model for the concrete bridge

A smaller size tower could have been used to achieve the deflection limit of L/300, but the design adopted minimum tower dimensions of 2 x 2.5. This dimension is considered as the minimum area needed to provide construction space for the placement of saddles on top of each tower.

Three finite element models were performed for the FRP deck with three different cable sizes to study the effect of the main cables size and deck stiffness on live load deflection. The cable size was increased beyond the size required for tension to control the deflection. Two other trials were made to control the deflection by increasing the depths of main girder web as shown in Figure 4.8 and Figure 4.9.

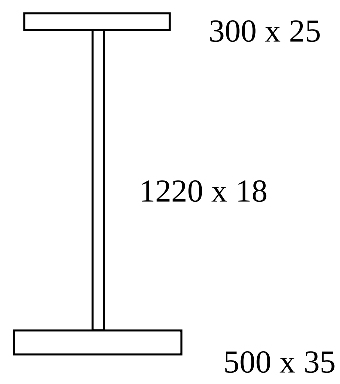

Figure 4.8: Main Girder Section

(All dimensions are in mm)

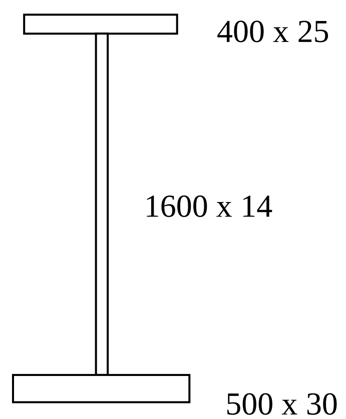

Figure 4.9: Modified Main Girder Section

(All dimensions are in mm)

The three models have common bridge elements with the same dimensions for each model. They are listed in Table 4.4.

Table 4.4: Element Dimensions for all FRP models

Item	Unit	Dimensions
Girder (top flange)	mm	400 x 25
Girder (web)	mm	1600 x 14
Girder (bottom flange)	mm	500 x 35
Cross-beam (top flange)	mm	220 x 12
Cross-beam (web)	mm	800 x 10
Cross-beam (bottom flange)	mm	250 x 14
Main tower	m	2.0 x 1.65
Hanger diameter	m	0.0636
Strand main cable	m	0.06

The details of the finite element model results with the three different cable size for the FRP deck are shown in Table 4.5.

Table 4.5: Live Load Deflection for the FRP Case

Item	Units	Model 1	Model 2	Model 3
Number of strands	No	6	8	10
Equivalent main cable diameter	m	0.146	0.169	0.189
Live load deflection	m	1.07	0.85	0.63

(yellow)	Selected model for the FRP bridge
(orange)	Live load deflection

4.4 Design Data and Results of the 200 m Free Span Suspension Bridge

This section presents the design process, data, and results of a 200 m suspension bridge with a concrete deck and an FRP deck. The detailed design of the decks are shown in Appendix II.

4.4.1 Bridge Geometry

A 200 m free span suspension bridge was designed using concrete deck and FRP deck. The bridge consists of two longitudinal girders and cross-girders supporting a concrete deck or FRP deck.

The details of the bridge geometry are summarized as shown in Table 4.6.

Table 4.6: Geometry of the Two Cases

Geometry	Unit	200 m main span with a concrete deck on steel girders	200 m main span with an FRP deck on steel girders
Main span length	m	200	200
Sag ratio	-	0.1	0.1
Sag height	m	20	20
Tower height above DL (Deck level)	m	25	25
Tower height below DL	m	20	20
Total tower height	m	45	45
Spacing of hangers at main span	m	10	10

4.4.2 Design of the Main Cables of the 200 m Span Bridge with a Concrete Deck

Two methods were used for the design of the main cable: the linear elastic method and three-dimensional finite element non-linear analysis. The linear elastic approach for the design of the main cables is summarized in Table 4.7.

Table 4.7: Linear Elastic Approach for the Design of the Main Cables of the Concrete Deck

Item	Unfactored loads	Factored loads	Unit	Difference (%)
Load from concrete slab	20,000	25,000	kN	25%
Up-stand parapets	300	375	kN	25%
Loads from steel girders	5,673	7,091	kN	25%
Asphalt wearing surface	5,520	6,900	kN	25%
Central reservation	250	313	kN	25%
Main cables self-weight	2,900	3,625	kN	25%
Hangers self-weight	86	108	kN	25%
Live loads	3,673	4,959	kN	35%

Item	Unfactored loads	Factored loads	Unit	Difference (%)
Total loads (W)	38,402	48,370	kN	26%
Load per each cable = Total load /2	19,201	24,185	kN	26%
Load intensity (w) = Load per each cable /Span	96	121	kN/m	26%
Horizontal tension in main cables H = w L2/8d	24,001	30,143	kN	26%
T = Tension in the main cables = H/cosα, $\alpha=31.5^{o}$	28,149	35,354	kN	26%

Using the linear elastic approach, the maximum main cables tension was found to be 35,354 kN.

From the software (MIDAS-Civil) generated results, the maximum factored tension in the main cables is 31,040.00 kN, as shown in Figure 4.10.

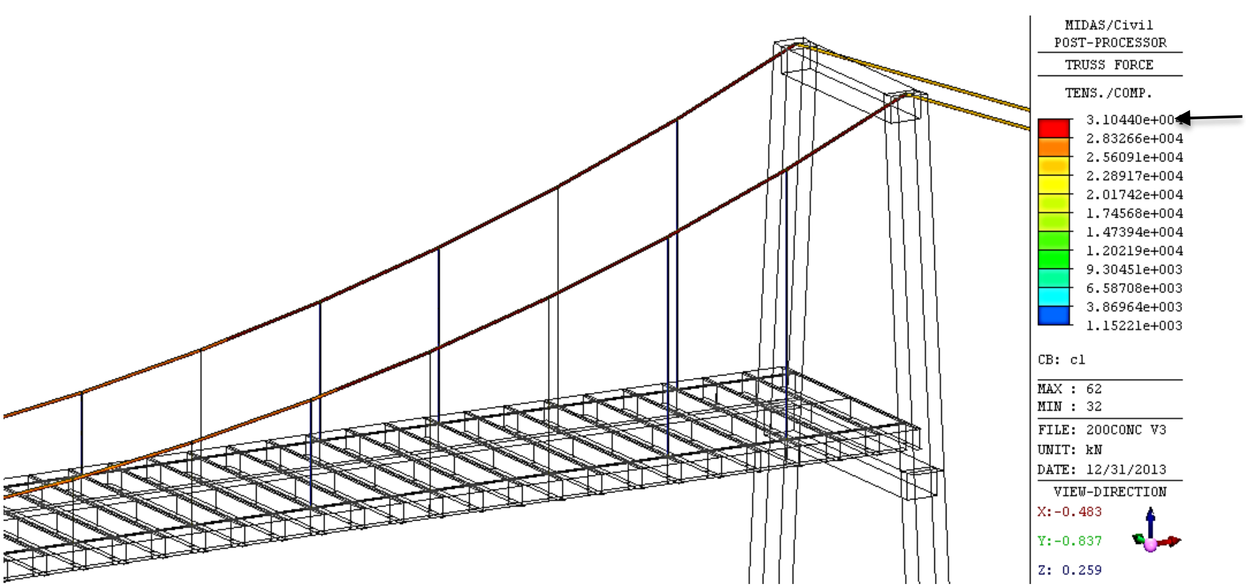

Figure 4.10: Tension in the Main Cables of the 200 m Span Bridge with a Concrete Deck

The higher value of the main cables tension of 35,354 kN was obtained from the linear elastic theory and was used for the design of the main cable. F_u is the characteristic tension force for 70 mm spiral strands and is equal to 4,700 kN. The calculations for the size of the main cables are summarized as shown in Table 4.8.

Table 4.8: Calculations for the Size of the Main Cables of the Concrete Deck

Item	Quantities	Value	Unit
F_u		4700	kN
F_d	4700/1.5	3133.33	kN
Number of strands		14	
The overall capacity of 14 strands	4700 x 14	65,800	kN
Factor of Safety	65,800/28,149	2.3	

4.4.3 Design of the Hangers of the 200 m Span Bridge with a Concrete Deck

Tension in the hangers from the three-dimensional finite element analysis is 1,357.00 kN. Two 60 mm diameter strands per hanger were selected for the design of the hangers. The ultimate strength of the strands, F_u, is 1,957 kN and the design strength, F_d, is 1,778.67 kN for each hanger. The design force of 1,778.67 kN is more than the applied force of 1,357.00 kN and thus the design is adequate.

4.4.4 Live Load Deflection Calculations of the 200 m Span with a Concrete Deck

Live load deflection was calculated in accordance to clause 3.6.1.3.2 of AASHTO—2012. Live load deflection was calculated for the HS-25 truck. Front and rear axle loads for HS-25 were calculated by increasing HS-20 axle loads by 25%. HS-20 truck load is shown in Figure 4.11 and HS-20 truck configuration is shown in Figure 4.12.

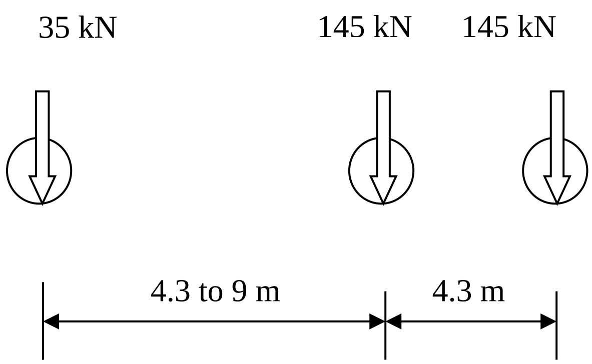

Figure 4.11: HS-20 Truck

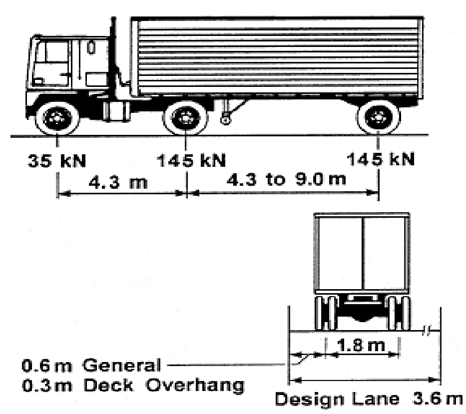

Figure 4.12: HS-20 Truck Load Configuration

(Adopted from AASHTO 2012)

Lane load was applied to the bridge using four lanes with a multiple presence factor of 0.65 in accordance to AASHTO specifications. The deflection was calculated for asymmetric load cases (for multiple positions of the design truck). The load was applied to produce the maximum deflection as shown in Figure 4.13.

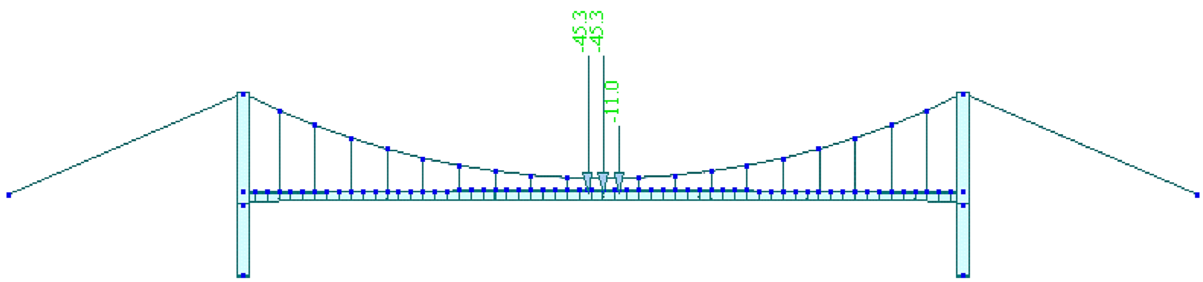

Figure 4.13: Live Load Application on the Bridge Model

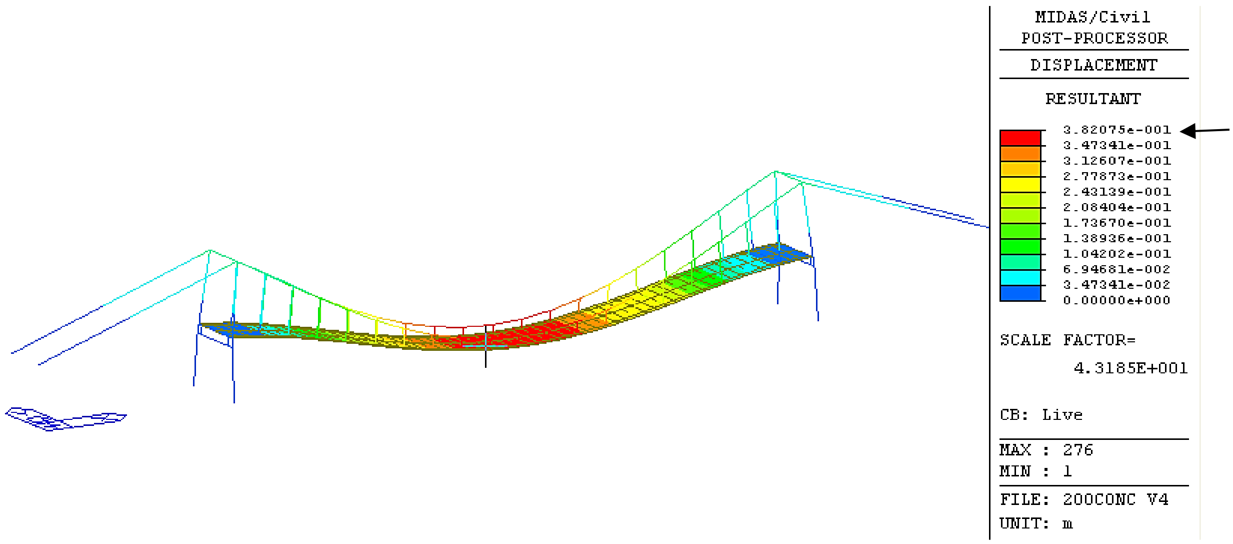

Figure 4.14: Live Load Deflection of the 200 m Span Bridge with a Concrete Deck (0.38 m)

The maximum live load deflection computed by the finite element analysis is 0.38 m as shown in Figure 4.14. The maximum deflection is within the limit of L/300 (0.67 m). For simplicity of the design process and for this comparative study, the longitudinal girder was designed as a constant steel section throughout the length of the bridge. Table 4.9 summarizes the quantities of steel and cables for the concrete deck.

Table 4.9: Summary of Steel and Cable Weight for the Concrete Deck

Item	**Quantity (ton)**
Steel	567.3
Main Cable	178
Hangers	8.7

4.4.5 Design of the 200 m Free Span Suspension Bridge with an FRP Deck

The 200 m span suspension bridge with an FRP deck on steel girders was designed in a similar fashion to the 200 m span bridge with a concrete deck.

4.4.6 Design of the Main Cables of the 200 m Span Bridge with an FRP Deck

The linear elastic approach for the design of the main cables is summarized in Table 4.10.

Table 4.10: Linear Elastic Approach for the Design of the Main Cables of the FRP Deck

Item	Unfactored loads	Factored loads	Unit	Difference (%)
Deck weight (FRP)	4,800	6,000	kN	25%
Up-stand parapets	300	375	kN	25%
Loads from steel girders	2,963	3,704	kN	25%
Main cables self-weight	1,522	1,903	kN	25%
Hangers self-weight	48	60	kN	25%
Live loads	3,673	4,959	kN	35%
Total loads (W)	13,306	17,000	kN	28%
Load per each cable = total load/2	6,653	8,500	kN	28%
Load intensity (w) = load per each cable/span	33	42	kN/m	29%
Horizontal tension in main cables H = w L2/8d	8,316	10,666	kN	28%

Item	Unfactored loads	Factored loads	Unit	Difference (%)
T = tension in the main cables = H/cosα, α=31.5°	9,753	12,509	kN	28%

Using the linear elastic approach, the maximum main cables tension was found to be 12,509 kN. From the software (MIDAS-Civil) results, the maximum factored tension in the main cables is 11,600 kN, as shown in Figure 4.14.

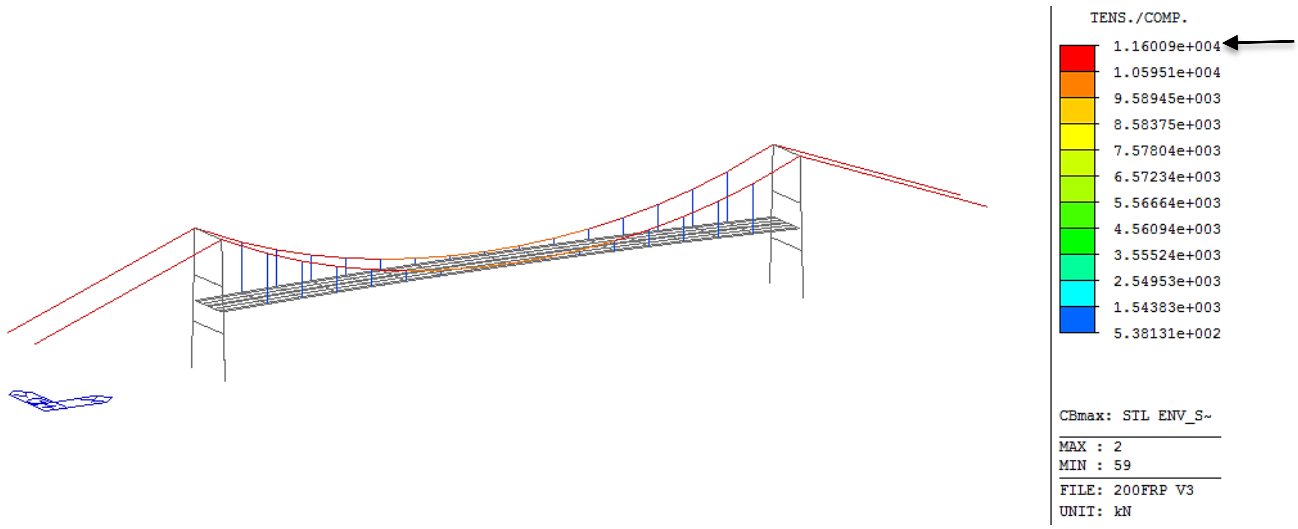

Figure 4.15: Tension in the Main Cables of the 200 m Span Bridge with an FRP Deck

The higher value of the main cables tension of 12,509 kN was obtained from the linear elastic theory and was used for the design of the main cable. F_u is the characteristic tension force for 70 mm spiral strands and is equal to 3,450 kN.

The detailed design of the main cables is summarized as shown as shown in Table 4.11.

Table 4.11: Calculations for the Size of the Main Cables of the FRP Deck

Item	Quantities	Value	Unit
F_u		3450	kN
F_d	3450/1.5	2300	kN
Number of strands		10	
The overall capacity of 10 strands	3450 x 10	34,500	kN
Factor of Safety	34,500/9,753	3.54	

4.4.7 Design of the Hangers of the 200 m Span Bridge with an FRP Deck

The tension in the hanger computed by the three-dimensional finite element analysis is 538.00 kN. Two 45 mm diameter strands per hanger were selected for the design of the hangers. The ultimate strength of the strands, F_u, is 968 kN and the design strength, F_d, is 645.00 kN for each hanger. The design force of 645 kN is more than the applied force of 538 kN and thus the design is adequate.

4.4.8 Live Load Deflection Calculations of the 200 m Span with an FRP Deck

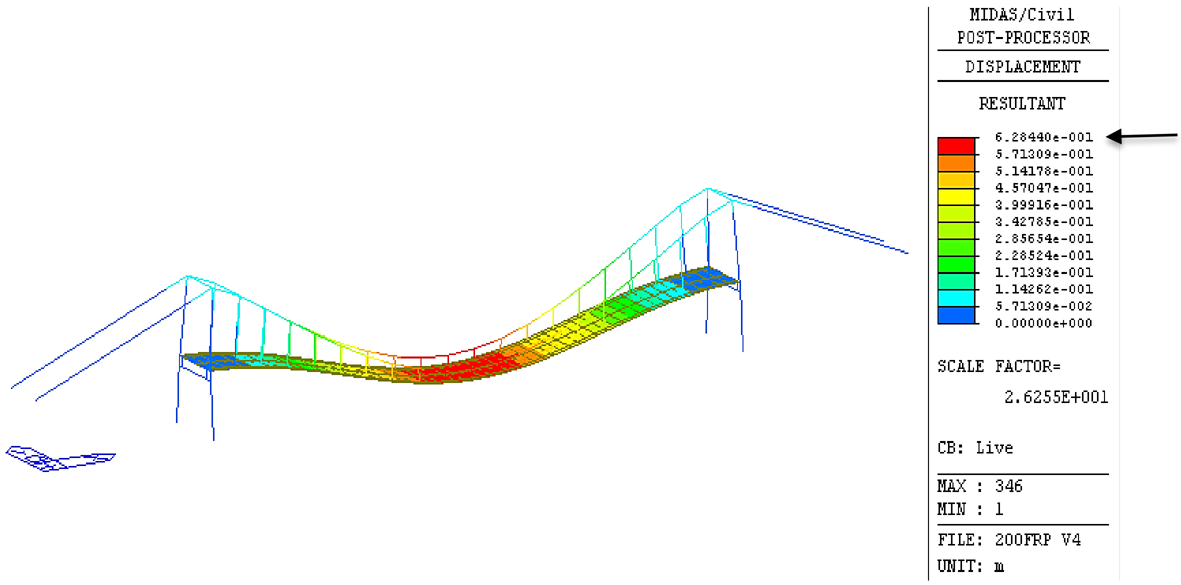

Figure 4.16: Live Load Deflection of the 200 m Span Bridge with an FRP Deck (0.63 m)

Live load deflection was computed based on AASHTO. Loading and lane loading were both considered for deflection calculations as shown in Figure 4.16. The live load deflection based on a three-dimensional finite element analysis was found to be 0.63 m, which is within the deflection limit of L/300 (0.64 m).

Table 4.12 summarizes the quantities of steel and cables for the FRP deck.

Table 4.12: Summary of Steel and Cable Weight for the FRP Deck

Item	Quantity (ton)
Steel	296.3
Main cable	98
Hanger	4.8

4.5 Tower Design

This section describes the design process, data, and results of the tower designs for 200 m suspension bridges with FRP and concrete decks. The design process adopted a minimum area for each leg of the towers to allow for saddle erection. In each case, the size provided was larger than what was needed to support the axial loads acting in the tower from the main cables tension.

Leg of the Tower Dimensions:

For suspension bridge with a concrete deck:

2.5 m x 2.00 m, as shown in Figure 4.17.

For suspension bridge with an FRP deck 2.0 m x 1.65 m.

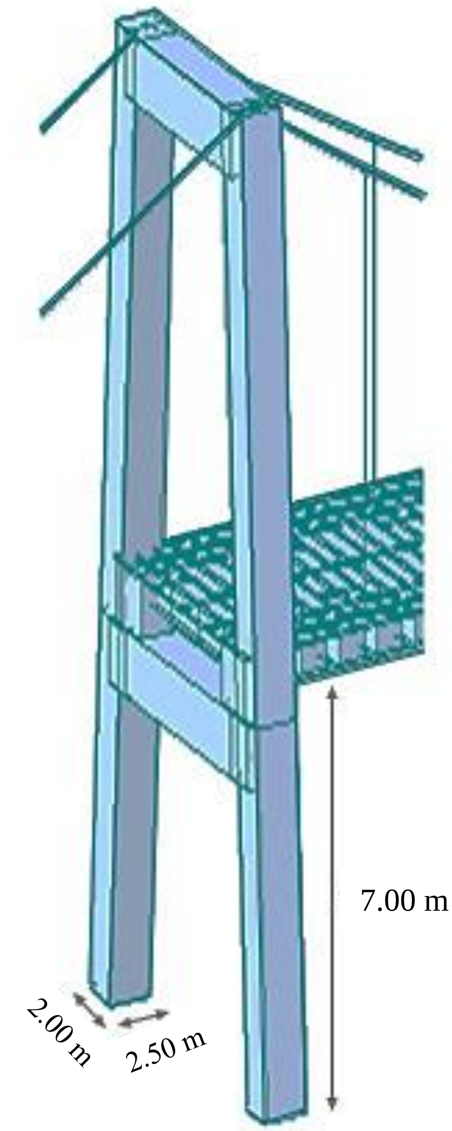

Figure 4.17: Tower Dimensions

4.5.1 Tower Design: Concrete-Case

The axial force acting on the towers of the 200 m suspension bridge were calculated. To simplify the tower design process, only the axil force was considered in the design. The allowable stresses for the tower concrete was limited by 70% to allow for other loads such as wind Then the design was performed by limiting the stresses produced by this axial force to 70% of the allowable stresses of concrete. (Gimsing, 1997).

The detailed design of the towers as described in Section 4.5.1 is summarized in Table 4.13.

Table 4.13: Tower Design: Concrete-Case

Item	Quantities	Value	Unit
Area	2.5 x 2	5	m^2
Density		25	kN/m^3
Length per one leg		114	m
Weight	5 x 25 x 114	14,250	kN
Axial force on tower		31,400	kN
Total load		45,650	kN
Stress limit	0.7 x 35	24.5	N/mm^2
Stress on concrete	45650/5000	9.13	N/mm^2

4.5.2 Tower Design: FRP-Case

The design of the towers was performed for the FRP case similarly to the design for the concrete case in Section 4.5.1. The detail design of the towers is summarized in Table 4.14.

Table 4.14: Tower Design: FRP-Case

Item	Quantities	Value	Unit
Area	2.0 x 1.65	3.3	m^2
Density		25	kN/m^3
Length per one leg		114	m
Weight	3.3 x 25 x 114	9,405	kN
Axial force on tower		11,150	kN
Total load		20,555	kN
Stress limit	0.7 x 35	24.5	N/mm^2
Stress on concrete	20555/3,300	6.22	N/mm^2

4.6 Discussion of Design Results

The results for the main cables tension obtained from the linear elastic analysis and those obtained from the three-dimensional finite element analysis were close and within 8% for the concrete case and 13% for the FRP case.

The steel floor girders design was performed using composite action for the concrete deck and non-composite action for the FRP deck. This design approach is conservative and resulted in heavier steel floor girders than if the FRP deck was designed similarly to the concrete deck as a composite deck.

The design of the 200 m suspension bridge with an FRP deck was controlled by the deflection limit of L/300. During the iterative design process to get the deflection limit of the FRP model, the main cables size had to be increased beyond its capacity to carry the maximum tension.

If the deflection limit could be increased, the main cables size of the FRP model could be reduced, which would have produced a more economical FRP bridge. The maximum tension obtained from the three-dimensional finite element analysis of the main cables for the concrete model was 31.04 MN, while it was 33.67 MN from the linear elastic analysis (Table 4.4). As expected, the linear elastic approach was conservative and higher by 8%. The results obtained using the two different methods were very close. In the case of the FRP deck, the main cables tension was 11.6 MN using the three-dimensional finite element model while it was 13.16 MN from the linear elastic analysis (Table 4.4). The results using the two methods were very close, within 13% for the FRP bridge. The main cables diameter is 0.262 m for the concrete model and 0.198 m for the FRP model, which is a 24% reduction.

The flutter speed computed using the finite element model was 100 m/s for the concrete model and 65 m/s for the FRP model. Flutter speeds as computed by the linear elastic method were 92 m/s and 60 m/s, respectively. The difference between the values of the flutter speed using the two methods is within 8% for the concrete model and within 7.7% for the FRP model. As expected by the initial hypothesis of this research, the use of a lighter deck, such as FRP, will reduce the aerodynamic stability of a suspension bridge and reduce the critical flutter speed (the minimum speed that can cause the bridge to experience flutter).

The flutter speed was reduced from an average speed of 96 m/s for the concrete model to 62.5 m/s for the FRP model (a reduction of 35%). Both critical flutter speeds of 96 m/s for the concrete model and 62.5 m/s for the FRP model are higher than the standard required design speed.

Chapter 5 - Design of 400 m and 600 m Suspension Bridges with Concrete and FRP Decks

This chapter describes the detailed design data and results of the 400 m and 600 m span bridges with concrete and FRP decks. Moreover, it summarizes the final estimated quantities of main cable, hangers and steel girders for each bridge.

5.1 Common Elements

Two 400 m and two 600 m suspension bridges were designed. In each pair, one bridge was designed using concrete deck; the other was designed using FRP deck. The linear elastic method and finite element three-dimensional non-linear analysis were both used in the design process. A typical detailed deck design is presented in Appendix I.

5.1.1 Bridge Geometry and Material Properties

Table 5.1 shows the geometry of a 400 m free span bridge and a 600 m free span bridge.

Table 5.1: Geometry of the Two Cases

Geometry	Unit	400 m span with a concrete and an FRP deck on steel girders	600 m span with a concrete and an FRP deck on steel girders
Main span length	m	400	600
Sag ratio	-	0.1	0.1

Geometry	**Unit**	**400 m span with a concrete and an FRP deck on steel girders**	**600 m span with a concrete and an FRP deck on steel girders**
Sag height	m	40	60
Tower height above DL (Deck level)	m	45	65
Tower height below DL	m	20	20
Total tower height	m	65	85
Spacing of hangers at main span	m	10	10

Of the 400 m bridge, the tower height above deck level was 45 meters. This was calculated by adding 40-meter sag to 5 meters more as clearance to avoid fouling with deck cambered by 1% as shown in Figure 5.1.

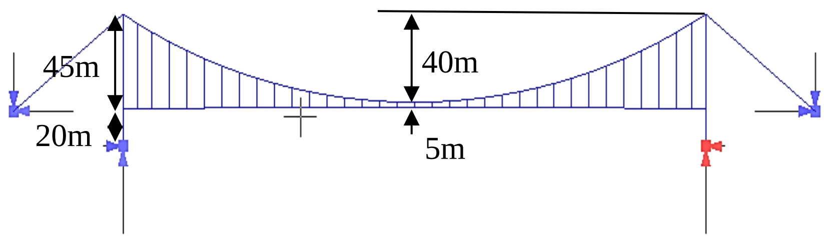

Figure 5.1: Tower Height Dimensions of the 400 m Free Span Bridges

Of the 600 m bridge, the tower height above deck level was 65 meters. This was calculated by adding 60-meter sag to 5 meter (minimum hanger length) as shown in Figure 5.2.

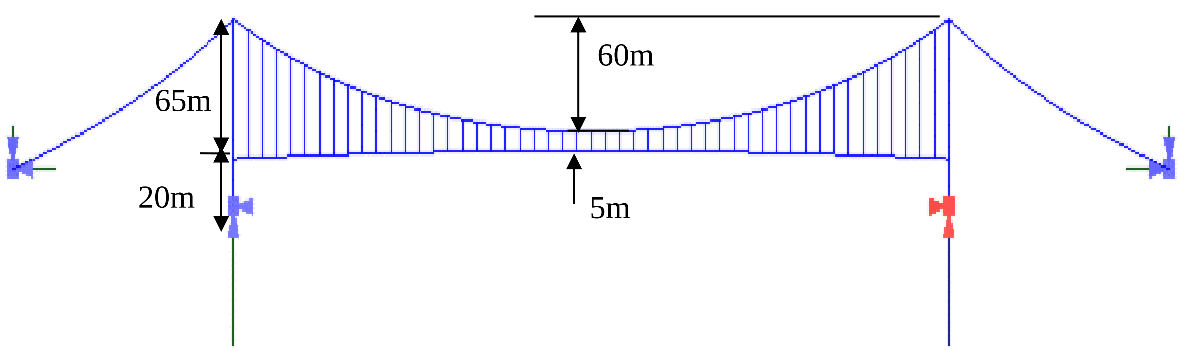

Figure 5.2: Tower Height Dimensions of the 600 m Free Span Bridges

The material properties used are similar to that of the base model (200 m suspension bridge) and are listed in Table 3.1.

5.1.2 Bridge Layout

Both bridges have a width of 20 m. The deck includes two footways, 1.5 m wide, at each side of the deck. Longitudinal girders with cross-girders carry the deck. Hangers spaced at 10 m transmit the loads to the main cable.

5.1.3 Section of the Steel Girders of the 400 m and 600 m Span Bridges with Concrete Decks

The steel sections used for the longitudinal and cross-girders of the 400 m and 600 m span suspension bridges with concrete decks were the same as the sections used of the 200 m span suspension bridge with the a concrete deck.

5.2 Concrete Deck

This section describes the design of the main cables and hangers of the 400 m span and 600 m span suspension bridges with a concrete deck. In addition, it shows the deflection calculations and results for each bridge.

5.2.1 Main Cables of the 400 m Span Bridge with a Concrete Deck

Two methods were used for the design of the main cable: the linear elastic method and three-dimensional finite element non-linear analysis. The linear elastic approach for the design of the main cables is summarized in Table 5.2.

Table 5.2: Linear Elastic Approach for the Design of the Main Cables of the 400 m Span Bridge with a Concrete Deck

Item	Unfactored loads	Factored loads	Unit	Difference (%)
Load from concrete slab	40,000	50,000	kN	25%
Up-stand parapets	600	750	kN	25%
Loads from steel girders	11,348	14,185	kN	25%
Asphalt wearing surface	11,040	13,800	kN	25%
Central reservation	500	625	kN	25%
Main cables self-weight	11,763	14,704	kN	25%
Hangers self-weight	218	273	kN	25%
Live loads	7,346	9,917	kN	35%
Total loads (W)	82,815	104,253	kN	26%
Load per each cable = total load /2	41,407	52,127	kN	26%
Load intensity (w) = load per each cable /span	104	130	kN/m	25%

Item	Unfactored loads	Factored loads	Unit	Difference (%)
Horizontal tension in main cables H = w L2/8d	51,759	65,043	kN	26%
T = Tension in the main cables = H/cosα, α=31.5º	60,705	76,284	kN	26%

Using the linear elastic approach, the maximum main cables tension was found to be 76,284 kN. From the software (MIDAS-Civil) results, the maximum factored tension in the main cables is 68,972 kN, as shown in Figure 5.3.

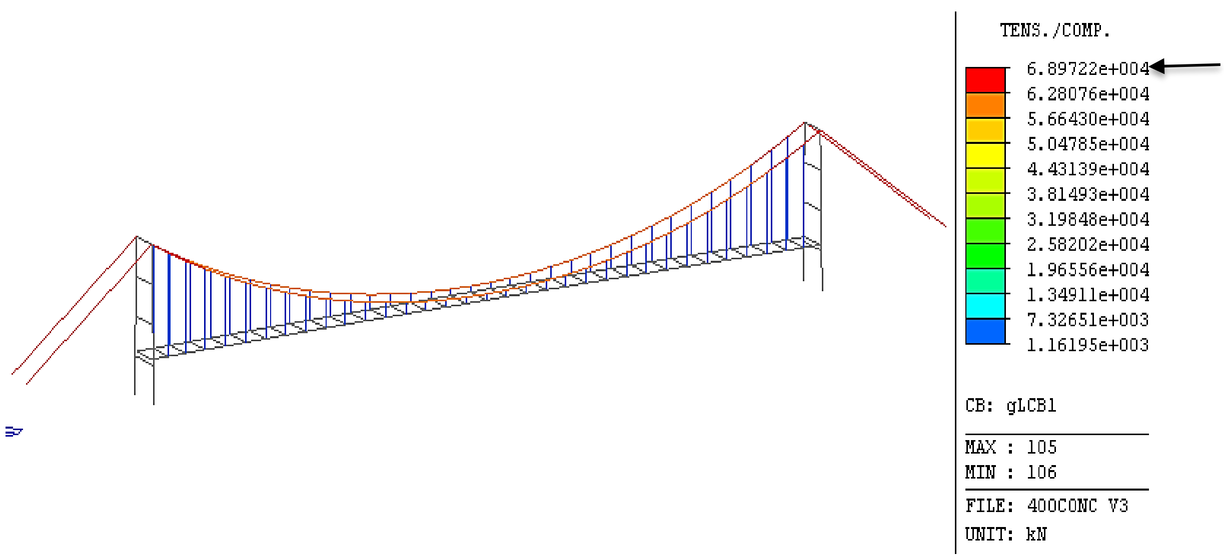

Figure 5.3: Tension in the Main Cables of the 400 m Span Bridge with a Concrete Deck

The higher value of the main cables tension of 76,284 kN was obtained from the linear elastic theory and was used for the design of the main cable. F_u is the characteristic tension force for 70 mm spiral strands and is equal to 4,700 kN. The details of the design of the main cables are summarized as shown in Table 5.3.

Table 5.3: Main Cables of the 400 m Span Bridge with a Concrete Deck

Item	Quantities	Value	Unit
F_u		4700	kN
F_d	4700/1.5	3133.33	kN
Number of strands		29	
The overall capacity of 29 strands	4700x29	136,300	kN
Factor of Safety	136,300/60,705	2.25	

5.2.2 Main Cables of the 600 m Span Bridge with a Concrete Deck

Two methods were used for the design of the main cable: the linear elastic method and three-dimensional finite element non-linear analysis. The linear elastic approach for the design of the main cables is summarized in Table 5.4.

Table 5.4: Linear Elastic Approach for the Design of the Main Cables of the 600 m Span Bridge with a Concrete Deck

Item	Unfactored loads	Factored loads	Unit	Difference (%)
Load from concrete slab	60,000	75,000	kN	25%
Up-stand parapets	900	1,125	kN	25%
Loads from steel girders	17,021	21,276	kN	25%
Asphalt wearing surface	16,560	20,700	kN	25%
Central reservation	750	938	kN	25%
Main cables self-weight	27,989	34,986	kN	25%
Hangers self-weight	346	433	kN	25%
Live loads	11,019	14,876	kN	35%
Total loads (W)	134,585	169,334	kN	26%
Load per each cable = total load / 2	67,292	84,667	kN	26%
Load intensity (w) = load per each cable /span	112	141	kN/m	26%
Horizontal tension in main cables H = w L2/8d	84,116	105,761	kN	26%
T = Tension in the main cables = H/ cosα , α=31.5º	98,653	124,039	kN	26%

The maximum main cables tension was found to be 124,039 kN using the linear elastic approach. From the software (MIDAS-Civil) results, the maximum factored tension in the main cables is 116,818 kN, as shown in Figure 5.4.

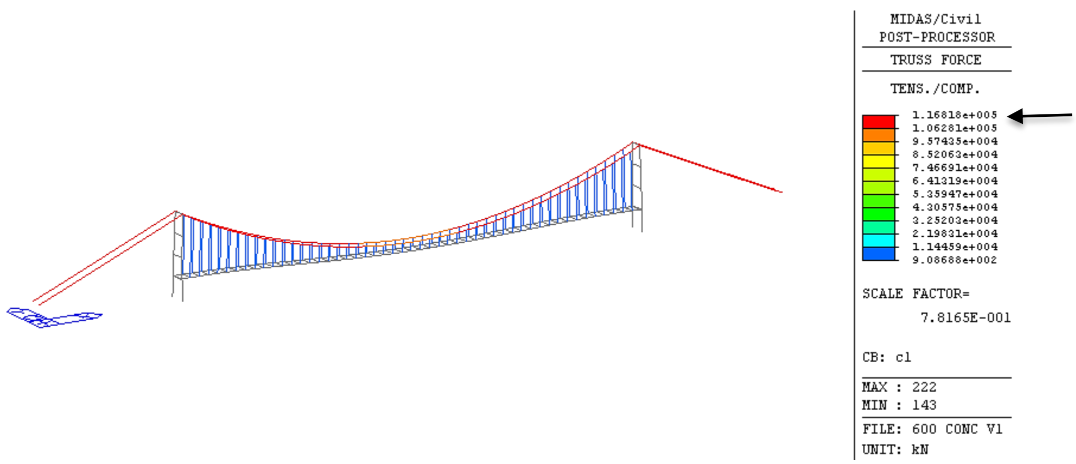

Figure 5.4: Tension in the Main Cables of the 600 m Span Bridge with a Concrete Deck

The higher value of the main cables tension of 124,039 kN was obtained from the linear elastic theory and was used for the design of the main cable. F_u is the characteristic tension force for 70 mm spiral strands and is equal to 4,700 kN. The details of the design of the main cables are summarized as shown in Table 5.5.

Table 5.5: Main Cables of the 600 m Span Bridge with a Concrete Deck

Item	Quantities	Value	Unit
F_u		4700	kN
F_d	4700/1.5	3133.33	kN
Number of strands		47	
The overall capacity of 47 strands	4700 x 47	220,900	kN
Factor of Safety	220,900/98,653	2.24	

5.2.3 Hangers of the 400 m Span Bridge with a Concrete Deck

Of the 400 m bridge, the tension in the hangers obtained from the three-dimensional finite element analysis was 1,924.8 kN. Two 65 mm diameter strands per hanger were selected for the design of the hangers. The ultimate strength of the strands, F_u, is 4,240 kN and the design strength, F_d, is 2,826.78 kN for each hanger. The design force of 2,826.78 kN is greater than the applied force of 1,924.8 kN and thus the design is adequate.

5.2.4 Hangers of the 600 m Span Bridge with a Concrete Deck

Of the 600 m bridge, the tension in the hangers obtained from the three-dimensional finite element analysis was 1,878.0 kN. Two 80 mm diameter strands per hanger were selected for the design of the hangers. The ultimate strength of the strands, F_u, is 5,300 kN and the design strength, F_d, is 3,533.3 kN for each hanger. The design force of 3,533.3 kN is greater than the applied force of 1,878.0 kN and thus the design is adequate.

5.2.5 Live Load Deflection Calculations of the 400 m and 600 m Span Bridges with a Concrete Deck

Live load deflection was computed based on AASHTO. Truck loading and lane loading were both considered for deflection calculations as shown in Figures 5.5 (400 m span) and 5.6 (600 m span).

Of the 400 m bridge, the live load deflection was found to be 1.2 m, which is within the deflection limit of L/300 (1.33 m). Of the 600 m bridge, the live load deflection was found to be 1.81 m, which is within the deflection limit of L/300 (2 m). Both values were determined using three-dimensional finite element analysis.

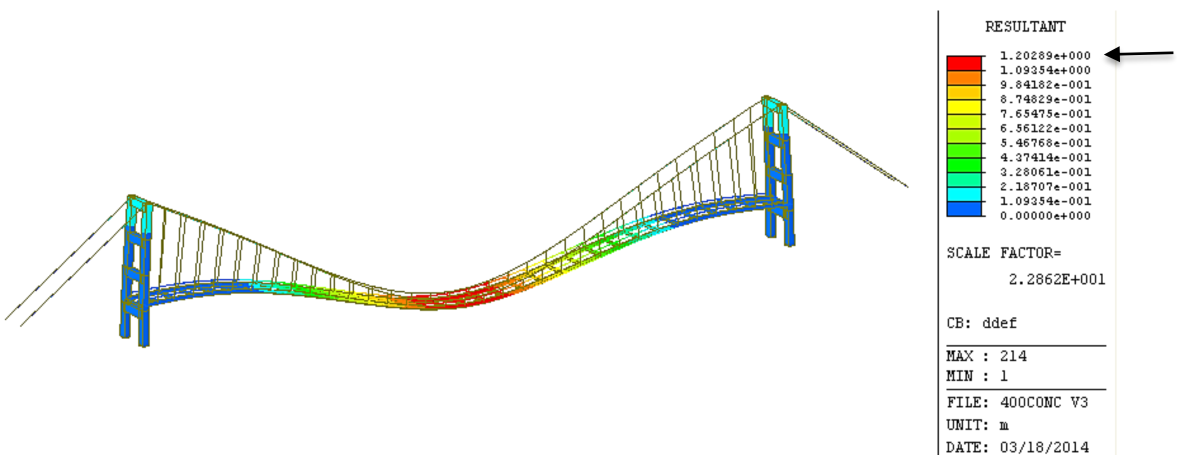

Figure 5.5: Live Load Deflection of the 400 m Span Bridge with a Concrete Deck (1.20 m)

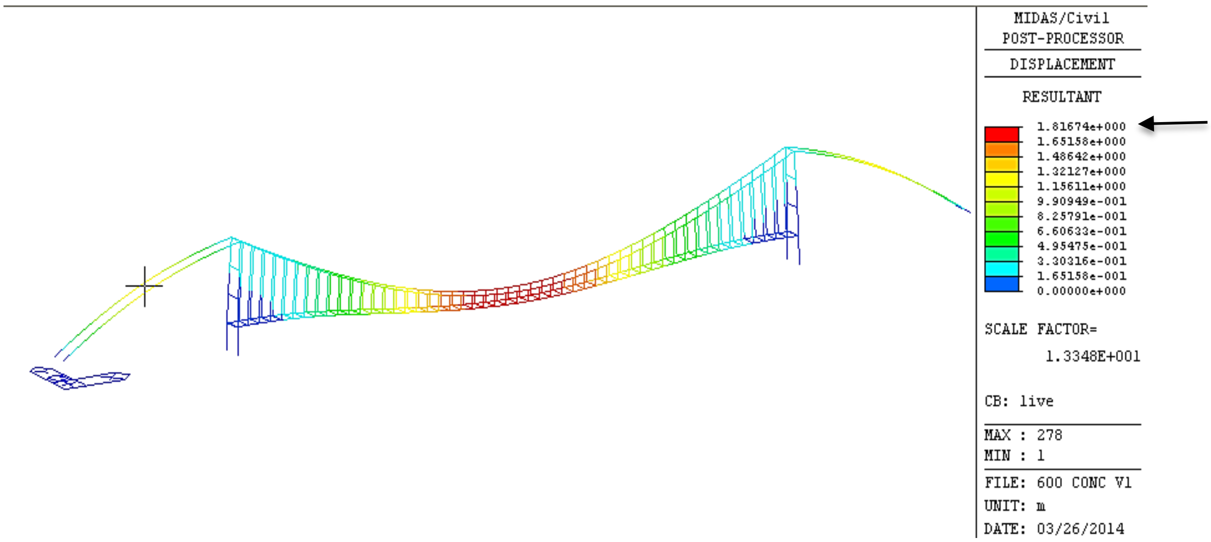

Figure 5.6: Live Load Deflection of the 600 m Span Bridge with a Concrete Deck (1.81 m)

The quantities of steel, including cross-girders, longitudinal girders, main cables, and hangers computed from the design are tabulated as shown in Table 5.6**.**

Table 5.6: Summary of Steel and Cable Weights for the FRP Deck of the 400 m Span Bridge and 600 m Span Bridge

Item	400 m Span Bridge Quantity (ton)	600 m Span Bridge Quantity (ton)
Steel	1157.2	1735.6
Main cable	732.9	1741
Hangers	26.1	56.9

5.3 FRP Deck

The same procedure used for the concrete deck bridges was used for the FRP deck bridges. The bridges were likewise analyzed using both the linear elastic method and three-dimensional finite element analysis. The results of both methods are described below.

5.3.1 Main Cables of the 400 m Span Bridge with an FRP Deck

The design of the main cables of the 400 m span bridge using the linear elastic approach is summarized in Table 5.7.

Table 5.7: Linear Elastic Approach for the Design of the Main Cables of the 400 m Span Bridge with an FRP Deck

Item	Unfactored loads	Factored loads	Unit	Difference (%)
Deck weight (FRP)	9,600	12,000	kN	25%
Up-stand parapets	600	750	kN	25%
Loads from steel girders	5,501	6,876	kN	25%
Central reservation	500	625	kN	25%
Main cables self-weight	6,854	8,568	kN	25%
Hangers self-weight	123	154	kN	25%

Item	Unfactored loads	Factored loads	Unit	Difference (%)
Live loads	7,346	9,917	kN	35%
Total loads (W)	30,523	38,890	kN	27%
Load per each cable = total load /2	15,262	19,445	kN	27%
Load intensity (w) = load per each cable /Span	38	49	kN/m	28%
Horizontal tension in main cables H = w L2/8d	19,077	24,244	kN	27%
T = Tension in the main cables = H/cosα, α=31.5º	22,374	28,434	kN	27%

Using the linear elastic approach, the maximum main cables tension was found to be 28,434 kN. From the MIDAS-Civil software results, the maximum factored tension for the main cables was found to be 23,618 kN, as shown in Figure 5.7.

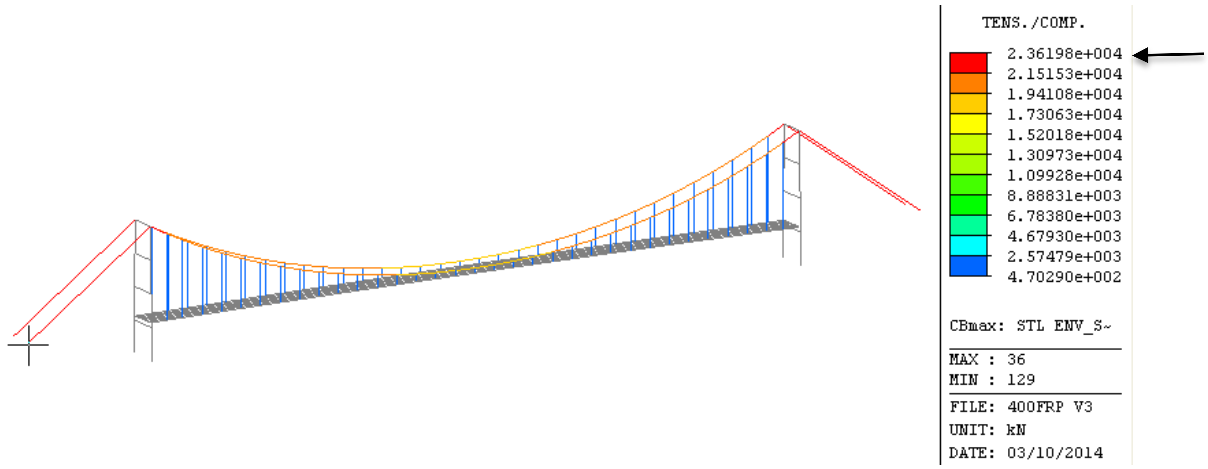

Figure 5.7: Tension of the Main Cables of the 400 m Span Bridge with an FRP Deck

The higher value of the main cables tension of 28,434 kN was obtained from the linear elastic theory and was used for the design of the main cable. F_u is the characteristic tension force for 70 mm spiral strands and is equal to 3,450 kN. The details of the design of the main cables are summarized in Table 5.8.

Table 5.8: Main Cables of the 400 m Span Bridge with an FRP Deck

Item	Quantities	Value	Unit
F_u		3450	kN
F_d	3,450/1.5	2300	kN
Number of strands		23	
The overall capacity of 23 strands	3,450x23	79,350	kN

Factor of Safety	79,350/22,374	3.55	

5.3.2 Main Cables of the 600 m Span Bridge with an FRP Deck

The linear elastic approach calculations of the 600 m span bridge are summarized in Table 5.9.

Table 5.9: Linear Elastic Approach for the Design of the Main Cables of the 600 m Span Bridge with an FRP Deck

Item	Unfactored loads	Factored loads	Unit	Difference (%)
Deck weight (FRP)	14,400	18,000	kN	25%
Up-stand parapets	900	1,125	kN	25%
Loads from steel girders	8,251	10,314	kN	25%
Central reservation	750	938	kN	25%
Main cables self-weight	16,093	20,116	kN	25%
Hangers self-weight	228	285	kN	25%
Live loads	11,019	14,876	kN	35%

Item	Unfactored loads	Factored loads	Unit	Difference (%)
Total loads (W)	51,641	65,654	kN	27%
Load per each cable = total load / 2	25,821	32,827	kN	27%
Load intensity (w) = load per each cable /span	43	55	kN/m	27%
Horizontal tension in main cables H = w L2/8d	32,276	40,961	kN	27%
T = Tension in the main cables = H / cosα, α=31.5º	37,854	48,847	kN	29%

Using the linear elastic approach, the maximum main cables tension of the 600 m bridge was found to be 48,847 kN. Using MIDAS-Civil software, the maximum factored main cables tension was found to be 43,280 kN, as shown in Figure 5.8.

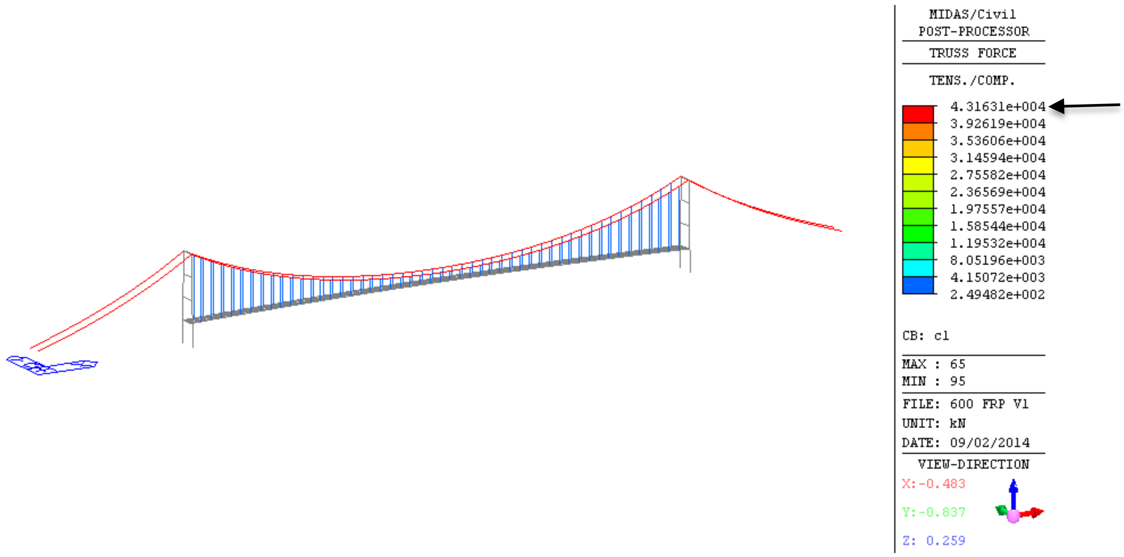

Figure 5.8: Tension in the Main Cables of the 600 m Span Bridge with an FRP Deck

The higher value of the main cables tension of 48,847 kN was obtained from the linear elastic theory and was used for the design of the main cable. F_u is the characteristic tension force for 70 mm spiral strands and is equal to 3,450 kN. The details of the design of the main cables are summarized as shown in Table 5.10.

Table 5.10: Main Cables of the 600 m Span Bridge with an FRP Deck

Item	Quantities	Value	Unit
F_u		3450	kN
F_d	3450/1.5	2300	kN
Number of strands		36	
The overall capacity of 36 strands	3450 x 36	124,200	kN
Factor of Safety	124,200/37,854	3.28	

5.3.3 Hangers of the 400 m Span Bridge with an FRP Deck

As determined by a three-dimensional finite element analysis, hanger tension of the 400 m bridge is 638.6 kN. Two 50 mm diameter strands per hanger were selected for hanger design. The ultimate strength of the strands, F_u, is 1,782 kN; the design strength, F_d, is 1,188.00 kN. The design force of 1,188.00 kN is greater than the applied force of 638.6 kN, and thus the design is adequate.

5.3.4 Hangers of the 600 m Span Bridge with an FRP Deck

As of the 600 m bridge, three-dimensional finite element analysis was used to determine hanger tension of 641.6 kN. For hanger design, two 65 mm diameter strands per hanger was selected. The ultimate strength of the strands, F_u, is 3,750 kN; the design strength, F_d, is 2,500.00 kN for each hanger. The design force of 2,500 kN is greater than the applied force of 641.6 kN, and therefore the design is adequate.

5.3.5 Live Load Deflection Calculations of the 400 m and 600 m Span Bridges with an FRP Deck

Live load deflection was computed based on AASHTO. Truck loading and lane loading were both considered for deflection calculations as shown in Figures 5.9 (400 m span) and 5.10 (600 m span).

Of the 400 m bridge, the live load deflection was found to be 1.25 m, which is within the deflection limit of L/300 (1.33 m). Of the 600 m bridge, the live load deflection was found to be 1.92 m, which is within the deflection limit of L/300 (2 m). Both values were determined using three-dimensional finite element analysis.

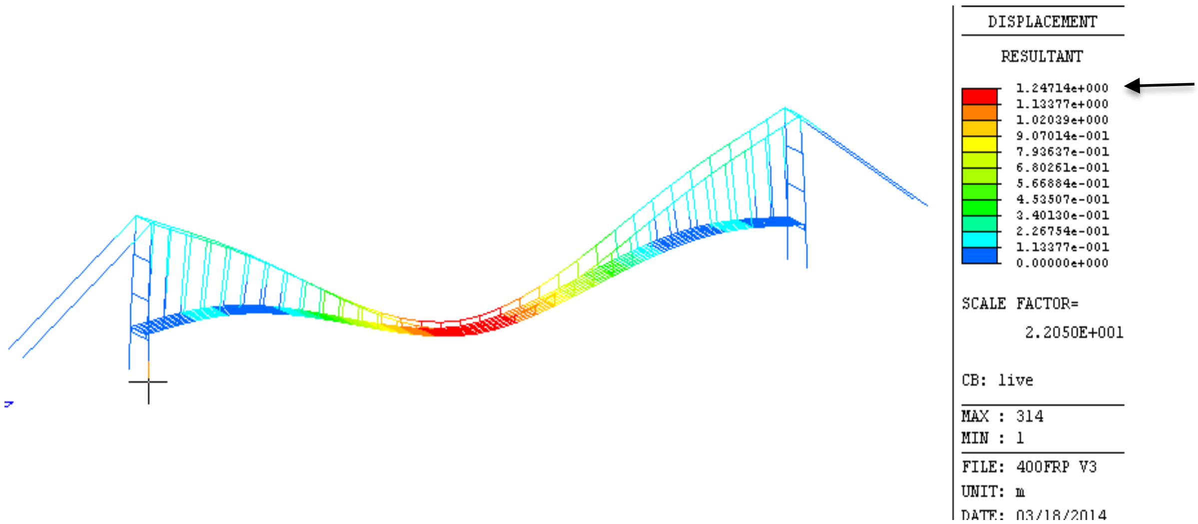

Figure 5.9: Live Load Deflection of the 400 m Span Bridge with an FRP Deck (1.25 m)

Figure 5.10: Live Load Deflection of the 600 m Span Bridge with an FRP Deck (1.92 m)

The quantities of steel, including cross-girders, longitudinal girders, main cable, and hangers from the design are tabulated as shown in Table 5.11.

Table 5.11: Summary of Steel and Cable Weights for the FRP Deck of the 400 m Span Bridge and the 600 m Span Bridge with an FRP Deck

Item	400 m Span Bridge Quantity (ton)	600 m Span Bridge Quantity (ton)
Steel	560.9	841.3
Main cable	427	1001.0
Hangers	15.4	35.1

Chapter 6 - Aerodynamic Parametric Analysis of 200 m, 400 m, and 600 m Suspension Bridges with a Concrete Deck and an FRP Deck

The critical flutter speed was calculated to compare the aerodynamic behavior of each bridge. Selberg's equation (Selberg 1961) was used to determine the critical flutter speed for each bridge. Critical flutter speed is the wind speed at which flutter will occur within the structure. Two methods were used to compute the torsional and vertical frequencies. The first approach used the linear elastic method. The torsional and vertical frequencies ($n_{t,}$ and n_v) were determined using spring constant equations as outlined in section 6.1. The second method used the results obtained from the three-dimensional finite element analysis utilizing MIDAS-Civil software.

6.1 Flutter Speed Calculations

Selberg's equation was used to determine the critical flutter speed for all the models.

$$\text{Flutter Speed} = 0.52 v_d \sqrt{\left[1-\left(\frac{n_v}{n^t}\right)^2\right]} \, b \sqrt{\frac{m}{I_m}} \tag{6-1}$$

Where:

$$v_d = \text{Divergence speed} = \frac{2}{b}\sqrt{\frac{c_t}{\pi p}} \tag{6-2}$$

n_t = Torsional frequency

n_v = Vertical frequency

c_t = Torsional spring constant = $0.5b^2$

Two approaches were used to determine the dynamic properties. The first approach used the linear elastic method. The torsional and vertical frequencies (n_t and n_v, respectively) were determined using spring constant equations.

$$C = \frac{\mathrm{EA}}{\mathrm{h}}$$ **(6-3)** [R. Vianna, 2005]

And,

$$\frac{\mathrm{n_v}}{\mathrm{n_t}} = \sqrt{\frac{4\mathrm{I_m}}{\mathrm{mb^2}}}$$ **(6-4)** [R. Vianna, 2005]

Where,

I_m is the bridge inertia

m is the bridge total mass

After obtaining the ratios of the torsional frequency, vertical frequency, the mass, and the inertia for each bridge, the critical flutter speed was calculated using Selberg's equation.

The second approach uses finite element analysis (FEA) as described in section 6.1.1.

6.1.1 Torsional and Vertical Frequencies using Finite Element Analysis

The other method used the finite element analysis (FEA) results from the (MIDAS-Civil) software to get the torsional and vertical frequencies. The vertical frequency of the 200 m span bridge with a concrete deck is 0.12 cycle/second as shown in Figure 6.1. The torsional frequency for the concrete deck, the vertical frequency for the FRP deck, and the torsional frequency of the FRP deck are shown in Figures 6.2, 6.3, and 6.4.

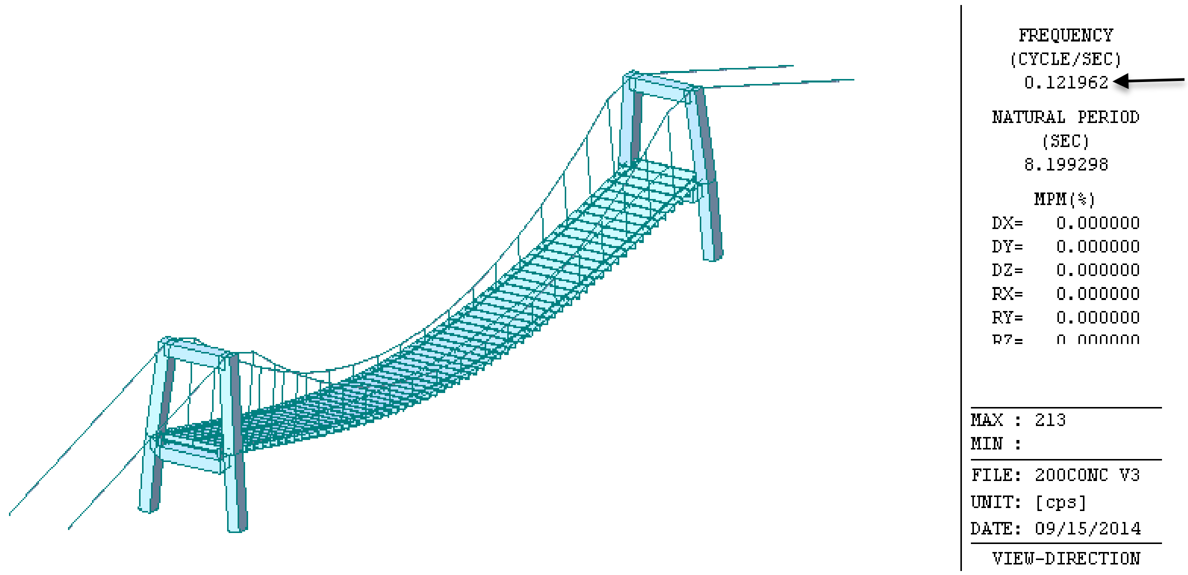

Figure 6.1: Vertical Frequency of the 200 m Span Bridge with a Concrete Deck

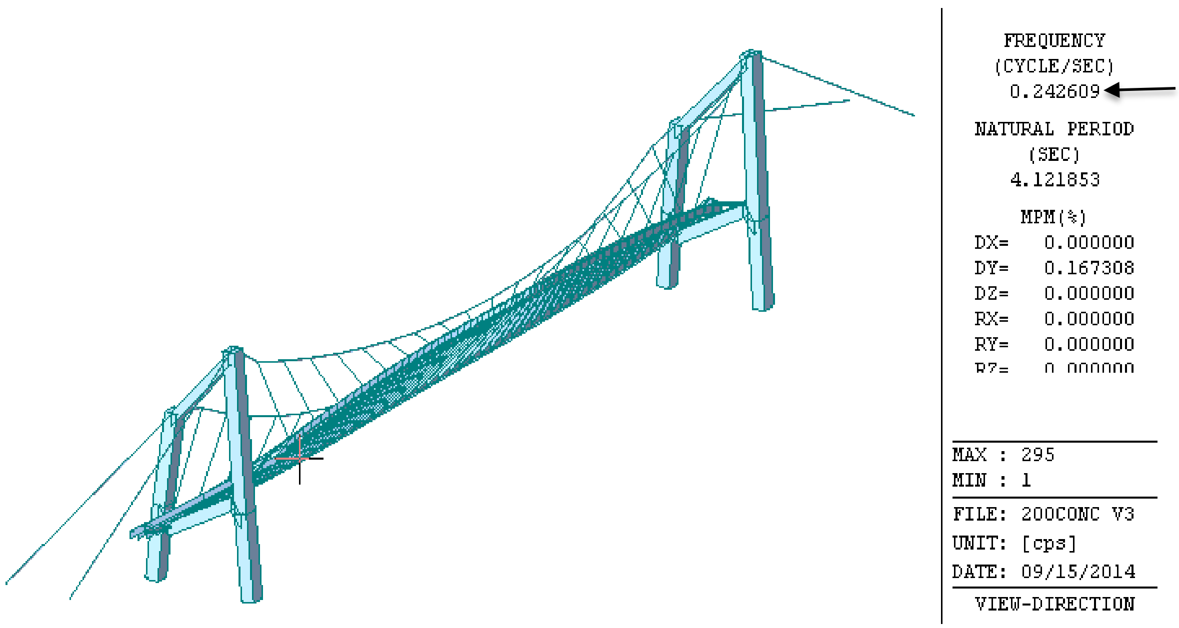

Figure 6.2: Torsional Frequency of the 200 m Span Bridge with a Concrete Deck

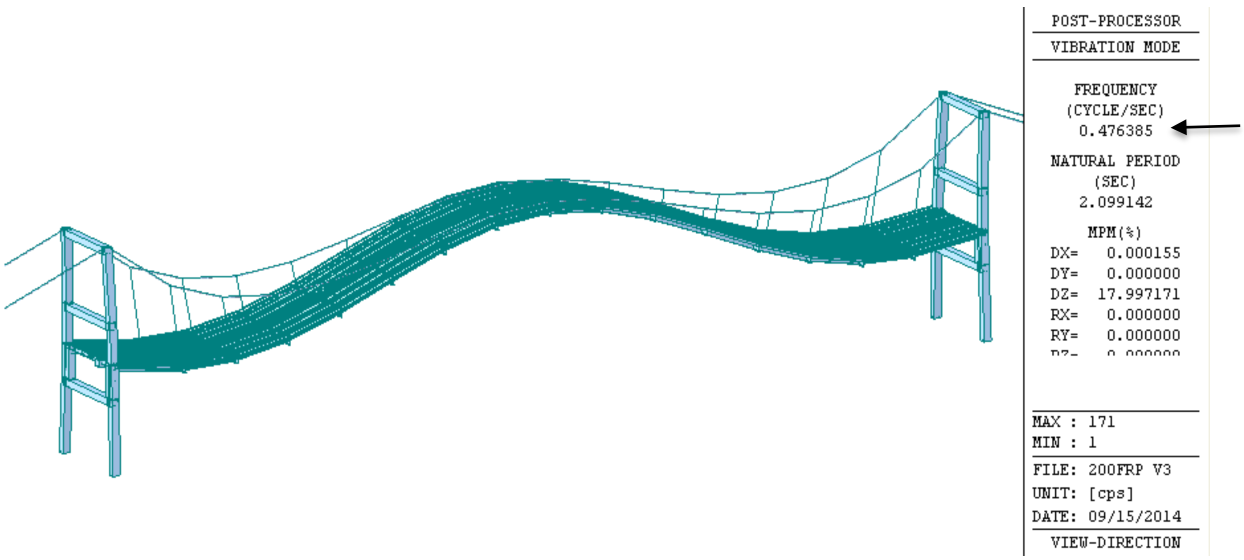

Figure 6.3: Vertical Frequency of the 200 m Span Bridge with an FRP Deck

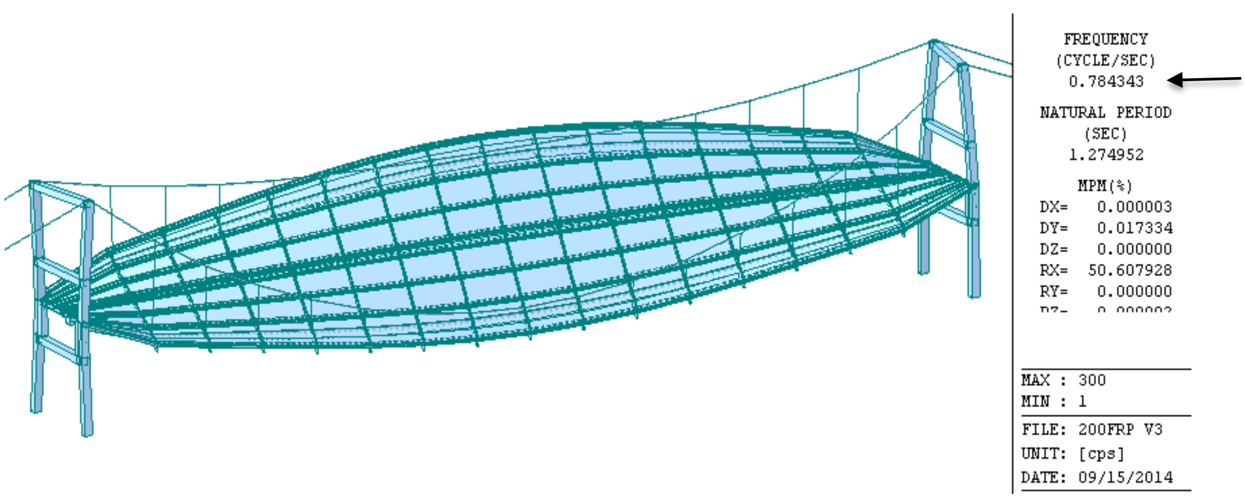

Figure 6.4: Torsional Frequency of the 200 m Span Bridge with an FRP Deck

The detailed calculations for the two cases (concrete deck and FRP deck) for 200 m suspension bridges are summarized in Table 6.1. The two approaches for calculating the critical flutter speed are also compared in Table 6.1.

Table 6.1: Comparison between the Three-Dimensional Finite Element Analysis and the Linear Elastic Analysis of Flutter Speed Calculations of the 200 m Span Bridges with a Concrete Deck and an FRP Deck

Item	Material used for the deck	Unit	Concrete	FRP
1	Concrete / FRP density	kN/m^2	5	1.2
2	Bridge length	m	200	200
3	Width	m	20	20
4	Deck weight	kN	2,0000	4800
5	Density of cross-girder	kN/m^3	78	78
6	Area of cross-girder	m^2	0.0379	0.018
7	Cross-girder total load	kN	2705.9	1498.3
8	Cross-girder total load	Ton	275.9	152.8

Item	Material used for the deck	Unit	Concrete	FRP
9	Density of cross-girder	kN/m^3	78	78
10	Area of main girder	m^2	0.09513	0.047
11	Main girder total load	kN	2966.9	1465.2
12	Main girder total load	Ton	302.6	149.4
13	Main cables density	kN/m^3	78	78
14	Number of strands		14	10
15	Area of single strand	m^2	0.004	0.003
16	Total area of main cable	m^2	0.056	0.03
17	Length of two main cable	m	690.5	690.5
18	Total load of main cable	kN	2900.4	1522.1
19	Total load of main cable	Ton	295.8	155.2
20	Hanger cable density	kN/m^3	78	78
21	Total area of hangers	m^2	0.006	0.003

Item	Material used for the deck	Unit	Concrete	FRP
22	Total length of hangers	m	193	193
23	Total load of hangers	kN	85.1	46.9
24	Total load of hangers	Ton	8.7	4.9
25	m_1	kg	606865.1	309385.1
26	m_2	kg	2877258.3	642028.5
27	Total mass	kg	3366590	889734
28	$I_1 = (m_1\ b_2)/4$	Kg.m^2	48933154	24770570
29	$I_2 = (\ m_1\ b_2)/12$	Kg.m^2	95908609.9	21400951.4
30	I total =	Kg.m^2	144841764	46171521
31	n_v/n_t using spring constant	ratio	0.656	0.72
32	Average height of hanger	m	17	17
33	Spring constant	kN/m	180045	101275
34	Divergence speed V_d	m/sec	311	233

Item	Material used for the deck	Unit	Concrete	FRP
35	n_v / n_t from FEA (MIDAS)	ratio	0.56	0.67
36	Flutter speed V_f (linear elastic method)	m/sec	214	141
37	Flutter speed V_f (FEA method)	m/sec	232	150
38	Critical flutter (linear elastic theory)	m/sec	92	60
39	Critical flutter (three-dimensional FEA model)	m/sec	100	65
40	% Difference between flutter speed from linear elastic and FEM methods		9	6.7

The other method used was three-dimensional finite element analysis. The values of torsional and vertical frequencies were obtained from the (MIDAS-Civil) software finite element analysis (FEA) results. Flutter speed calculations of the 400 m suspension bridges with a concrete deck and an FRP deck using the three-dimensional finite element approach and the linear elastic approach are summarized in Table 6.2.

Table 6.2: Comparison between the Three-Dimensional Finite Element Analysis and the Linear Elastic Analysis of Flutter Speed Calculations of the 400 m Suspension Bridges with a Concrete Deck and an FRP Deck

Item	Material used for the deck	Unit	Concrete	FRP
1	Concrete / FRP density	kN/m^2	5	1.2
2	Bridge length	m	400	400
3	Width	m	20	20
4	Deck weight	kN	40000	9600
5	Density of cross-girder	kN/m^3	78	78
6	Area of cross-girder	m^2	0.0379	0.018
7	Cross-girder total load	kN	5411.8	2570.3
8	Cross-girder total load	Ton	551.9	262.1
9	Density of cross-girder	kN/m^3	78	78
10	Area of main girder	m^2	0.09513	0.04696
11	Main girder total load	kN	5935.8	2930.3

Item	Material used for the deck	Unit	Concrete	FRP
12	Main girder total load	Ton	605.3	298.8
13	Main cables density	kN/m^3	78	78
14	Number of strands	No.	29	23
15	Area of single strand	m^2	0.0038	0.0028
16	Total area of main cable	m^2	0.11	0.06
17	Length of two main cable	m	826	826
18	Total load of main cable	kN	7186.8	4186.7
19	Total load of main cable	Ton	732.9	426.0
20	Hanger cable density	kN/m^3	78	78
21	Total area of hangers	m^2	0.0066	0.0039
22	Total length of hangers	m	494	494
23	Total load of hangers	kN	255.6	151.2
24	Total load of hangers	Ton	26.1	15.4

Item	Material used for the deck	Unit	Concrete	FRP
25	m_1	kg	1363734.9	741002.4
26	m_2	kg	5754516.6	1240596.5
27	Total mass	kg	7118251.5	1981598.9
28	$I_1 = (m_1\, b_2)/4$	$Kg.m^2$	136373486.7	74100236.9
29	$I_2 = (\, m_1\, b_2)/12$	$Kg.m^2$	191817219.8	41353216.8
30	I total =	$Kg.m^2$	328190706.5	115453453.8
31	n_v/n_t using spring constant	ratio	0.679	0.763
32	Average height of hanger	m	30	30
33	Spring constant	kN/m	119738.84	70851.38464
34	Divergence speed V_d	m/sec	254.2	195.6
35	n_v/n_t from FEA (MIDAS)	ratio	0.612	0.723
36	Flutter speed V_f (linear elastic method)	m/sec	167	106
37	Flutter speed V_f (FEA method)	m/sec	179	114

Item	Material used for the deck	Unit	Concrete	FRP
38	Critical flutter (linear elastic theory)	m/sec	72	46
39	Critical flutter (three-dimensional FEA model)	m/sec	77	49
40	% Difference between flutter speed from linear elastic and FEM methods	%	8	7

The torsional and vertical frequencies of the 600 m span bridge were obtained from the MIDAS-Civil software finite element analysis (FEA) results. Flutter speed calculations for the concrete deck and the FRP deck using the three-dimensional finite element approach and the linear elastic approach are summarized in Table 6.3.

Table 6.3: Comparison between the Three-Dimensional Finite Element Analysis and the Linear Elastic Analysis of Flutter Speed Calculations of the 600 m Suspension Bridges with a Concrete Deck and an FRP Deck

Item	Material used for the deck	Unit	Concrete	FRP
1	Concrete / FRP density	kN/m^2	5	1.2
2	Bridge length	m	**600**	**600**
3	Width	m	20	20
4	Deck weight	kN	60000	14400
5	Density of cross-girder	kN/m^3	78	78
6	Area of cross-girder	m^2	0.0379	0.018
7	Cross-girder total load	kN	8116.7	3855.4
8	Cross-girder total load	Ton	826.8	393.1
9	Density of cross-girder	kN/m^3	78	78
10	Area of main girder	m^2	0.09513	0.04696

Item	Material used for the deck	Unit	Concrete	FRP
11	Main girder total load	kN	8903.7	4395.5
12	Main girder total load	Ton	906.9	448.2
13	Main cables density	kN/m^3	78	78
14	Number of strands	No.	46	36
15	Area of single strand	m^2	0.0038	0.0028
16	Total area of main cable	m^2	0.1769	0.1017
17	Length of two main cable	m	1237	1237
18	Total load of main cable	kN	17072.1	9816.1
19	Total load of main cable	Ton	1740.9	1001.0
20	Hanger cable density	kN/m^3	78	78
21	Total area of hangers	m^2	0.0077	0.0047
22	Total length of hangers	m	930	930
23	Total load of hangers	kN	558.1	344.5

Item	Material used for the deck	Unit	Concrete	FRP
24	Total load of hangers	Ton	56.9	35.1
25	m_1	kg	2704780	1483798
26	m_2	kg	8631774.9	1860894.8
27	Total mass	kg	11336554.4	3344693.6
28	$I_1 = (m_1\, b_2)/4$	Kg.m^2	270477946.7	148379880.6
29	$I_2 = (\ m_1\, b_2)/12$	Kg.m^2	287725829.7	62029825.3
30	I total =	Kg.m^2	558203776.4	210409705.9
31	n_v/n_t using spring constant	ratio	0.702	0.793
32	Average height of hanger	m	43	43
33	Spring constant	kN/m	96885.14923	59811.75029
34	Divergence speed V_d	m/sec	228.7	179.7
35	n_v/n_t from FEA (MIDAS)	ratio	0.652	0.765
36	Flutter speed V_f(linear elastic method)	m/sec	143	90

Item	Material used for the deck	Unit	Concrete	FRP
37	Flutter speed V_f (FEA method)	m/sec	152	96
38	Critical flutter (linear elastic theory)	m/sec	**62**	**39**
39	Critical flutter (three-dimensional FEA model)	m/sec	**65**	**41**
40	% Difference between flutter speed from linear elastic and FEM methods	%	6	6

6.2 Discussion of Results

As expected by the hypothesis of this research, the critical flutter speed was lower in the case of FRP deck than for the concrete deck for all the bridge spans considered in this study. The predicted flutter speeds obtained from the linear elastic approach and the finite element approach were within 9% of each other for all the spans and deck materials. The reduction of the predicted flutter speed of the 200 m span suspension bridge, due to the use of FRP deck was 35% using the linear elastic method and finite element analysis (Figure 6.5 and Figure 6.6). The flutter speed reduction was 36% of the 400 m span bridge and 37% of the 600 m span bridge.

For the concrete deck, the average critical flutter speed was 96 m/s of the 200 m span bridge, 74.5 m/s of the 400 m span bridge, and 63.5 m/s of the 600 m span bridge. The average critical flutter speeds for the 200 m, 400 m, and 600 m bridges with an FRP deck, were 62.5 m/s, 46.5 m/s, and 40 m/s, respectively.

Matson, et al. (2001) performed an aerodynamic stability evaluation program of the Lion's Gate Suspension Bridge located in Vancouver, British Columbia, Canada. The evaluation consisted of full bridge aero-elastic models and section models. The bridge has a total span of 847 m with a free span of 472 m. The modified deck is concrete filled tee-grit deck and is 16.8 m wide. They reported a flutter speed of 70 m/s. This research calculated a flutter speed of the 600 m bridge of 63.5 m/s for concrete deck and 40 m/s for FRP deck.

These values appear to be comparable and consistent with those calculated and measured by Matson, et al. The width and the mass of the deck influence the calculations of flutter speed. While the total length of the Lion's Gate Bridge is 847 m, the free span is 472 m. The deck of the Lion's Gate Bridge is lighter than concrete deck but heavier than FRP deck. Comparing the results obtained for a 600 m bridge in this study with the flutter speed of the Lion's Gate Bridge, the flutter speed measured for Lion's Gate is 70 m/s, which is slightly higher than the 600 m bridge with a concrete deck (63.5 m/s). The Lion's Gate Bridge has a narrower deck (16.8 m versus 20 m) and lighter deck (concrete filled-steel grit versus a reinforced concrete deck).

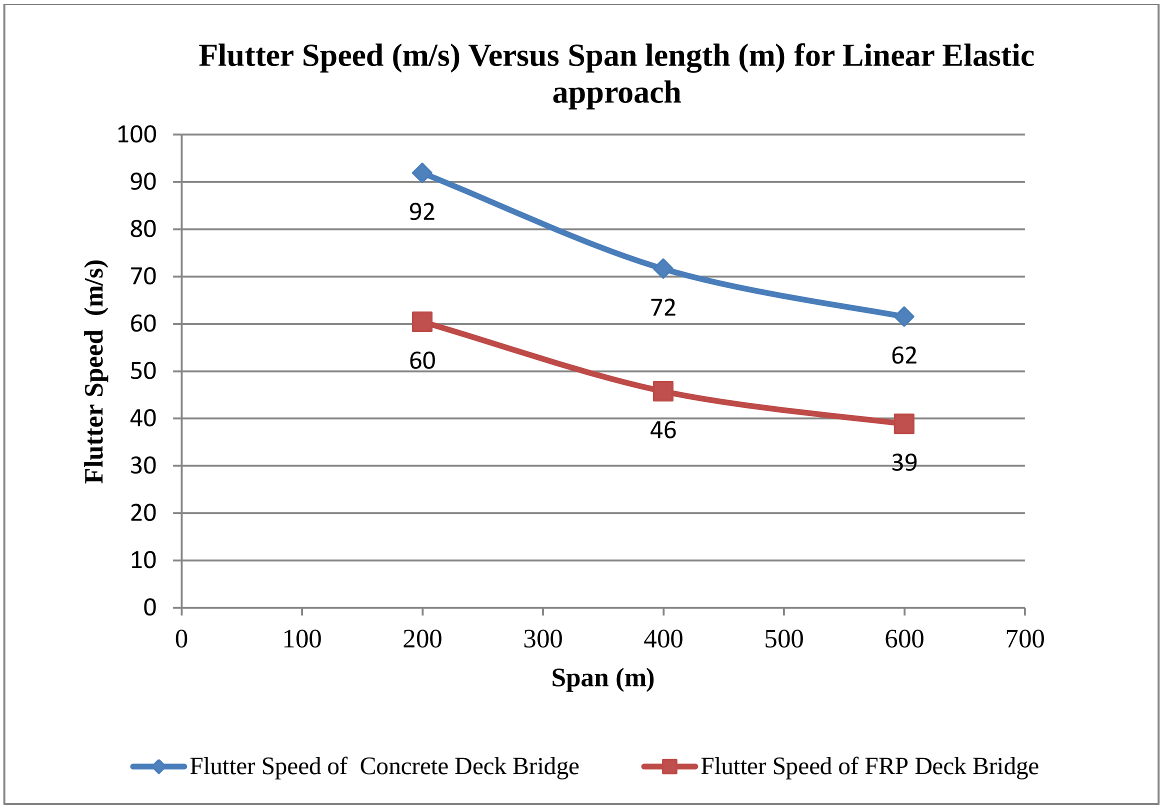

Figure 6.5: Critical Flutter Speed (m/s) Versus Bridge Span (m) using Linear Elastic Approach

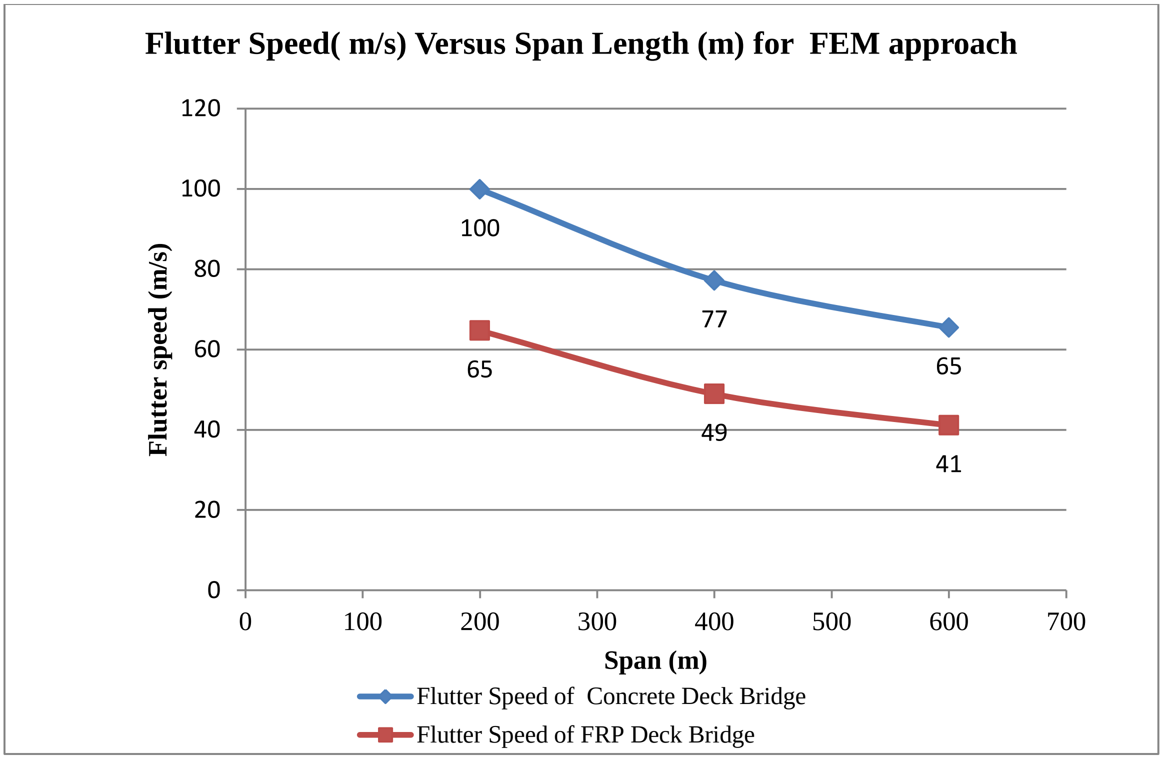

Figure 6.6: Critical Flutter Speed (m/s) Versus Bridge Span Using the FEM Approach

However, the redesign of the Lion's Gate Bridge improved the torsional rigidity of the deck and increased the aerodynamic stability of the bridge, which has led to a slightly higher flutter speed than the 600 m bridge considered in this research.

The flutter speed calculated of the 600 m bridge with an FRP deck was lower than the Lion's Gate Bridge's flutter speed. The 600 m bridge has a wider deck, which should result in a higher flutter speed, but the FRP deck is lighter than the concrete filled steel grit of Lion's Gate. In addition, significant changes were performed on the deck to increase torsional rigidity and consequently increase the flutter speed of Lion's Gate from 35 m/s to 70 m/s. The 600 m bridge flutter speed obtained in this research was 40 m/s, higher than the original flutter speed but lower than the final flutter speed of the Lion's Gate Bridge.

Meiarashi, et al. (2002) compared an all-steel suspension bridge with an all-composite suspension bridge. Their work was discussed extensively in Chapter 2. The all-composite bridge has a span length of 800 m with a free span of 500 m. The deck width is 25 m, which is wider than all the bridges considered in this research (20 m).

Meiarashi, et al. reported a flutter speed of 64 m/s for the all-composite bridge, which is almost the same as the flutter speed calculated in this research of the 600 m bridge with a concrete deck and significantly higher than the flutter speed computed for FRP deck case. The factors that might have contributed to the higher flutter speed for the all-composite bridge are:

- The all-composite bridge has a wider deck, which leads to higher flutter speed;
- The main cables and hangers are made of lighter composite materials. Lighter main cables and hangers could reduce the mass at the edges and increase the overall aerodynamic stability of the bridge and lead to a higher flutter speed [Gimsing 1997]; and
- Use of the streamlined aerodynamic shape of the deck for the all-composite bridge versus the H-shaped deck used in this research has improved the aerodynamic stability. Streamlined deck shapes have higher flutter speeds.

The results obtained by the linear elastic method and the finite element method were within 9% of each other. In addition, the flutter speeds calculated and tested by other researchers for other existing bridges that are similar to the bridges considered in this research were comparable to the speeds obtained in this study, if the differences between these bridges are taken into account. Two facts support the flutter speed results obtained in this research. First, the flutter speeds calculated using the linear elastic method and the finite element approach were close to each other. Second, the flutter speeds reported by several researchers for several comparable bridges were comparable to the flutter speeds computed in this research.

The design flutter speed varies and depends on many factors, including site location, nature of the terrain, exposure category, and specific bridge owner requirements. The computed design flutter speed for the Second Tacoma Narrows Bridge, located in the U.S. state of Washington was 38 m/s (Al-Assaf 2006). The aforementioned Lion's Gate Bridge, located in Vancouver, British Columbia, Canada targeted a design flutter speed of 45 m/s. The flutter speeds computed in this research for 200 m and 400 m suspension bridges with an FRP deck were higher than the design flutter speed for both the Second Tacoma Narrows Bridge and the Lion's Gate Bridge. Of the 600 m bridge span with an FRP deck, the flutter speed was less than the Lion's Gate Bridge's targeted design flutter speed and greater than the Second Tacoma Narrows Bridge's targeted design flutter speed. These results support the consideration of an FRP deck on suspension bridges for short and medium spans (as long as 600 m) without causing aerodynamic instability of the bridge. A higher value of flutter speed could be obtained for an FRP deck if the deck shape is streamlined. According to the results obtained in this research, a suspension bridge with a streamlined box-shaped FRP deck might be able to span more than 600 m.

Chapter 7 - Comparative Cost Analysis of 200 m, 400 m, and 600 m Suspension Bridges with a Concrete and an FRP Deck

The use of an FRP deck in suspension bridges reduces the forces and sizes of all the bridge components. The reduction in the main cables tension forces leads to reduction in the cable size, tower size, and anchorage. However, the anchorage savings will depend on the soil type. Where the soil is stronger, the anchorage savings will be higher. This chapter explores the variations of the total cost of the bridges based on the variations of the soil conditions. Three type of soils were considered: sound rock, medium sand, and stiff clay.

7.1 Material Unit Prices

The prices considered in this research did not include items that are common for both bridges, such as bridge furniture (lighting, railings, scuppers, etc.). The prices also did not include side spans, approaches, or the parapets, since those are also common for both bridges. Other cost such as contractor mobilization, temporary works and monitoring were not included since they are common for all the bridges.

The unit prices for the various each bridge element were obtained from the following sources:

- Average prices for the main cables and hangers were obtained from two suppliers: Wire Rope Corporation of America (St. Joseph, Missouri, USA) and Wire Rope Industries (Pointe-Claire, Quebec, Canada).

- The prices of the saddles, clamps, hangers, and the anchorage frame were obtained from Clodfelter Bridges and Structures CBS (Houston, Texas, USA) and American Bridge Company (Coraopolis, Pennsylvania, USA).
- The deck concrete and tower concrete prices were obtained from R. S. Means and Engineering News Record (ENR).
- The FRP deck unit prices were obtained from Creative Pultrusions (Alum Bank, Pennsylvania, USA) and Zell Comp Inc. (Durham, North Carolina, USA).

All of the material unit prices are summarized in Table 7.1.

Table 7.1: Material Unit Prices

Item	**Material**	**Unit**	**Unit Price (USD)**
1	Deck	m^2	300
2	Steel girder, cross-beams, stringers	Ton	2,800
3	Main cable	Ton	5,000
4	Anchorage	m^3	400
6	Tower (45 m height)	m^3	1,000

7.2 Comparative Cost Analysis of the 200 m Suspension Bridges

The 200 m suspension bridges with a concrete deck and an FRP deck were fully analyzed in Chapter 4. To study the impact of the soil conditions on using the FRP deck, three types of soil were considered: sound rock, medium sand, and stiff clay. The next three sections explore the cost implications of these different soil types.

7.2.1 Sound Rock

The soil characteristics of sound rock were shown in Table 3.2. The design of the anchorage system was performed by computing the mass of the anchorage block. Equations 3.3, 3.4, and 3.5 were used to design the anchorage block. The detailed design calculations of the anchorage block are summarized in Table 7.2 for sound rock.

Table 7.2: Design of the Anchorage System of the 200 m Suspension Bridges with a Concrete Deck and an FRP Deck on Sound Rock

No.	Item	Unit	Concrete	FRP
1	Tension in main cables *(T)*	MN	31.4	11.6
2	Cable angle (ϴ)	Degree	21.1	21.1
3	Horizontal component *(H)*	MN	116.8	43.2
4	Vertical component *(V)*	MN	42.7	15.8

No.	Item	Unit	Concrete	FRP
5	Factored horizontal component	MN	175.2	64.7
6	Concrete density (ɣ)	MN/m^3	0.024	0.024
7	Friction factor (µ)	-	0.7	0.7
8	Quantity of concrete $M=(H/\gamma\mu)+V/\gamma$	m^3	**12,209**	**4,510**

The quantities of the steel girders, main cables, and hangers for the concrete deck bridge and the FRP deck bridge were computed and summarized in Chapter 4. The quantities, prices, and price per square meter for a 200 m span bridge using both a concrete deck and an FRP deck were calculated for a sound rock soil condition. The results were tabulated in Tables 7.3 and 7.4.

Table 7.3: Estimated Quantities and Costs of Materials of the 200 m Suspension Bridge with a Concrete Deck on Sound Rock

Item	Material	Unit	Concrete Deck on Steel Girder		
			Amount	Unit Price (USD)	Cost (USD)
1	Deck	m^2	4000	300	1,200,000
2	Steel girder, cross-beams, stringers	Ton	578.6	2,800	1,619,988
3	Main cable	Ton	187	5,000	935,000
4	Anchorage	m^3	12,209	400	4,883,448
5	Erection	job	1.0	2,000,000	2,000,000
6	Tower (45 m height)	m^3	1230.0	1,000	1,230,000
7	Tower base + piling	job	1	1,500,000	1,500,000
	Total				**13,368,453**

Table 7.4: Estimated Quantities and Costs of Materials of the 200 m Suspension Bridge with an FRP Deck on Sound Rock

Item	Material	Unit	GFRP Deck on Steel Girder		
			Amount	Unit Price (USD)	Cost (USD)
1	Deck	m^2	4000	700	2,800,000
2	Steel girders, cross-beams, stringers	Ton	302.2	2,800	846,126
3	Main cable	Ton	98	5,000	490,000
4	Anchorage	m^3	4,510	400	1,804,076
5	Erection	job	1.0	1,800,000	1,800,000
6	Tower (45 m height)	m^3	461.3	1,000	461,250
7	Tower base + piling	job	1	1,200,000	1,200,000
	Total				**9,401,453**

This initial construction cost estimate for a 200 m main span suspension bridge with concrete on steel stringer deck with anchorage founded in sound rock was found to be $13,368,435 ($3,342/m^2). The price for an FRP deck bridge is $9,401,453 ($2,350/m^2). The use of FRP deck for a 200 m span bridge represents a 30% reduction in cost as compared to a concrete deck bridge.

7.2.2 Medium Sand

The soil properties of medium sand are shown in Table 3.2. The quantities, prices, and price per square meter are calculated for each bridge for medium sand soil condition. The results are tabulated in Tables 7.5 and 7.6.

Table 7.5: Estimated Quantities and Costs of Materials of the 200 m Suspension Bridge with a Concrete Deck on Medium Sand

Item	Material	Unit	Concrete Deck on Steel Girder		
			Amount	Unit Price (USD)	Cost (USD)
1	Deck	m³	4000	300	1,200,000
2	Steel girders, cross-beams, stringers	Ton	578.6	2,800	1,619,988
3	Main cable	Ton	187	5,000	935,000
4	Anchorage	m³	16,380	400	6,552,133
5	Erection	job	1.0	2,000,000	2,000,000
6	Tower (45 m height)	m³	1230.0	1,000	1,230,000

7	Tower base + piling	job	1	3,000,000	3,000,000
	Total				**16,537,121**

Table 7.6: Estimated Quantities and Costs of Materials of the 200 m Suspension Bridge with an FRP Deck on Medium Sand

Item	**Material**	**Unit**	**GFRP Deck on Steel Girder**		
			Amount	**Unit Price (USD)**	**Cost (USD)**
1	Deck	m^2	4000	700	2,800,000
2	Steel girders, cross-beams, stringers	Ton	302.2	2,800	846,126
3	Main cable	Ton	98	5,000	490,000
4	Anchorage	m^3	6,051	400	2,420,533
5	Erection	job	1.0	1,800,000	1,800,000
6	Tower (45 m height)	m^3	461.3	1,000	461,250
7	Tower base + piling	job	1	2,400,000	2,400,000
	Total				**11,217,910**

For the medium sand soil condition, the price of anchorage, tower base, and piling increase significantly. The initial construction cost estimate of the concrete on steel stringer deck with anchorage founded in medium sand was found to be \$16,537,121 (\$4,134/m^2). The price for an FRP deck bridge is \$11,217,910 (\$3,040/m^2). The use of FRP deck for a 200 m span bridge represents a 32% of reduction in cost as compared to a concrete deck bridge.

7.2.3 Stiff Clay

For the stiff clay soil condition, the anchorage block is greater in size than the anchorage block in the case of medium sand. The results are tabulated in Tables 7.7 and 7.8.

Table 7.7: Estimated Quantities and Costs of Materials of the 200 m Suspension Bridge with a Concrete Deck on Stiff Clay

Item	Material	Unit	Concrete Deck on Steel Girder		
			Amount	Unit Price (USD)	Cost (USD)
1	Deck	m^2	4000	300	1,200,000
2	Steel girders, cross-beams, stringers	Ton	578.6	2,800	1,619,988
3	Main cable	Ton	187	5,000	935,000
4	Anchorage	m^3	20,031	400	8,012,233
5	Erection	job	1.0	2,000,000	2,000,000

Item	Material	Unit	Concrete Deck on Steel Girder		
			Amount	Unit Price (USD)	Cost (USD)
6	Tower (45 m height)	m^3	1230.0	1,000	1,230,000
7	Tower base + piling	job	1	3,000,000	3,000,000
	Total				17,997,221

Table 7.8: Estimated Quantities and Costs of Materials of the 200 m Suspension Bridge with an FRP Deck on Stiff Clay

Item	Material	Unit	GFRP Deck on Steel Girder		
			Amount	Unit Price (USD)	Cost (USD)
1	Deck	m^2	4000	700	2,800,000
2	Steel girders, cross-beams, stringers	Ton	302.2	2,800	846,126
3	Main cable	Ton	98	5,000	490,000
4	Anchorage	m^3	7,400	400	2,959,933

5	Erection	job	1.0	1,800,000	1,800,000
6	Tower (45 m height)	m^3	461.3	1,000	461,250
7	Tower base + piling	job	1	2,400,000	2,400,000
	Total				**11,757,310**

For the stiff clay, the initial construction cost estimate of the concrete on steel stringer deck with anchorage founded in stiff clay was $17,997,221 ($4500/m^2). The price for an FRP deck bridge is $11,757,310 ($3,939/m^2). The use of FRP deck for a 200 m span bridge represents a 34% reduction in cost as compared to a concrete deck bridge.

7.3 Comparative Cost Analysis of 400 m Suspension Bridges

The 400 m suspension bridges with a concrete deck and an FRP deck were fully analyzed in Chapter 5. To study the impact of the soil conditions on using the FRP deck, three types of soil were considered: sound rock, medium sand, and stiff clay. Section 7.3.1 describes the detailed comparative cost analysis calculations for sound rock soil type. Section 7.5.2 and 7.5.3 summarize the cost comparative analysis for medium sand and stiff clay soil types.

7.3.1 Sound Rock

The anchorage block of the 400 m span bridge was designed similarly to the anchorage block of the 200 m span bridge in section 7.2.1. The detailed design calculations for the anchorage block are summarized in Table 7.9 for sound rock.

Table 7.9: Design of the Anchorage System for 400 m Suspension Bridges with a Concrete Deck and an FRP Deck on Sound Rock

No.	Item	Unit	Concrete	FRP
1	Tension in main cables *(T)*	MN	68.9	23.6
2	Cable angle (Θ)	Degree	21.1	21.1
3	Horizontal component *(H)*	MN	256.3	87.8
4	Vertical component *(V)*	MN	93.7	32.1
5	Factored horizontal component	MN	384.5	131.7
6	Concrete density (ɣ)	MN/m^3	0.024	0.024
7	Friction factor (μ)	-	0.7	0.7
8	Quantity of concrete $M=(H/\gamma\mu)+V/\gamma$	m^3	**26,789**	**9,176**

The soil properties of sound rock are shown in Table 3.2. The quantities, prices, and price per square meter is calculated for each bridge for sound rock soil condition. The results are tabulated in Tables 7.10 and 7.11.

Table 7.10: Estimated Quantities and Costs of Materials of the 400 m Suspension Bridge with a Concrete Deck on Sound Rock

Item	Material	Unit	Concrete Deck on Steel Girder		
			Amount	Unit Price (USD)	Cost (USD)
1	Deck	m^2	8000	300	2,400,000
2	Steel girder, cross-beams, stringers	Ton	1157.1	2,800	3,795,000
3	Main cable	Ton	759	5,000	2,730,000
4	Anchorage	m^3	26,789	400	10,715,590
5	Erection	job	1.0	4,000,000	4,000,000
6	Tower (65 m height)	m^3	6205.5	1,250	7,756,875
7	Tower base + piling	job	1	3,000,000	3,000,000
	Total				**34,907,441**

Table 7.11: Estimated Quantities and Costs of Materials of the 400 m Suspension Bridge with an FRP Deck on Sound Rock

Item	Material	Unit	GFRP Deck on Steel Girder		
			Amount	Unit Price (USD)	Cost (USD)
1	Deck	m^2	8000	700	5,600,000
2	Steel girder, cross-beams, stringers	Ton	560.9	2,800	1,570,522
3	Main cable	Ton	443	5,000	2,215,000
4	Anchorage	m^3	9,176	400	3,670,362
5	Erection	job	1.0	3,600,000	3,600,000
6	Tower (65 m height)	m^3	2364.0	1,250	2,955,000
7	Tower base + piling	job	1	2,400,000	2,400,000
	Total				**22,010,884**

The initial construction cost estimate of the concrete on steel stringer deck with anchorage founded in sound rock was \$33,907,441 (\$4,238/m^2). The price for FRP deck bridge is \$22,010,884 (\$2,751/m^2). The use of FRP deck for a 400 m span bridge represents a 35% of reduction in cost as compared to a comparable bridge built with a concrete deck.

7.4 Comparative Cost Analysis of 600 m Suspension Bridges

The 600 m suspension bridges with a concrete deck and an FRP deck were fully analyzed in Chapter 5. To study the impact of the soil conditions on using the FRP deck, three types of soil were considered; Sound rock, medium sand, and stiff clay. Section 7.4.1 describes the detailed comparative cost analysis calculations for the sound rock soil type. Section 7.5.2 and 7.5.3 summarize the cost comparative analysis for medium sand and stiff clay soil types.

7.4.1 Sound Rock

The anchorage block of the 600 m span bridge was designed similarly to the anchorage block of the 200 m span bridge as seen in in section 7.2.1.

The detailed design calculations of the 600 m bridge anchorage block in sound rock are summarized in Table 7.12.

Table 7.12: Design of the Anchorage System of the 600 m Suspension Bridges with a Concrete Deck and an FRP Deck on Sound Rock

No.	Item	Unit	Concrete	FRP
1	Tension in main cables *(T)*	MN	116.8	44.1
2	Cable angle (Θ)	Degree	21.1	21.1
3	Horizontal component *(H)*	MN	434.5	164.1

No.	Item	Unit	Concrete	FRP
4	Vertical component *(V)*	MN	158.8	60.0
5	Factored horizontal component	MN	651.7	246.1
6	Concrete density (ɣ)	MN/m^3	0.024	0.024
7	Friction factor (µ)	-	0.7	0.7
8	Quantity of concrete $M=(H/\gamma\mu)+V/\gamma$	m^3	**45,413**	**17,147**

The soil properties of sound rock were shown in Table 3.2. The quantities, prices, and price per square meter are calculated for each bridge for the sound rock soil condition.

The results are tabulated in Tables 7.13 and 7.14.

Table 7.13: Estimated Quantities and Cost of Materials of the 600 m Suspension Bridge with a Concrete Deck on Sound Rock

Item	Material	Unit	Concrete Deck on Steel Girder		
			Amount	Unit Price (USD)	Cost (USD)
1	Deck	m^2	12,000	300	3,600,000
2	Steel girders, cross-beams, stringers	Ton	1735.7	2,800	4,859,963
3	Main cable	Ton	1800	5,000	9,000,000
4	Anchorage	m^3	45,413	400	18,165,181
5	Erection	job	1.0	10,000,000	10,000,000

Item	Material	Unit	Concrete Deck on Steel Girder		
6	Tower (85 m height)	m^3	17034.9	1,500	25,552,313
7	Tower base + piling	job	1	4,500,000	4,500,000
	Total				**75,677,456**

Table 7.14: Estimated Quantities and Cost of Materials of the 600 m Suspension Bridge with an FRP Deck on Sound Rock

Item	Material	Unit	GFRP Deck on Steel Girder		
			Amount	Unit Price (USD)	Cost (USD)
1	Deck	m^2	12,000	700	8,400,000
2	Steel girders, cross-beams, stringers	Ton	841.4	2,800	2,355,782
3	Main cable	Ton	1036	5,000	5,180,000
4	Anchorage	m^3	17,147	400	6,858,600
5	Erection	job	1.0	7,400,000	7,400,000
6	Tower (85 m height)	m^3	7504.9	1,500	11,257,313
7	Tower base + piling	job	1	3,600,000	3,600,000
	Total				**45,051,695**

The initial construction cost estimate for the concrete on steel stringer deck with anchorage founded in sound rock was $75,677,456 ($6,306/m^2). The initial construction cost for the FRP deck bridge was $45,051,695 ($3,754/m^2). The use of FRP deck for a 600 m span bridge represents a 41% reduction in cost as compared to a similar bridge with a concrete deck.

7.5 Sensitivity Cost Analysis of 200 m, 400 m, and 600 m Suspension Bridges with a concrete and an FRP deck on Three Different Soil Types

The use of FRP deck reduces the forces and sizes of all of the components of suspension bridges. The reduction in the main cables tension forces leads in reductions in the cable size, tower size and anchorage. However, the anchorage savings will depend on the soil type. Where the soil is strong, the anchorage savings will not be as high as it would be if the soil were weaker. This fact is demonstrated in Section 7.2 above of the 200 m model. The cost savings of using FRP deck for sound rock was 30%, increased to 32% for medium sand, and increased to 34% for stiff clay. This section explores the variation of the total cost based on variation of soil type for all of the bridge models considered in this research.

7.5.1 Sound Rock

The quantities resulted from the design of all the models on sound rock is tabulated below in Table 7.15. For sound rock soil type, the cost reduction due to the use of FRP deck increased from 30% for 200 m span bridge to 35% for a 400 m span bridge and 41% for a 600 m span bridge as shown in Table 7.15 and Figure 7.1. This shows that the use of the FRP deck is more advantageous as the free span of suspension bridges increases.

Table 7.15: Estimated Cost of 200 m, 400 m, and 600 m Suspension Bridges with a Concrete Deck and FRP Deck on Sound Rock (USD)

Span (m)	**200**	**400**	**600**
Cost for concrete deck	13,368,435	33,842,441	75,677,456
Cost for concrete deck/m^2	3342	4230	6306
Cost for FRP deck	9,401,453	21,670,884	45,051,695
Cost for FRP deck/m^2	2350	2709	3754
Percentage cost reduction	30	35	41

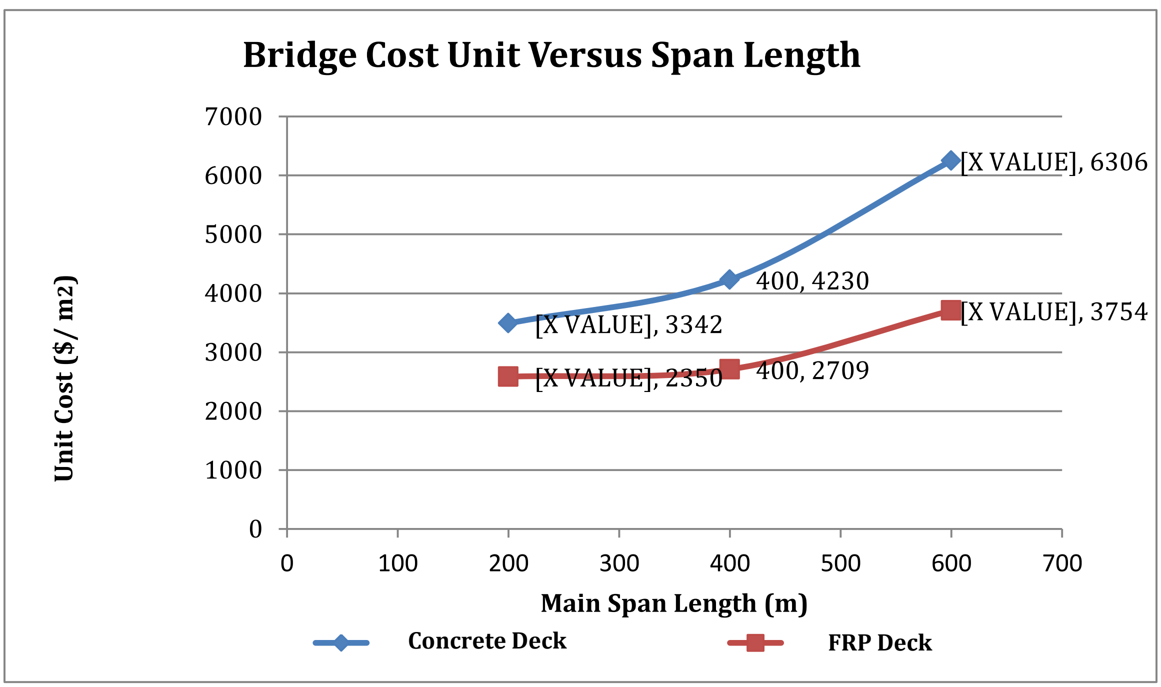

Figure 7.1: Estimated Cost of 200 m, 400 m, and 600 m Span Bridges with a Concrete and an FRP Deck on Sound Rock

7.5.2 Medium Sand

Similar analysis was performed for medium sand; the results are tabulated in Table 7.16.

Table 7.16: Estimated Cost of 200 m, 400 m, and 600 m Suspension Bridges with a Concrete Deck and an FRP Deck on Medium Sand (USD)

Span (m)	200	400	600
Cost for concrete deck	16,537,213	41,568,983	86,384,542
Cost for concrete deck/m^2	4134	5196	7199
Cost for FRP deck	11,217,910	25,665,055	50,995,295
Cost for FRP deck/m^2	2804	3208	4250
Percentage cost reduction	32	38	41

Similar to the sound rock soil type, the cost savings increases as the span increases from 32% to 41% as shown in Table 7.16 and Figure 7.2. However, the overall savings were higher for each model than in the case of sound rock soil type.

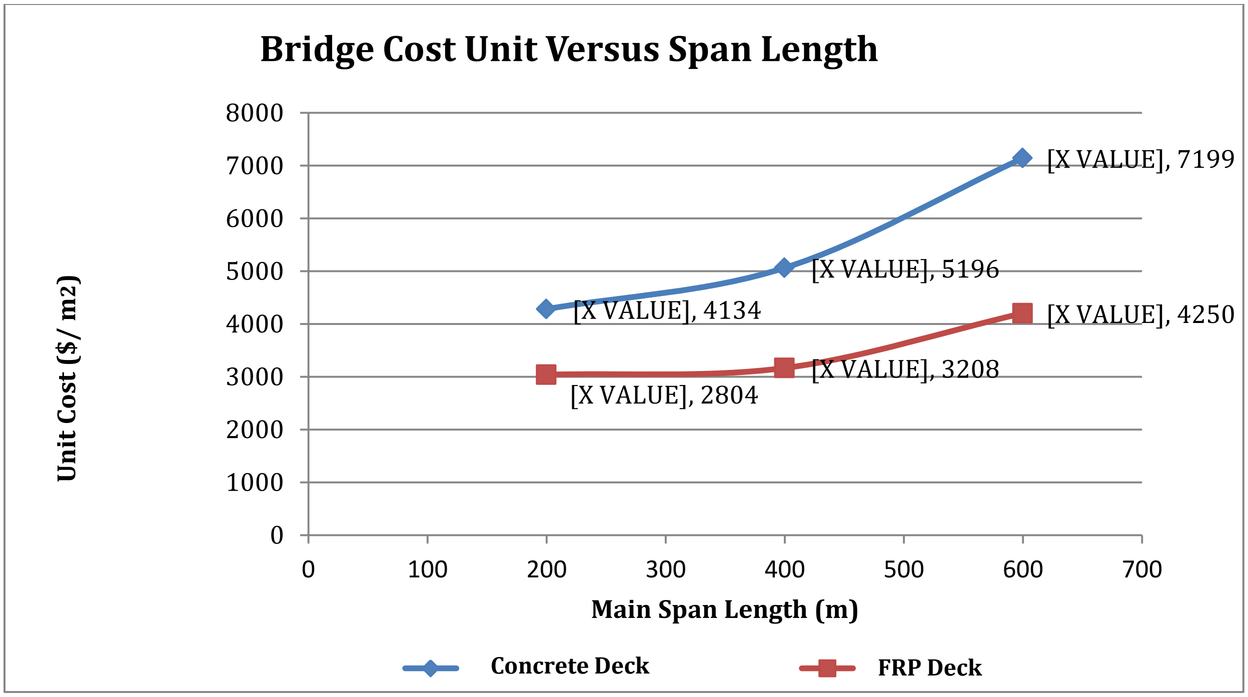

Figure 7.2: Estimated Cost in (USD) of 200 m, 400 m, and 600 m Span Bridges with a Concrete and an FRP Deck on Medium Sand

7.5.3 Stiff Clay

Similar analysis was performed for stiff clay soil type. The results are shown in Table 7.17.

Table 7.17: Estimated Cost of 200 m, 400 m, and 600 m Suspension Bridges with a Concrete Deck and an FRP Deck on Stiff Clay (USD)

Span (m)	200	400	600
Cost for concrete deck	17,997,721	44,772,833	91,815,739
Cost for concrete deck/m^2	4499	5597	7651
Cost for FRP deck	11,757,310	26,762,455	53,045,945
Cost for FRP deck/m^2	2939	3345	4420
Percentage cost reduction	34	40	42

The estimated bridge costs of the 200 m, 400 m, and 600 m span bridges with concrete decks and FRP decks on stiff clay were plotted in Figure 7.3.

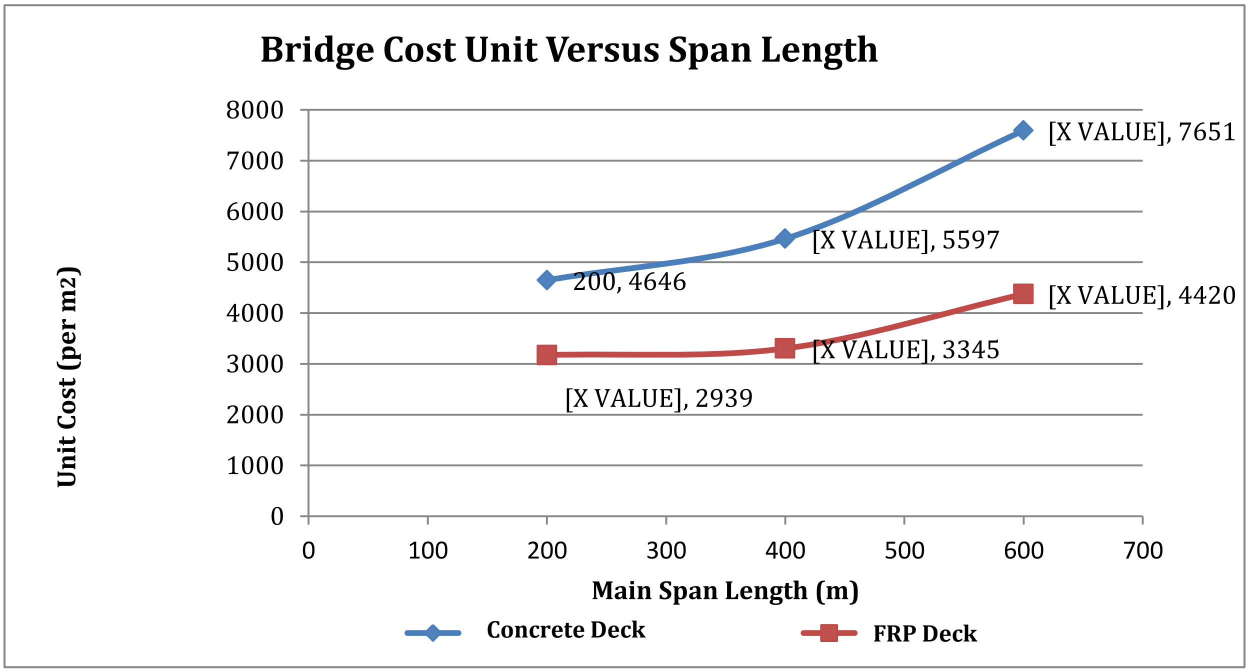

Figure 7.3: Estimated Cost of 200 m, 400 m, and 600 m Span Bridges with a Concrete and an FRP Deck on Stiff Clay

The cost of all bridges with span lengths of 200 m, 400 m, and 600 m with a concrete deck and FRP deck founded in the three different soil conditions (sound rock, medium sand, and stiff clay) are shown in Figure 7.4.

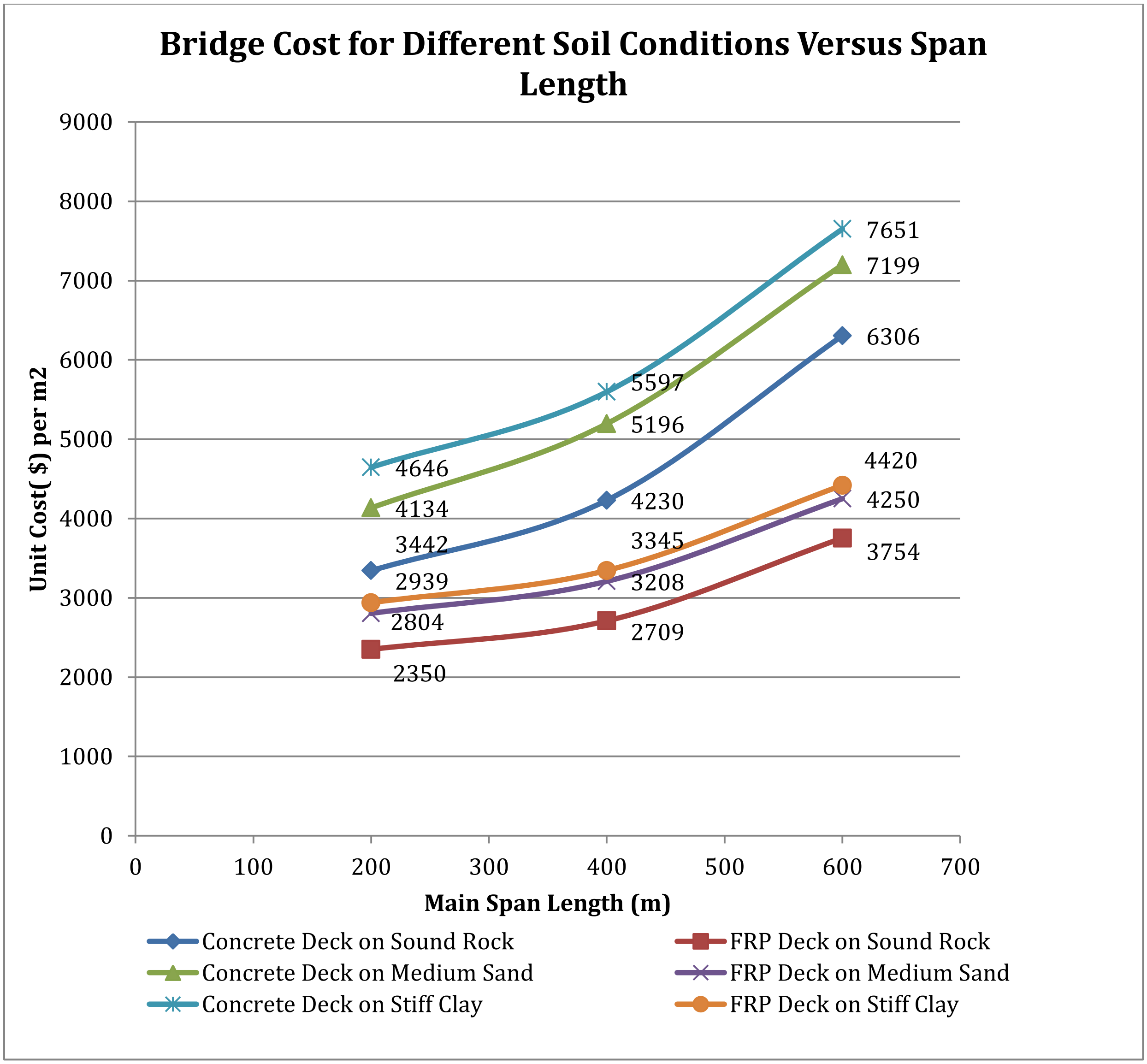

Figure 7.4: Bridge Cost in USD for Different Soil Conditions (Sound Rock, Medium Sand and Stiff Clay) Versus Span Length (200 m, 400 m, and 600 m)

7.6 Discussion of Results

Consistent with the research hypothesis, while the cost of the FRP deck is more than twice the cost of the concrete deck, the overall cost of the bridge using an FRP deck was predicted to be 30% to 42% less than the cost of the bridge using a concrete deck. Significant savings on all the other items, including steel girders, main cable, anchorage system towers, and towers foundation was achieved by using FRP deck. The design was controlled by deflection, so the steel girders and cable size provided was larger than required to resist the main cables tension. This increase of steel girders section and increase in cable size were designed to provide more stiffness to meet the deflection criteria. If the deflection limit is increased, then a more efficient design could be accomplished which will result in further cost reduction.

The total cost of all the bridges with a concrete deck or FRP deck increased with the increase of the span length. The increase is not linear because the increase of the main cables tension is based on the square of the span length. The main cables tension affects the quantities and cost of the main cable, the towers, and the anchorage. However, the increase of the bridge span length causes a linear increase in the quantities and cost of the deck area and the steel girders supporting the deck for both concrete and FRP decks. Accordingly, the total cost increase was higher than a linear increase with the bridge span length but less than an increase proportional with the square of the bridge span length.

The cost reduction depends on the span length and soil type. The maximum reduction was realized for the longer span of 600 m and the least resistant soil type (stiff clay). The use of FRP deck reduces the main cables tension force and consequently the anchorage quantities and cost. This reduction in the tension forces has less impact when the soil type has high resistance properties. The lowest cost computed for all the bridges was in the case of sound rock. The cost obtained for all the bridges was close in the cases of medium sand and stiff clay soil type.

The cost of all the bridges with spans of 200 m, 400 m, and 600 m with FRP decks founded in all the soil types were lower than all of the bridges with concrete decks founded in all of the soil types (Figure 7.4).

The lowest cost of the bridges is when the bridge is founded in sound rock. The highest bridge cost was when the bridge is founded in stiff clay. Even the lowest cost of the 200 m span bridge with a concrete deck was found to be 14% higher than the highest cost of the 200 m span bridge with an FRP deck (Figure 7.4).

Chapter 8 - Conclusions and Recommendations

This research addressed the use of FRP composites as deck materials for suspension bridges. FRP composites were used only for the deck; conventional construction materials were used for all other elements of the bridge—reinforced concrete for the towers and steel strands for the main cables and suspenders. The main objective of this research was to explore the aerodynamic and economic implications of reducing the dead weight of the deck when FRP composites are used.

The hypothesis of this research led to the following questions:

1. Would suspension bridges constructed with an FRP deck be more or less cost-effective than those constructed with reinforced concrete deck? How do the costs compare and what impact does soil condition have on the comparison?
2. How would suspension bridges constructed with an FRP deck behave aerodynamically?

To answer these questions, two groups of suspension bridges with 200 m, 400 m, and 600 m free spans, one group using reinforced concrete deck and the other group using the much lighter FRP deck were designed for three different soil conditions. Then, the aerodynamic stability of all the models was examined using Selberg's approach.

Three-dimensional finite element analysis was performed for each bridge to obtain the values for the torsional moment of inertia and the vertical and torsional frequencies. These values were used in Selberg's equation to determine the flutter speed of each bridge. A linear elastic analysis was performed to validate the three-dimensional finite element analysis results. The predicted flutter speeds obtained from the linear elastic approach and the finite element approach were within 9% for all the spans and deck materials. Because of the use of FRP deck, the reductions in the predicted flutter speed of the 200 m span bridge, 400 m span bridge, and 600 m span bridge were 35%, 36%, and 37%, respectively. Several researchers performed analysis and wind tunnel tests to get the flutter speeds of some existing suspension bridges, including the Second Tacoma Narrows Bridge (USA) and the Lion's Gate Bridge (Canada). The flutter speeds calculated and tested for these bridges were comparable to the flutter speeds obtained in this research. As discussed in Chapter 6, streamlined box-shaped FRP deck can attain higher values for flutter speeds than the H-shaped deck that was considered in this research. Thus, it can be concluded from this research that suspension bridges constructed from streamlined box-shaped FRP deck could span more than 600 m.

The comparative cost analysis indicated that the overall cost savings resulting from the use of FRP deck varies from 30% to 42% in spite the fact that the cost of the FRP deck is more than twice the cost of the concrete deck. Significant savings on all the other items, including steel girders, main cables, anchorage system towers, and tower foundation, was achieved by using FRP deck. In addition, these research findings show that the soil conditions influence the cost reduction. Maximum cost savings were obtained in the cases of stiff clay and medium sand.

The current practice in bridge construction limits the use of FRP deck for small-scale bridges and rehabilitation of existing bridges. This research explored the use of FRP deck in suspension bridges. Most previous researchers used FRP deck for small bridges. They have shown that FRP deck can be advantageous when the design lifetime of the bridge is long and significant savings can be realized from maintenance cost savings.

The other effective use for FRP deck demonstrated in previous research is in the rehabilitation of bridges to increase their live load capacity. While earlier research has demonstrated that bridges constructed with an FRP deck could be cost effective in the long term because they require less maintenance, the findings of this research showed that the use of FRP deck could also result in a lower *initial* construction cost.

To build on the findings of this research, future research on the implications of using an FRP streamlined box shaped deck for aerodynamic stability is recommended. For suspension bridges with span lengths longer than 600 m, a wind tunnel test will be highly recommended to investigate its aerodynamic stability.

The study of the aerodynamic stability of suspension bridges using lighter weight deck materials will help explore another solution for long-term maintenance of aging suspension bridges. Some suspension bridges have been in service for well over 70 years, such as the Bronx-Whitestone Bridge. They experience heavier loads than they were originally designed to support. Future research that addresses the aerodynamic challenges of using lighter deck in such bridges will be very useful. Using a lighter deck solution will help such bridges to support heavier live loads and avoid the need for total replacement.

Chapter 9 - References

www.fhwa.dot.gov

www.ncn-uk.co.uk

www.midasuser.com

Podolny, W. (2006) Structural Steel Designer's Handbook: AISC, AASHTO, AISI, ASTM, AREMA and ASCE-07 Design Standards, Fourth Edition- Chapter 15. New York, NY: McGraw-Hill.

Ammann, O.H. (1939), Discussion of Preliminary Design of Suspension Bridges. Trans. Am. Soc. Civ. Eng., 104, 625.

Simiu, E. and Scanlan, R., Wind Effects on Structures, 3rd Ed., Wiley, New York, 1986.
Strouhal, V., On a particular way of tone generation (German), Vol. 5, 1878.

Parkinson, G. (1989), Phenomena and Modeling of Flow-Induced Vibrations of Bluff Bodies, Aerospace Science, Vol. 16 (1989), pp. 169-224.

Rothman, H. (1984), One Hundred Years of Suspension Bridges: From the Era of the Brooklyn Bridge to Today. Bridge to the Future; A Centennial Celebration of the Brooklyn Bridge, Ann. N.Y. Acad. Sci., 424, 107-128.

Selberg, A., Oscillation and Aerodynamic Stability of Suspension Bridges, Acta Polytechnia Scandinavia, Civil Engineering and Construction, Series 13, Trondheim, 1961.

Alagusundar, A., Harik, E. and Choo, C. (2006), Structural Behavior of FRP Composite Bridge Deck Panels, Journal of Bridge Engineering, ASCE, pp. 384-399. July-August, 2006.

Farhey D. (2006), Long-Term Performance Monitoring of the Tech 21 All-Composite Bridge, Journal of Composites for Construction, pp. 255-262. May-June, 2006.

Wu, H., Fu, R. Gibson, A. Yan, Warnemuende, K.and Anumandla, V. (2006), Durability of FRP Composite Bridge Deck Materials under Freeze-Thaw and Low Temperature Conditions, Journal of Bridge Engineering, ASCE, pp. 433-451. July-August, 2006.

Wattanadechachan, P., Riyadaboutaha, O. Hag-Elsafi, and Alampalli, S., (2006), Thermal Compatibility and Durability of Wearing Surfaces on GFRP Bridge Decks. Journal of Bridge Engineering, ASCE, pp. 465-473. July-August, 2006.

Nishizaki, I. (2006), A Case Study of Life Cycle Cost based on a Real FRP Bridge, Third International Conference on FRP Composites in Civil Engineering (CICE 2006) December 13-15 2006, Miami, Florida, USA.

Mark A.Ehlen and Harold E. Marshall (1996) The Economics of New – Technology Materials.
Meiarashi, S., Nishizaki, I. and Kishima, T. (2002), Life Cycle Cost of All-Composite Suspension Bridge. Journal of Composites for Construction, pp. 206- 213. November 2002.

Ehlen, M. (1999), Life Cycle Costs of Fiber-Reinforced-Polymer Bridge Decks, Journal of Materials in Civil Engineering / August 1999.

Key, S. (2005), Vortex Formation and Turbulence on Soap Film, Report Project, St John's College.

M. Matsumoto, H. Matsumiya, S. Fujiwara, Y. Ito, New Consideration on Flutter Properties basing on SBS-Fundamental Flutter Mode, Similar Selberg's Formula, Torsional Divergence Instability, and New Coupled Flutter Phenomena affected by Structural Coupling ; BBAA VI International Colloquium on: Bluff Bodies Aerodynamics & Applications ; Milano, Italy, July, 2008.

Fiber-Reinforced Polymer Composites for Construction (2002), Journal of Composites for Construction May (2002).

Wang, X. Wu, Z., (2010) Integrated High-Performance Thousand-Metre Scale Cable-Stayed Bridge with Hybrid FRP Cables. Composites Part B, 41, 166-175. (2010)

Adanur, S., Mosallam, S., Shinozuka, M., Gumusel, L. (2011) A comparative study on static and dynamic responses of FRP composite and steel suspension bridges. Journal of Reinforced Plastics and Composites; 30 (15) 1265-1279. (2011).

Kuyumcu Z and Ates, S. (2012) Soil-Structure Foundation Effects on Stochastic Response Analysis of Cable-Stayed Bridges. Structural Engineering and Mechanics, 43 (5) 63. (2012).

Yao, J., YANG, Y. (2008) Bridging Capacity and Aerodynamic Challenge of Long-Span Suspension Bridges; January 24-26, 2008.

Toshio Miyata (2003), Historical View of Long-Span Bridge Aerodynamics; Journal of Wind Engineering and Industrial Aerodynamics, (2003) .

René Walther, David Amsler; (1994), Hybrid Suspension Systems for Very Long Span Bridges: Aerodynamic Analysis and Cost Estimates, 15 October 1994.

Ehlen, M., Marshall, H. (1996),The Economics of New Technology Materials: A Case Study of FRP Bridge Decking, National Institute of Standard & Technology, July 1996.

The United Kingdom Design Manual for Bridges BD 49/01 Standard (Volume 1, Section 3, Part 3)

The United Kingdom Design Manual for Bridges BD 90/05 Standard (Volume 1, Section 3, Part 17)

Ammann, O.H. (1953), Present Status of Design of Suspension Bridges with Respect to Dynamic Wind Action, Trans. Boston Soc. Eng., 40(3), 231-253.

Steinman, D.B. (1943), Rigidity and Aerodynamic Stability of Suspension Bridges. Proceedings American Society of Civil Engineering, 69, 1361-1367

Zdravokovich, M. (1996), Different Modes of Vortex Shedding: an Overview, Journal of Fluids and Structures, Vol. 10 (1996), pp. 427-437.

Sakata, H. (1971), A Study of Suspension Bridge with Shallow Box-Type Suspended Structure, Proc. Wind Effects on Buildings and Structures, Saikon, Tokyo: 953-964, 1971.

Scanlan, R., and Budlong, K. (1972), Flutter and Aerodynamic Response Considerations for Bluff Objects in a Smooth Flow, Flow-Induced Structural Vibrations, Proceedings Symposium. VTAM-IAHR, Karlsruhe, Springer, Berlin, Germany: 39-354, 1972.

Scanlan, R.H. (1979), on the State of Stability Considerations for Suspended Span Bridges under Wind, Proceedings of IUTAM-IAHR Symposium, Karlsruhe, Germany, Paper F1:595-618, 1979.

Kim, H., Kim, S. and Lee, Y. (2004). Design of GFRP Deck and Deck-to-Girder Connections for Girder Bridges, ASCE Journal of Civil Engineering, January 2004.

Gimsing, N. (1997), Cable Supported Bridges, Concept & Design, Second Edition, Chichester, United Kingdom: John Wiley & Sons.

Vickneswaran, S. and Eyre, J. (2011), Deck Stiffness Selection in the Design of Long Span Cable Stayed Bridges, ICSECM - Kandy - Sri Lanka - (15th to 17th December 2011).

Xinzhong, C. (2007), Improved Understanding of Bimodal Coupled Bridge Flutter Based on Closed-Form Solutions, Journal of Structural Engineering, Vol. 133, No. 1, January 1, 2007.

Panneer, R, Govindaswamy, S., (2001), Aero-elastic Analysis of Bridge Girder Section Using Computer Modeling, Report for Blackwell Transportation Center, May 2001.

Viana, R., Freitas, M.Grebogi, C. (2005), Estimation of Model Parameters in Nonlinear Engineering Systems: The Case of Suspension Bridge Oscillations, Proceedings of the Workshop on Nonlinear Phenomena Modeling and Their Applications. Saint Paulo, Brazil

Bleich, F. (1948), Dynamic Instability of Truss-Stiffened Suspension Bridges under Wind Action, Proc., ASCE, 1948.

Morgenthal, G. Advances in Numerical Bridge Aerodynamics and Recent Applications, Structural Engineering International, IABSE, Zurich, Vol. 15, No. 2, (2005).

Szabó, F.and Györgyi., J. (2009), Three-Dimensional Fluid-Structure Interaction Analysis for Bridge Aero-elasticity, Proceedings of the World Congress on Engineering and Computer Science 2009 Vol. II WCECS 2009, October 20-22, 2009, San Francisco, USA.

Davenport A. and King, J. (1985), The Incorporation of dynamic Wind Loads into the Design Specifications for Long Span Bridges, ASCE Fall Convention, New Orleans, La., 1985.

Brockenbrough, R. Merritt, F., Structural Steel Designer's Handbook: AISC, AASHTO, AISI, ASTM, AREMA, and ASCE-07 Design Standard, Fourth Edition. (McGraw-Hill Professional, 2006).

Koichi Yokoyama. (1998), New Challenges for Long-Span Bridges Crossing Japan's Stairs in 21 St Century, The International Seminar on Bridge Aerodynamics Perspective, ISBAP, 1998, Long-Span Bridge and Aerodynamics, Kobe, Japan, 1998.

Davenport, A.G., J.P.C. King. Dynamic Wind Forces on Long Span Bridges, the IABSE Congress, Vancouver, B.C., Sep. 3-7, 1984, pp. 705-712.

Nystrom, H., Watkins, S., Nanni, A., and Murray, S. (2003), Financial Viability of Fiber-Reinforced Polymer (FRP) Bridges, Journal of Management in Engineering, pp. 2-8. January 2003.

Wei- Xin, R. et al. (2004), Roebling Suspension Bridge. I: Finite Element Model and Free Vibration Response. Journal of Bridge Engineering, pp. 110-118. April 2004.

Wei- Xin, R. et al. (2004), Roebling Suspension Bridge. II: Ambient Testing and Live Load Response. Journal of Bridge Engineering, pp. 119-126. April 2004.

Stiller, W., Gergely, J. and Rochelle, R. (2006), Testing, Analysis, and Evaluation of GFRP Deck on Steel Girders, Journal of Bridge Engineering, ASCE, pp. 394-400. July-August, 2006.

Zhang, Y., Cai, C., Shi, X. and Wang, C. (2006), Vehicle-Induced Dynamic Performance of FRP versus Concrete Slab Bridge, Journal of Bridge Engineering, ASCE, pp. 410-419. July-August, 2006.

Cheng, L. and Karbhari, V., Fatigue Behavior of a Steel-Free FRP-Concrete Modular bridge deck System. Journal of Bridge Engineering, ASCE, pp. 474-488.

Cole, T., Lopez M. and Ziehl, P. (2006), Fatigue behavior and Nondestructive Evaluation of Full- Scale FRP Honeycomb Bridge Specimen, Journal of Bridge Engineering, ASCE, pp. 420-429. July-August, 2006.

AASHTO LRFD Bridge Design Specifications, 7th Edition. (2012). American Association of State Highway and Transportation Officials, Washington, D.C.

Wight, R., Erki, M., Shyu, C., Tanovic, R. and Heffernan, P. (2006), Development of FRP Short-Span Deployable Bridge-Experimental Results, Journal of Bridge Engineering, ASCE, pp 489-498 July-August, 2006.

Hines, E., Buonopane, S., Garlock, M., Festschrift Billington (2012), International Network for Structural Art, (2012)

Huebner, K. H., Thornton, E. A., and Byron, T. G. (1995), The Finite Element Method for Engineers. New York, NY: Wiley, John and Sons

Milne-Thomson, L.M. (1996), Theoretical Aerodynamics. New York: Dover Publications.
Buonopane, S. , Billington, D. (1993), Theory and History of Suspension Bridge Design from 1823 to 1940, Journal of Structural Engineering, Volume 119, Number 3, March 1993.

M. Barelli, J. White, D. Billington (2006), History and Aesthetic of the Bronx-Whitestone Bridge, Journal of Bridge Engineering, April 2006

Appendix I. Detailed Design Calculations for the Longitudinal and Cross-Girders of the Concrete and FRP Decks of the 200 m, 400 m, and 600 m Suspension Bridges

I.1 Introduction

Appendix I describes the detailed serviceability design calculations of the concrete deck and FRP deck. A panel spanning between the hangers consists of two longitudinal girders and cross-girders as shown in Figure I.2 was analyzed and designed. The design of the cross-girders and longitudinal girders was based on ultimate limit state (ULS) and checked for serviceability limit state (SLS). The typical deck panel was used for all the bridges: 200 m, 400 m, and 600 m free spans. The material properties used are as indicated in Table I.1 below.

Table I.1: Material Properties

Materials	**Unit**	**Concrete-30**	**GFRP**	**Steel**	**Strands**	
Elements		Deck Case-1	Deck Case-2	Girders	Main Cable	Hangers
Density	KN/m³	25	-	78	78	78
Weight	KN/m²	5	1.2	-	-	-
Elastic modulus	GPa	23	25	205	197	197
Poisson's ratio		0.2	0.25	0.3	0.3	0.3

I.2 Methodology

First, one unit of the deck system for the two cases, composite concrete deck and GFRP deck, is modeled alone for moving load analysis case. One unit of a typical panel of cross-girders and longitudinal girders was designed in accordance to AASHTO 2012 specifications. The steel girders were designed as composition for the concrete deck and non-composite for the FRP deck. The girder arrangements are shown in Figure I.2 for the concrete deck and the FRP deck.

The installation process of the FRP deck is shown in Figure I.1 below. The arrangements of the cross-girders and longitudinal girders are different for the concrete deck and FRP deck. Thus, there are differences in the arrangement of the deck-supporting beams for concrete and FRP as shown in Figure I.2.

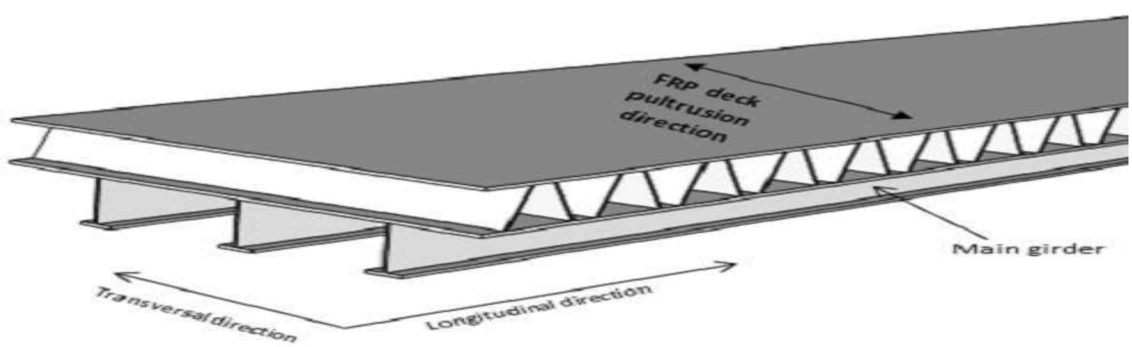

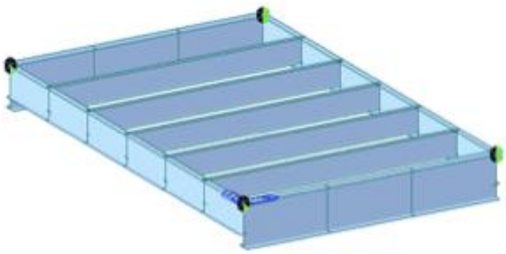

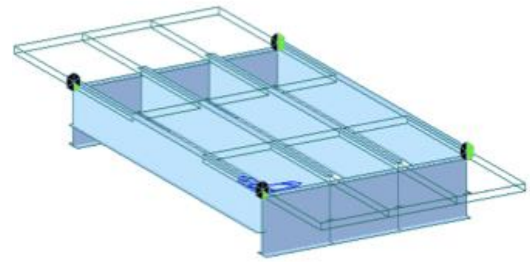

Concrete Deck **FRP Deck**

Figure I.2: Arrangements of the Deck-Supporting Beams

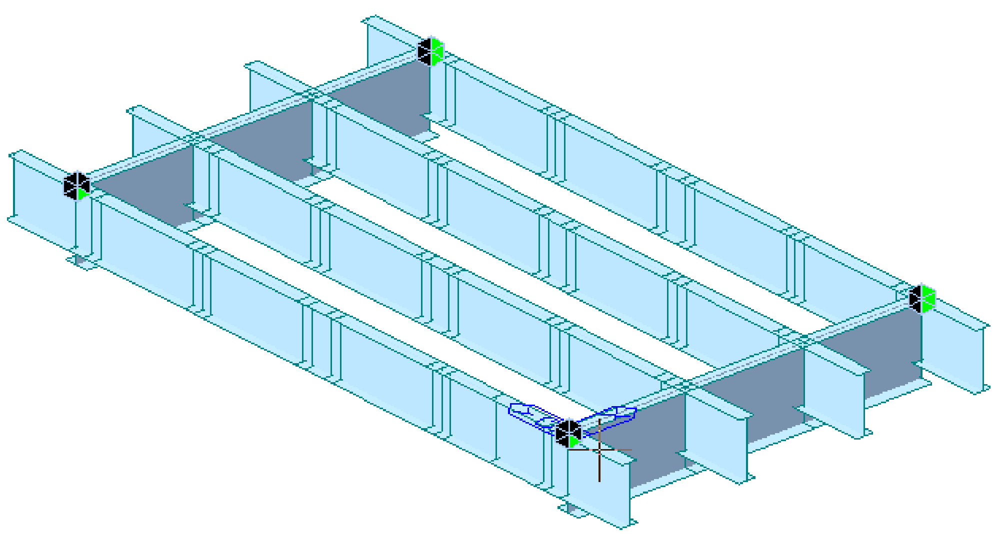

Figure I.3: Typical Deck Panel between Hangers (FEA Model)

I.3 Design Specifications

The design was performed in accordance with AASHTO LRFD Bridge Design Specifications, 2012.

I.4 Deck Description

The typical deck has a width of 20 m that includes two footways 1.5 m wide at each side. The cross-girders are framed into and supported by longitudinal-girders. The hangers are spaced every 10 m and supported by the longitudinal-girders. The hangers transmit the loads carried by the deck to the main cables. The typical cross-section is shown in Figure I.4 of the 200 m span bridge; it is similar to the 400 m and 600 m span bridges.

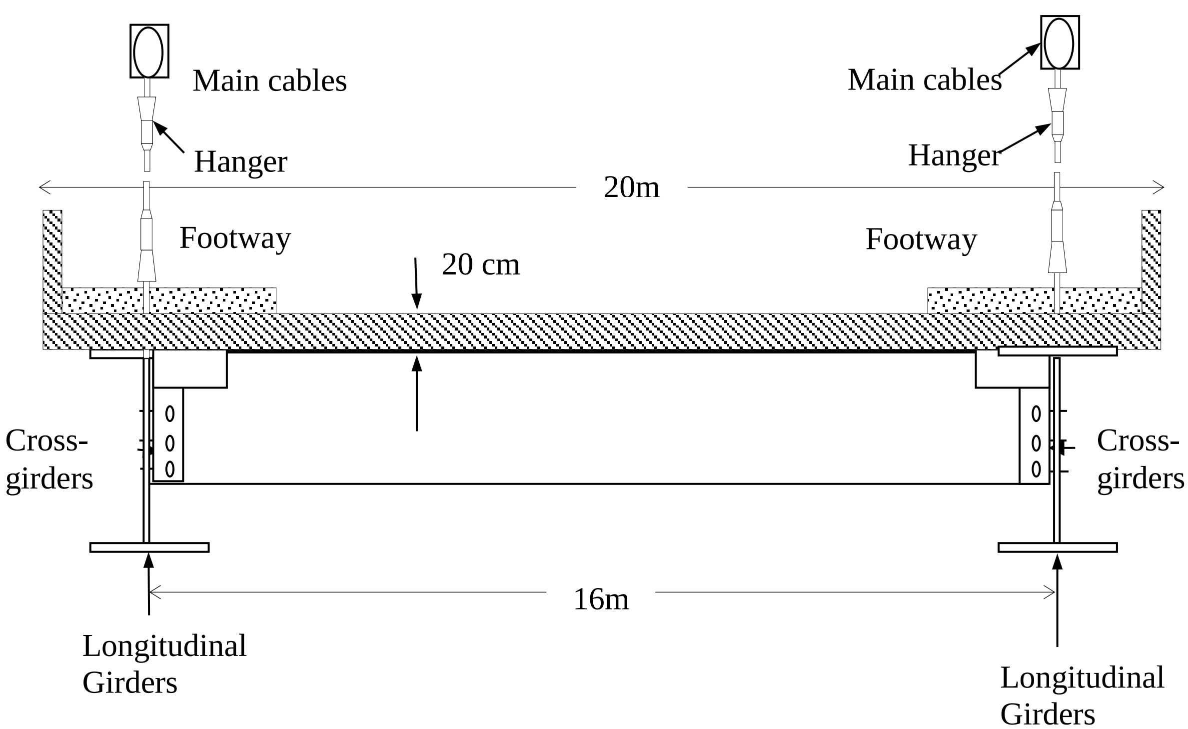

Figure I.4: Typical Cross-Section of the Suspension Bridge

I.5 Design of a Typical Panel Supporting a Concrete Deck

The plan of the 200 m span bridge is detailed in Figure I.5.

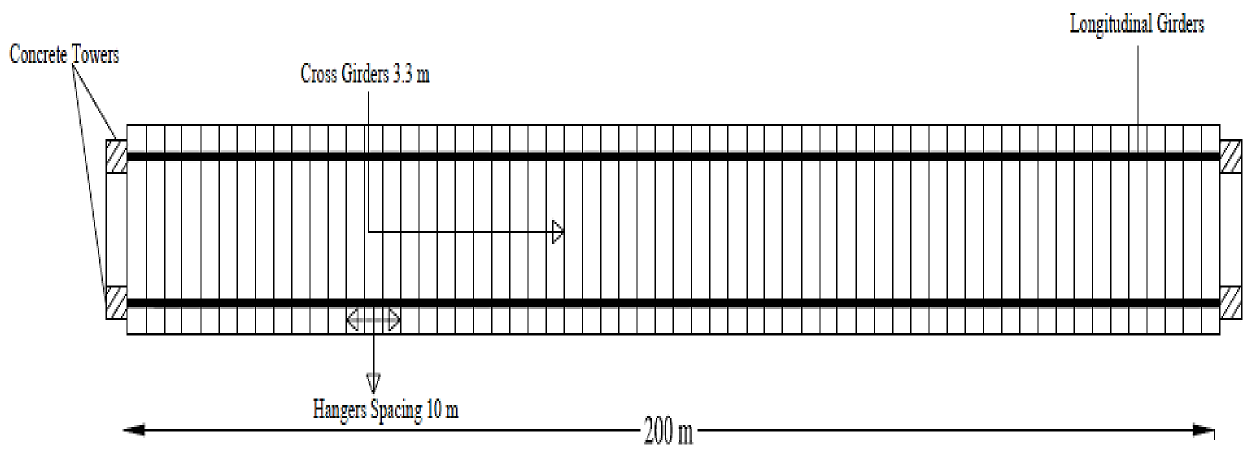

Figure I.5: Plan (Concrete Deck)

I.6 Design Loads

This section describes the dead loads and live loads used for the design of steel girders supporting the concrete deck.

I.6.1 Dead Load

The concrete self-weight was calculated by multiplying the total deck thickness of 0.2 m and the concrete density of 25 kN/m^3 . The deck weight used in the design is 5 kN/m^2.

I.6.2 Steel Section

The section of the cross-girder is shown in Figure I.6. The cross-girder weight is 2.9 N/m and is spaced at 3.33 m with a span of 16 m.

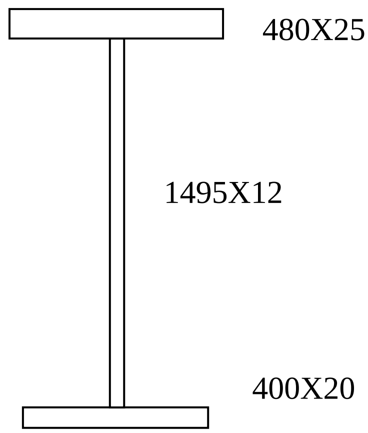

Figure I.6: Typical Steel Section

(All dimensions are in mm)

I.6.3 Superimposed Dead Load

Asphalt thickness = 60.0 mm

Asphalt density = 23.0 kN/m^3

Asphalt wt = 23x0.06 = 1.38 kN/m^2

I.7 Design Vehicular Live Load

Vehicular live load on the bridge designated HL-93 AASHTO-LRFD, which shall consist of combination of both design truck or design tandem, and the design lane load.

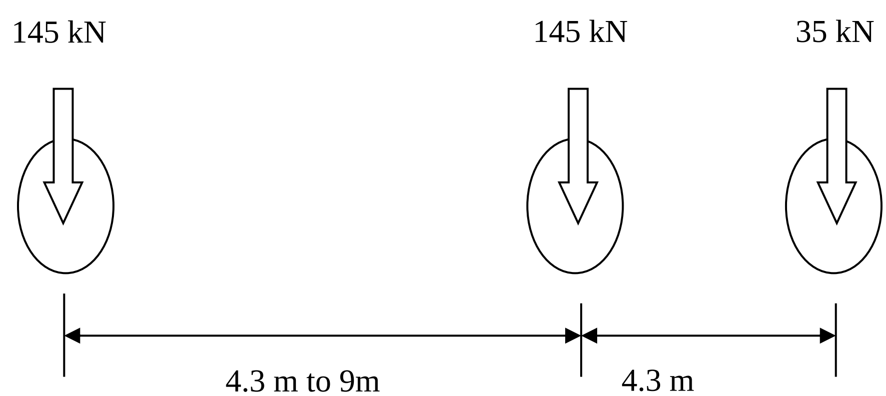

Figure I.7: Truck Loading Configuration
(*Adopted from AASHTO –2012)*

I.8 Truck Load

Standard vehicle live loads have been ASHTO-LRFD for use in bridge design as shown in Figure I.8.

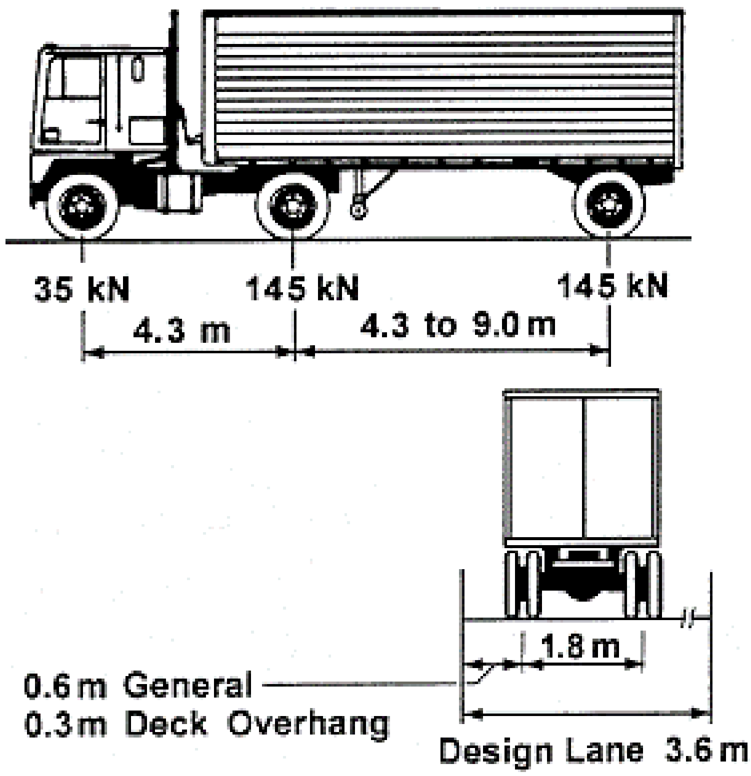

Figure I.8: HL-93 Truck

(Adopted from AASHTO S-LRFD Specifications)

I.9 Tandem Load

Tandem loading is used to model heavy trucks of a pair of 110 kN. Tandem refers to two closely spaced axles. Legally defined by the distance between the axles with 1.2 m, the transverse spacing of wheels shall be considered 1.8 m.

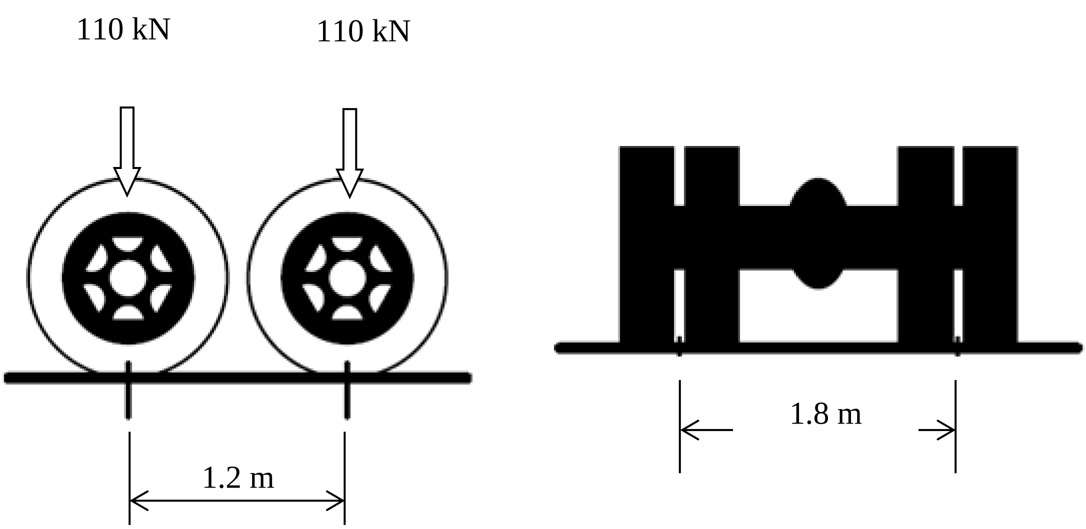

Figure I.9: Tandem Load

(Adopted from AASHTO S-LRFD Specifications)

I.10 Lane Load

The design lane load shall consist of a load of 9.3 N/mm uniformly distributed in the longitudinal direction transversely, the design lane load shall be assumed to be uniformly distributed over a 3.0 m width. The force effects from the design lane load shall not be adjusted to a dynamic load allowance.

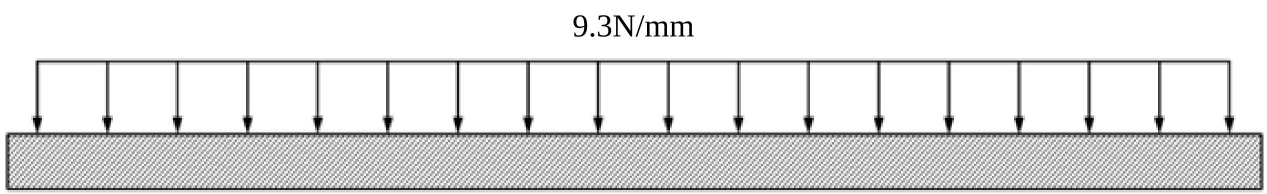

Figure I.10: Lane Load

(Adopted from *AASHTO Standard Specifications*)

I.11 Load Combination and Load Factors

Table I.2: Load Factors for Permanent Loads

Limit State Load Combination	Dead Load	Live Load + Impact	Superimposed Loads
Service I	1.00	1.00	1.00
Service II	1.00	1.30	1.00
Service III	1.00	0.80	1.00

I.12 Critical Loading

Truck load + lane load or tandem load + lane load

The critical loading envelope, which indicate tandem load + lane load, controls the design. The results are summarized in Table I.3 for the cross – girder and the longitudinal girder for the concrete deck.

Table I.3: Moment and Shear Results for the Concrete Deck

Tandem loads + lane loads control

No.	Element	Moment (kN.m)	Shear (kN)
1	Cross-girder	4,044	592
2	Longitudinal girders	7,930	1,100

I.12.1 Serviceability Limit Service Check (Concrete Deck)

A serviceability limit state check was performed on the cross-girders and the longitudinal girders. Section I.12.2 describes the serviceability check for the cross-girders, while Section I.12.3 describes the serviceability check for the longitudinal girders.

I.12.2 Cross-Girder Check (Concrete Deck)

Cross-girders section properties:

Section modulus Z is define by equation (I.1)

Section modulus Z = 1.45 E+07 mm^3 **(I.1)**

Applied Stress on Cross-girder is define by equation (I.2)

Applied Stress on Cross-girder = $M/Z = 4044 \times 10^6 / 1.45E+07 = 278.90\ N/mm^2$ **(I.2)**

Allowable stress for grade is = $298.7\ N/mm^2 > 278.9\ N/mm^2$

I.12.3 Longitudinal Girder Check (Concrete Deck)

Composite section properties:

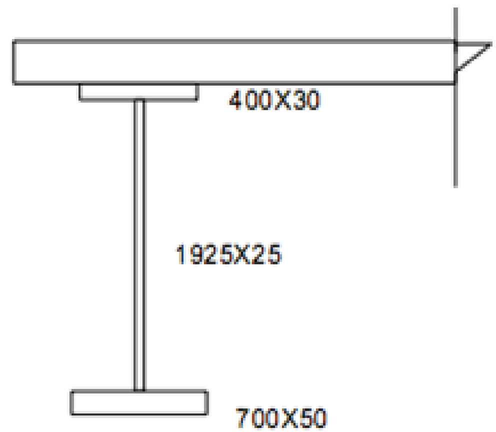

Figure I.11: Longitudinal Girder

(All dimensions are in mm)

I = $1.19E+11\ mm^4$ **(I.3)**

A_Y = $9.77E+07\ mm^3$ **(I.4)**

Calculate shear flow

Shear Stress

q = $V A_y / I$ **(I.5)**

Shear Force *(V)* = 1,100 kN

q = $9.07E-01\ kN/mm$ **(I.6)**

Use 2 rows of shear studs:

The moment capacity of section = 9,339.00 kN.m

The applied moment from Table I.3 = 7,930.00 kN.m

Since the applied moment is less than moment capacity, the longitudinal girder section is adequate.

I.13 Design of a Typical Panel Supporting the FRP Deck

A typical plan for the FRP deck includes longitudinal girders, cross-girders, and secondary longitudinal girders as shown in Figure I.12.

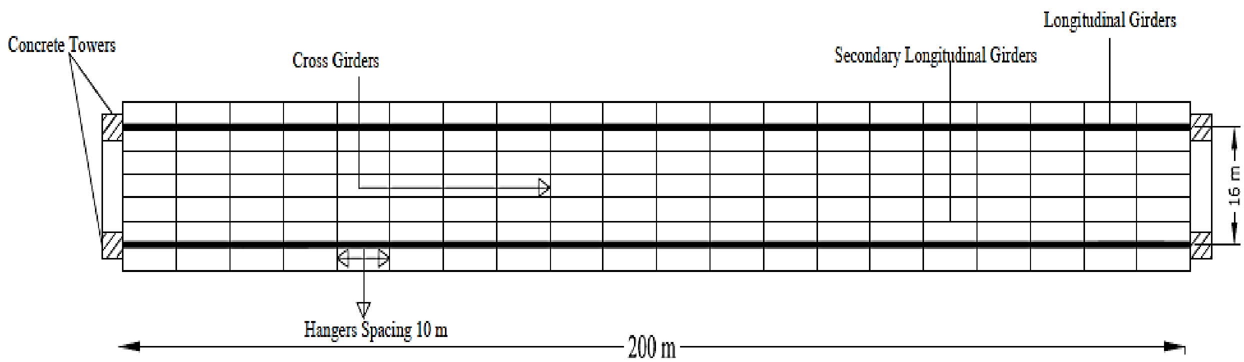

Figure I.12: Plan (FRP Deck)

The typical deck plan is shown for a 200 m span suspension bridge with an FRP deck on steel girders. The typical deck is similar of the 400 m and 600 m span suspension bridges.

I.13.1 Design of Cross-girders (FRP Deck)

The section dimension is shown in Figure I.13 is used for the design of the cross-girder supporting the FRP deck.

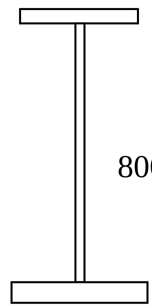

Figure I.13: Cross-Girder Design

(All dimensions are in mm)

I.13.1.1 Dead Load

The dead load calculations are summarized in Table I.5.

Table I.4: Dead Load Calculation

Item	Value	Unit
FRP including wearing services	1.2	kN/m^2
Total deck weight	4800	kN
Cross-girder weight	1.10	kN/m
Cross-girder spacing	10	m
Span	16	m

Cross-girder total dead load	336	kN
Stringer weight	1162	kN
Total dead moment (Sls)	124	kN.m

I.13.1.2 Live Load

Live load (including lane load and tandem loading), which controls the design, was calculated and the results are shown in Table I.6.

Table I.5: Live Load Calculations

Item	**Value**	**Unit**
Span between longitudinal girders	16	m
Cross-girder spacing	10.5	m
Equivalent point load on beam	96	kN
Tandem load	110	kN
Reaction on cross-girder (0.95 X 2P)	2.09	kN
Equivalent point load on beam (110 X 1.9 X 1.06/2)	110.8	kN/per wheel

I.13.1.3 Lane Load

Lane load was applied to the bridge using four lanes with a multiple presence factor of 0.65 in accordance to AASHTO–LRFD specifications. The complete results are shown in Table I.7.

Table I.6: Moment and Shear Results for the FRP Deck

Tandem loads + lane loads control

No.	Element	Moment (kN.m)	Shear (kN)
1	Cross-girder	2526	292
2	Longitudinal girders	4,078	597

I.13.2 Serviceability Limit State Check (FRP Deck)

Serviceability limit state check was performed on cross-girders and longitudinal girders for the FRP deck similar to Section I.13.2 as described in Table I.8.

Table I.7: Serviceability Limit State Check

Item	Value	Unit
Total moment	2526	kN.m
Section modulus *(Z)*	8.78 E+06	mm^3
Applied stress on cross-girder (=2526x10^6/8.78E+06)	287.5	N/mm^2
Allowable stress for grade 345 (=345/1.1/1.05)	298.7	N/mm^2

This applied stress of 287.5 N/mm^2 is less than 298.7 N/mm^2 and thus the section is adequate.

I.13.3 Longitudinal Girder Design (FRP Deck)

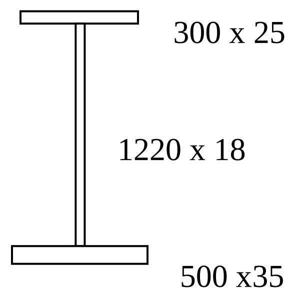

Figure I.14: Longitudinal Girder Design

(All dimensions are in mm)

Section properties

I	=	5.93E+10 mm^4
A_y	=	4.88E+07 mm^3

Using two rows of shear studs:

The moment capacity of section	=	4,537 kN.m
The applied moment	=	4,078 kN.m

Since the applied moment is less than the moment capacity, the longitudinal girder is adequate.

Appendix II. Detailed Calculations for Comparative Cost Analyses of 200 m, 400 m, and 600 m Suspension Bridges on Rock, Sand, and Clay

II.1 Sound Rock

This section presents the calculations for the comparative cost analysis of 200 m, 400 m, and 600 m suspension bridges with a concrete and an FRP deck on sound rock.

II.1.1 Cost Analysis of 200 m Suspension Bridge with a concrete and an FRP deck on Sound Rock

Two 200 m span suspension bridges with a concrete and an FRP deck were designed. The calculations of the quantities and cost for the two bridges were tabulated in Table II.1. The Items for the following tables shown in Appendix II are: 1 is Deck, 2 is Main steel girder, cross-girders, and stringers, 3 is Main cable, 4 is Anchorage, 5 is Erection, 6 is Towers, 7 is Towers base+piling, and 8 is Total Cost.

Table II.1: Cost Analysis of the 200 m Suspension Bridges with a Concrete Deck and an FRP Deck on Sound Rock

Item	Unit	Concrete Deck on Steel Girder			GFRP Deck on Steel Girder		
		Amount	Unit Price (USD)	Cost (USD)	Amount	Unit Price (USD)	Cost (USD)
1	m^2	4000	300	1,200,000	4000	700	2,800,000
2	Ton	578.6	2,800	1,619,988	302.2	2,800	846,126
3	Ton	187	5,000	935,000	98	5,000	490,000
4	m^3	12,209	400	4,883,448	4,510	400	1,804,076
5	job	1.0	2,000,000	2,000,000	1.0	1,800,000	1,800,000
6	m^3	1230.0	1,000	1,230,000	461.3	1,000	461,250
7	job	1	1,500,000	1,500,000	1	1,200,000	1,200,000
8				13,368,435			9,401,453

II.1.2 Cost Analysis of 400 m Suspension Bridge with a concrete and an FRP deck on Sound Rock

Two 400 m span suspension bridges with a concrete and an FRP deck were designed. The calculations of the quantities and cost for the two bridges were tabulated in Table II.2.

Table II.2: Cost Analysis of the 400 m Suspension Bridges with a Concrete Deck and an FRP Deck on Sound Rock

Item	Unit	Concrete Deck on Steel Girder			GFRP Deck on Steel Girder		
		Amount	Unit Price (USD)	Cost (USD)	Amount	Unit Price (USD)	Cost (USD)
1	m^2	8000	300	2,400,000	8000	700	5,600,000
2	Ton	1157.1	2,800	3,239,975	560.9	2,800	1,570,522
3	Ton	546	5,000	2,730,000	375	5,000	1,875,000
4	m^3	26,789	400	10,715,590	9,176	400	3,670,362
5	job	1.0	4,000,000	4,000,000	1.0	3,600,000	3,600,000
6	m^3	6205.5	1,250	7,756,875	2364.0	1,250	2,955,000
7	job	1	3,000,000	3,000,000	1	2,400,000	2,400,000
8				33,842,441			21,670,884

II.1.3 Cost Analysis of 600 m Suspension Bridge with a concrete and an FRP deck on Sound Rock

Two 600 m span suspension bridges with a concrete and an FRP deck were designed. The calculations of the quantities and cost for the two bridges were tabulated in Table II.3.

Table II.3: Cost Analysis of the 600 m Suspension Bridge with a Concrete Deck and an FRP Deck on Sound Rock

Item	Unit	Concrete Deck on Steel Girder			GFRP Deck on Steel Girder		
		Amount	Unit Price (USD)	Cost (USD)	Amount	Unit Price (USD)	Cost (USD)
1	m^2	12,000	300	3,600,000	12,000	700	8,400,000
2	Ton	1735.7	2,800	4,859,963	841.4	2,800	2,355,782
3	Ton	1800	5,000	9,000,000	1036	5,000	5,180,000
4	m^3	45,413	400	18,165,181	17,147	400	6,858,600
5	job	1.0	10,000,000	10,000,000	1.0	7,400,000	7,400,000
6	m^3	17034.9	1,500	25,552,313	7504.9	1,500	11,257,313
7	job	1	4,500,000	4,500,000	1	3,600,000	3,600,000
8				75,677,456			45,051,695

II.2 Medium Sand

This section presents the calculations for the comparative cost analysis of 200 m, 400 m, and 600 m suspension bridges with a concrete and an FRP deck on medium sand.

II.2.1 Cost Analysis of 200 m Suspension Bridge with a concrete and an FRP deck on Medium Sand

Two 200 m span suspension bridges with a concrete and an FRP deck were designed. The calculations of the quantities and cost for the two bridges were tabulated in Table II.4.

Table II.4: Cost Analysis of the 200 m Suspension Bridge with a Concrete Deck and an FRP Deck on Medium Sand

Item	Unit	Concrete Deck on Steel Girder			GFRP Deck on Steel Girder		
		Amount	Unit Price (USD)	Cost (USD)	Amount	Unit Price (USD)	Cost (USD)
1	m^2	4000	300	1,200,000	4000	700	2,800,000
2	Ton	578.6	2,800	1,620,080	302.2	2,800	846,126
3	Ton	187	5,000	935,000	98	5,000	490,000
4	m^3	16,380	400	6,552,133	6,051	400	2,420,533
5	job	1.0	2,000,000	2,000,000	1.0	1,800,000	1,800,000
6	m^3	1230.0	1,000	1,230,000	461.3	1,000	461,250
7	job	1	3,000,000	3,000,000	1	2,400,000	2,400,000
8				16,537,213			11,217,910

II.2.2 Cost Analysis of 400 m Suspension Bridge with a concrete and an FRP deck on Medium Sand

Two 400 m span suspension bridges with a concrete and an FRP deck were designed. The calculations of the quantities and cost for the two bridges were tabulated in Table II.5.

Table II.5: Cost Analysis of the 400 m Suspension Bridges with a Concrete Deck and an FRP Deck on Medium Sand

Item	Unit	Concrete Deck on Steel Girder			GFRP Deck on Steel Girder		
		Amount	Unit Price (USD)	Cost (USD)	Amount	Unit Price (USD)	Cost (USD)
1	m^2	8000	300	2,400,000	8000	700	5,600,000
2	Ton	1157.1	2,800	3,239,975	560.9	2,800	1,570,522
3	Ton	759	5,000	3,795,000	443	5,000	2,215,000
4	m^3	35,943	400	14,377,133	12,311	400	4,924,533
5	job	1.0	4,000,000	4,000,000	1.0	3,600,000	3,600,000
6	m^3	6205.5	1,250	7,756,875	2364.0	1,250	2,955,000
7	job	1	6,000,000	6,000,000	1	4,800,000	4,800,000
8				41,568,983			25,665,055

II.2.3 Cost Analysis of 600 m Suspension Bridge with a Concrete and an FRP Deck on Medium Sand

Two 600 m span suspension bridges with a concrete and an FRP deck were designed. The calculations of the quantities and cost for the two bridges were tabulated in Table II.6.

Table II.6: Cost Analysis of the 600 m Suspension Bridges with a Concrete Deck and an FRP Deck on Medium Sand

Item	Unit	Concrete Deck on Steel Girder			GFRP Deck on Steel Girder		
		Amount	Unit Price (USD)	Cost (USD)	Amount	Unit Price (USD)	Cost (USD)
1	m^2	12,000	300	3,600,000	12,000	700	8,400,000
2	Ton	1735.7	2,800	4,859,963	841.4	2,800	2,355,782
3	Ton	1800	5,000	9,000,000	1036	5,000	5,180,000
4	m^3	60,931	400	24,372,267	23,006	400	9,202,200
5	job	1.0	10,000,000	10,000,000	1.0	7,400,000	7,400,000
6	m^3	17034.9	1,500	25,552,313	7504.9	1,500	11,257,313
7	job	1	9,000,000	9,000,000	1	7,200,000	7,200,000
8				86,384,542			50,995,295

II.3 Stiff Clay

This section presents the calculations for the comparative cost analysis of 200 m, 400 m, and 600 m suspension bridges with a concrete and an FRP deck on stiff clay.

II.3.1 Cost Analysis of 200 m Suspension Bridge with a Concrete and an FRP Deck on Stiff Clay

Two 200 m span suspension bridges with a concrete and an FRP deck were designed. The calculations of the quantities and cost for the two bridges were tabulated in Table II.7.

Table II.7: Cost Analysis of the 200 m Suspension Bridges with a Concrete Deck and an FRP Deck on Stiff Clay

Item	Unit	Concrete Deck on Steel Girder			GFRP Deck on Steel Girder		
		Amount	Unit Price (USD)	Cost (USD)	Amount	Unit Price (USD)	Cost (USD)
1	m^2	4000	300	1,200,000	4000	700	2,800,000
2	Ton	578.6	2,800	1,619,988	302.2	2,800	846,126
3	Ton	187	5,000	935,000	98	5,000	490,000
4	m^3	20,031	400	8,012,233	7,400	400	2,959,933
5	job	1.0	2,000,000	2,000,000	1.0	1,800,000	1,800,000
6	m^3	1230.0	1,000	1,230,000	461.3	1,000	461,250
7	job	1	3,000,000	3,000,000	1	2,400,000	2,400,000
8				17,997,221			11,757,310

II.3.2 Cost Analysis of 400 m Suspension Bridge with a Concrete and an FRP Deck on Stiff Clay

Two 400 m span suspension bridges with a concrete and an FRP deck were designed. The calculations of the quantities and cost for the two bridges were tabulated in Table II.8.

Table II.8: Cost Analysis of the 400 m Suspension Bridges with a Concrete Deck and an FRP Deck on Stiff Clay

Item	Unit	Concrete Deck on Steel Girder			GFRP Deck on Steel Girder		
		Amount	Unit Price (USD)	Cost (USD)	Amount	Unit Price (USD)	Cost (USD)
1	m^2	8000	300	2,400,000	8000	700	5,600,000
2	Ton	1157.1	2,800	3,239,975	560.9	2,800	1,570,522
3	Ton	759	5,000	3,795,000	443	5,000	2,215,000
4	m^3	43,952	400	17,580,983	15,055	400	6,021,933
5	job	1.0	4,000,000	4,000,000	1.0	3,600,000	3,600,000
6	m^3	6205.5	1,250	7,756,875	2364.0	1,250	2,955,000
7	job	1	6,000,000	6,000,000	1	4,800,000	4,800,000
8				44,772,833			26,762,455

II.3.3 Cost Analysis of 600 m Suspension Bridge with a Concrete and an FRP Deck on Stiff Clay

Two 600 m span suspension bridges with a concrete and an FRP deck were designed. The calculations of the quantities and cost for the two bridges were tabulated in Table II.9.

Table II.9: Cost Analysis of the 600 m Suspension Bridges with a Concrete Deck and an FRP Deck on Stiff Clay

Item	Unit	Concrete Deck on Steel Girder			GFRP Deck on Steel Girder		
		Amount	Unit Price (USD)	Cost (USD)	Amount	Unit Price (USD)	Cost (USD)
1	m^2	12,000	300	3,600,000	12,000	700	8,400,000
2	Ton	1735.7	2,800	4,859,960	841.4	2,800	2,355,782
3	Ton	1800	5,000	9,000,000	1036	5,000	5,180,000
4	m^3	74,509	400	29,803,467	28,132	400	11,252,850
5	job	1.0	10,000,000	10,000,000	1.0	7,400,000	7,400,000
6	m^3	17034.9	1,500	25,552,313	7504.9	1,500	11,257,313
7	job	1	9,000,000	9,000,000	1	7,200,000	7,200,000
8				91,815,739			53,045,945

Appendix III. Software (MIDAS Civil) Procedure for Completed State Analysis and Initial Forces at Hangers and Main Cable

III.1 Introduction

The completed state analysis is performed to check the behavior of the completed bridge. At the initial equilibrium state, the structure is in balance under self-weight, and the deflection due to the self-weight has already occurred. The initial equilibrium state analysis will provide the coordinates and tension forces in the cables. The completed state analysis of the suspension bridge is performed to check the behavior of the structure under additional loads such as live, seismic and wind loadings. The self-weight loading in the initial equilibrium state will also be added to the total loading for the completed state analysis. The process is shown in Figure III.1.

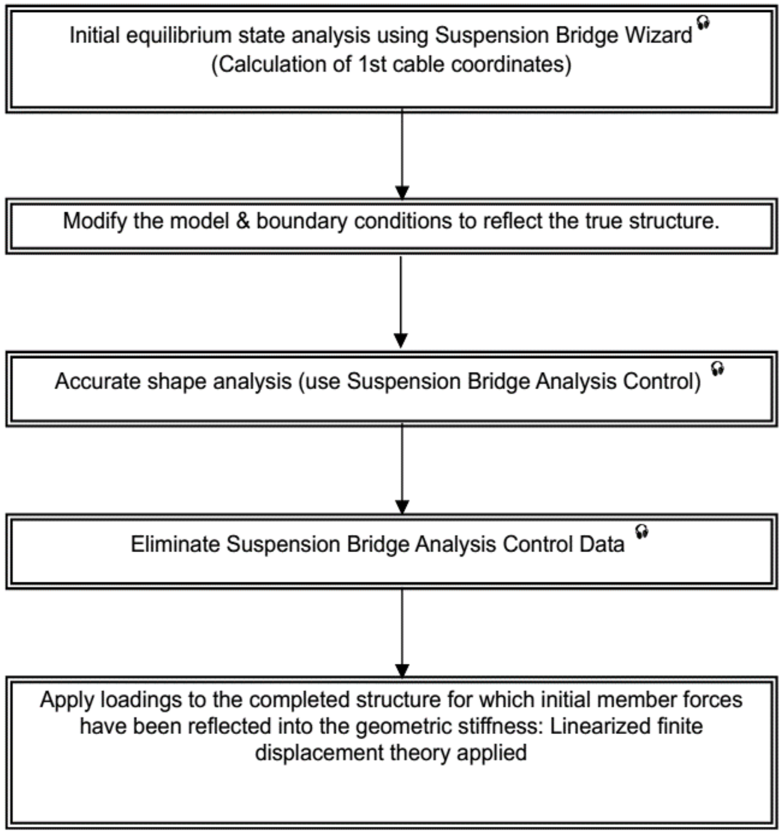

Figure III.1: Procedure for Completed State Analysis
(MIDAS-Civil Software User's Manual)

III.2 Initial Equilibrium State Analysis

Deflections due to self-weight have already occurred, and the structure has come to an equilibrium state (Figure III.2). In this initial equilibrium state, the cable coordinates and tension forces are not simply assumed by the designer, but rather they are automatically determined by using equilibrium equations within the program. Using the Suspension Bridge Wizard function, the coordinates of the cables and the initial tension forces within the cables and hangers and the forces in the pylons can be calculated automatically. The initial equilibrium state is determined by inputting the basic dimensions of cable sag, hanger spacing and the self-weight applied to each hanger. The cable and hanger tension forces determined by the Suspension Bridge Wizard are automatically converted into increased geometric stiffness using the Initial Force for Geometric Stiffness function within the program (MIDAS-Civil User's Manual).

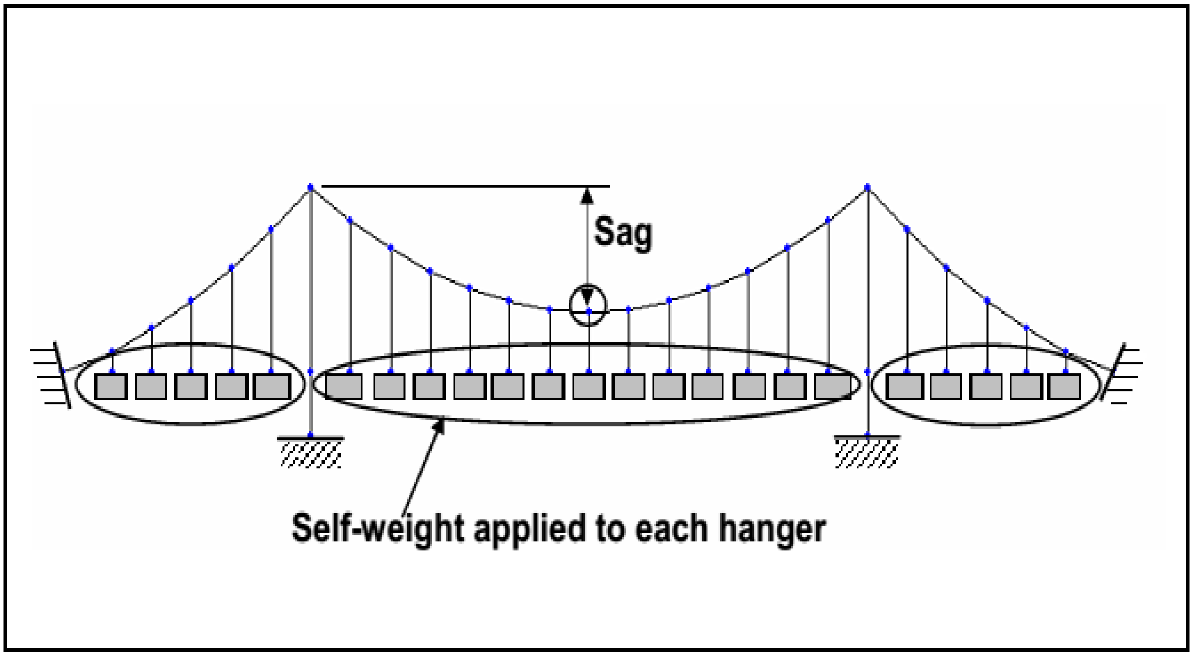

Figure III.2: Description of the Initial Equilibrium State

(Taken from MIDAS-Civil Software User's Manual)

III.3 Initial Equilibrium Results

Table III.1 indicates the results of the calculations for the forces in the concrete case while Table III.2 indicates the results of the calculations for the forces in the FRP case. Figure III.3 indicates the designation numbers of the elements at the models.

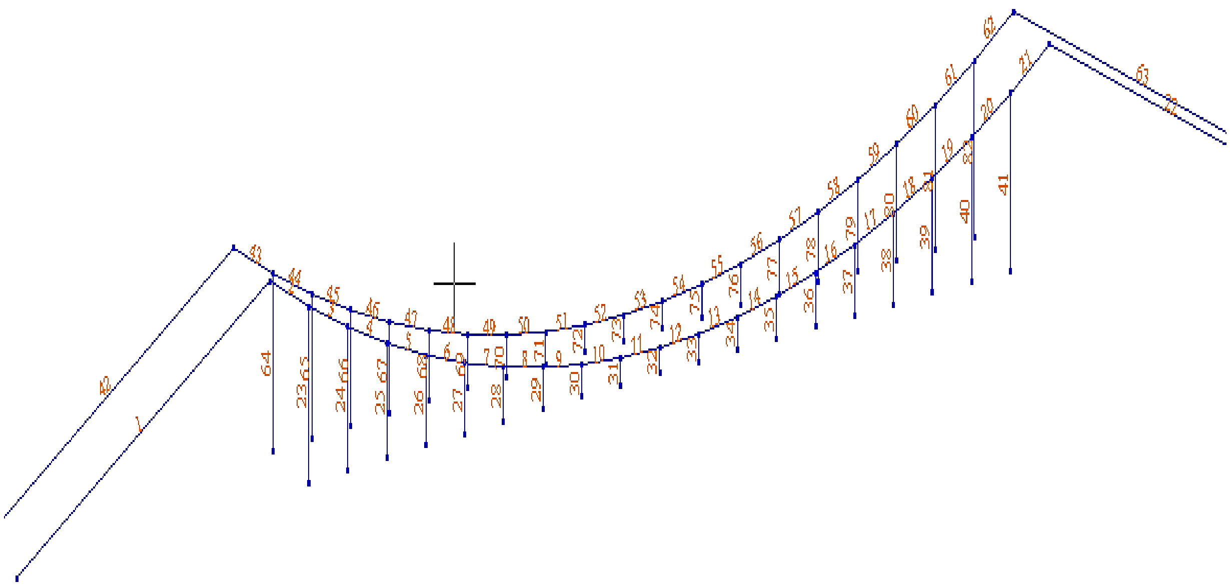

Figure III.3: Element Designation Numbers of the 200 m Span Bridge with a Concrete Deck and an FRP Deck

The results of the initial equilibrium forces in the main cables and hangers are tabulated in Table III.1 for the 200 span bridge with a concrete deck and in Table III.2 of the 200 m span bridge with an FRP deck.

Table III.1: Initial Equilibrium Force in the Main Cables and Hanger for 200 Span with a Concrete Deck

Member No.	Tension Force	(kN)
1	Axial	1678.7430
2	Axial	1673.3513
3	Axial	1647.9178
4	Axial	1626.8675
5	Axial	1608.9638
6	Axial	1593.9981
7	Axial	1581.7932
8	Axial	1572.2029
9	Axial	1565.1110
10	Axial	1560.4309
11	Axial	1558.1052
12	Axial	1558.1052

Member No.	Tension Force	(kN)
13	Axial	1560.4309
14	Axial	1565.1110
15	Axial	1572.2029
16	Axial	1581.7932
17	Axial	1593.9981
18	Axial	1608.9638
19	Axial	1626.8675
20	Axial	1647.9178
21	Axial	1673.3513
22	Axial	1678.7430
23	Axial	20.8454
24	Axial	16.0309
25	Axial	14.0105

Member No.	**Tension Force**	**(kN)**
26	Axial	12.2761
27	Axial	10.8205
28	Axial	9.6377
29	Axial	8.7228
30	Axial	8.0721
31	Axial	7.6827
32	Axial	7.5531
33	Axial	7.6827
34	Axial	8.0721
35	Axial	8.7228
36	Axial	9.6377
37	Axial	10.8205
38	Axial	12.2761

Member No.	**Tension Force**	**(kN)**
39	Axial	14.0105
40	Axial	16.0309
41	Axial	20.8454
42	Axial	1678.7430
43	Axial	1673.3513
44	Axial	1647.9178
45	Axial	1626.8675
46	Axial	1608.9638
47	Axial	1593.9981
48	Axial	1581.7932
49	Axial	1572.2029
50	Axial	1565.1110
51	Axial	1560.4309

Member No.	Tension Force	(kN)
52	Axial	1558.1052
53	Axial	1558.1052
54	Axial	1560.4309
55	Axial	1565.1110
56	Axial	1572.2029
57	Axial	1581.7932
58	Axial	1593.9981
59	Axial	1608.9638
60	Axial	1626.8675
61	Axial	1647.9178
62	Axial	1673.3513
63	Axial	1678.7430
64	Axial	20.8454

Member No.	**Tension Force**	**(kN)**
65	Axial	16.0309
66	Axial	14.0105
67	Axial	12.2761
68	Axial	10.8205
69	Axial	9.6377
70	Axial	8.7228
71	Axial	8.0721
72	Axial	7.6827
73	Axial	7.5531
74	Axial	7.6827
75	Axial	8.0721
76	Axial	8.7228
77	Axial	9.6377

Member No.	Tension Force	(kN)
78	Axial	10.8205
79	Axial	12.2761
80	Axial	14.0105
81	Axial	16.0309
82	Axial	20.8454

Table III.2: Initial Equilibrium Force in the Main Cables and the Hanger for a 200 m Span Bridge with an FRP Deck

Member No.	Tension Force	(kN)
1	Axial	472.9738
2	Axial	463.5372
3	Axial	454.2508
4	Axial	447.3702
5	Axial	441.7005

Member No.	**Tension Force**	**(kN)**
6	Axial	437.0960
7	Axial	433.4354
8	Axial	430.6205
9	Axial	428.5745
10	Axial	427.2416
11	Axial	426.5843
12	Axial	426.5843
13	Axial	427.2416
14	Axial	428.5745
15	Axial	430.6205
16	Axial	433.4354
17	Axial	437.0960
18	Axial	441.7005

Member No.	Tension Force	(kN)
19	Axial	447.3702
20	Axial	454.2508
21	Axial	463.5372
22	Axial	472.9738
23	Axial	16.4215
24	Axial	12.2525
25	Axial	10.8101
26	Axial	9.5826
27	Axial	8.5602
28	Axial	7.7345
29	Axial	7.0990
30	Axial	6.6487
31	Axial	6.3799

Member No.	Tension Force	(kN)
32	Axial	6.2906
33	Axial	6.3799
34	Axial	6.6487
35	Axial	7.0990
36	Axial	7.7345
37	Axial	8.5602
38	Axial	9.5826
39	Axial	10.8101
40	Axial	12.2525
41	Axial	16.4215
42	Axial	472.9738
43	Axial	463.5372
44	Axial	454.2508

Member No.	Tension Force	(kN)
45	Axial	447.3702
46	Axial	441.7005
47	Axial	437.0960
48	Axial	433.4354
49	Axial	430.6205
50	Axial	428.5745
51	Axial	427.2416
52	Axial	426.5843
53	Axial	426.5843
54	Axial	427.2416
55	Axial	428.5745
56	Axial	430.6205
57	Axial	433.4354

Member No.	Tension Force	(kN)
58	Axial	437.0960
59	Axial	441.7005
60	Axial	447.3702
61	Axial	454.2508
62	Axial	463.5372
63	Axial	472.9738
64	Axial	16.4215
65	Axial	12.2525
66	Axial	10.8101
67	Axial	9.5826
68	Axial	8.5602
69	Axial	7.7345
70	Axial	7.0990

Member No.	Tension Force	(kN)
71	Axial	6.6487
72	Axial	6.3799
73	Axial	6.2906
74	Axial	6.3799
75	Axial	6.6487
76	Axial	7.0990
77	Axial	7.7345
78	Axial	8.5602
79	Axial	9.5826
80	Axial	10.8101
81	Axial	12.2525
82	Axial	16.4215